Novel Functional Aspects of Follicular Dendritic Cells

Dissertation

Zur

Erlangung der naturwissenschaftlichen Doktorwürde

(Dr. sc. nat.)

vorgelegt der

Mathematisch-naturwissenschaftlichen Fakultät

der

Universität Zürich

von

Jan Kranich

aus

Deutschland

Promotionskomitee

Prof. Dr. med. Dr. sc. h.c. Adriano Aguzzi

Prof. Dr. Annette Oxenius

Prof. Dr. Manfred Kopf

Zürich 2008

1 Table of contents

2 Summary

Follicular dendritic cells (FDCs) constitute an important cell type in the germinal center (GC) reaction. They are thought to supply GC B cells with essential survival signals, drive affinity maturation and control generation and maintenance of memory B cells.

The exact molecular mechanisms of these processes are not well defined and despite their central role in the GC reaction, FDCs are probably one of the most poorly understood cell types of the immune system.

Apart from their beneficial role in adaptive immunity FDCs also exert a noxious role in certain pathologies. It is well established that FDCs trap large amounts of HIV virions and thereby contribute to the pathogenesis of AIDS. Furthermore, FDCs also participate in prion diseases by replication and accumulation of disease-associated PrP^{Sc} in lymphoid organs.

To gain deeper insights into FDC-biology by identifying FDC-specific genes and also to identify important factors that make FDCs such efficient prion replicators, an unbiased transcriptomic screen has been conducted. One interesting candidate found was the phosphatidylserine (PS)-binding protein Mfge8, which was further investigated here.

The observation that FDCs of *Mfge8*$^{-/-}$ mice lacked FDC-M1 expression, one of the most specific markers used to define FDCs, but of unknown identity, let to the discovery that FDC-M1 and Mfge8 are identical. This discovery enables new methods to study FDCs.

The role of Mfge8 in the removal of apoptotic cells is well established. It binds to PS on the surface of apoptotic cells, which is then recognized by integrins expressed on macrophages. This interaction then induces the internalization of the apoptotic cell. Consequently, tangible body macrophages (TBMϕs) of *Mfge8*$^{-/-}$ mice exhibit a phagocytosis defect leading to impaired removal of apoptotic B cells from the GC. This was reported to result in the autoimmune disease systemic lupus erythematosus (SLE). However, this report claimed that Mfge8 was produced by TBMϕs and not by FDCs.

This view was refuted here by a detailed analysis of *Mfge8* expression in the spleen using reciprocal bone marrow (BM) chimeras between wild-type (WT) and *Mfge8*$^{-/-}$ mice. In these mice *Mfge8* expression was restricted to radiation resistant FDCs.

Radiation sensitive TBMϕs failed to show any detectable *Mfge8* RNA expression. However, Mfge8 protein was easily detectable in TBMϕs when FDCs expressed *Mfge8*. This has led to a novel model of apoptotic cell removal in the GC, in which FDCs produce Mfge8 and opsonize apoptotic cells to target them for removal by TBMϕs. Cell death occurs frequently in the GC, but TBMϕs are a rare cell type, which might be limiting for apoptotic corpse removal. Thus, by supplying TBMϕs with detailed topological information were to engulf apoptotic cells FDCs guarantee a rapid and efficient removal of dying cells.

The question whether Mfge8 also contributes to prion pathogenesis was also addressed here. Mfge8 produced by FDCs seemed to be irrelevant for prion replication and accumulation in lymphoid organs. In contrast to this, *Mfge8*$^{-/-}$ mice showed a drastically accelerated prion pathogenesis after intracerebral inoculation, where disease progression is independent of prion replication in lymphoid organs. This acceleration was associated with higher levels of PrP^{Sc} in the brain. However, this phenotype was dependent on the genetic background. Whether *Mfge8*-deficiency leads to impaired removal of prions from the brain and why this occurs only in a specific genetic background will be addressed in the future.

3 Zusammenfassung

Follikuläre dendritische Zellen (FDCs) stellen einen wichtigen Zelltyp in der Keimzentrumsreaktion dar. Man nimmt an, dass sie B Zellen im Keimzentrum mit wichtigen Überlebenssignalen versorgen, die Affinitätsreifung von B Zellen kontrollieren, sowie die Entstehung und Erhaltung von B-Gedächtniszellen regulieren.

Die genauen molekularen Mechanismen dieser Prozesse sind nicht genau bekannt, und trotz ihrer wichtigen Rolle in der Keimzentrumsreaktion, sind FDCs einer der wohl am schlechtesten verstandenen Zelltypen des Immunsystems.

Ausser ihrer nützlichen Rolle in der adaptiven Immunabwehr, spielen FDCs auch eine schädliche Rolle in bestimmten Krankheiten. Es ist bekannt, dass FDCs grosse Mengen an HIV-Virionen binden und dadurch zur AIDS-Pathogenese beitragen. Desweiteren sind FDCs auch an Prionenerkrankungen beteiligt, indem sie das pathologische PrP-Konformer PrP^{Sc} in lymphatischen Organen vermehren und anreichern.

Um ein genaueres Verständnis der FDC-Biologie duch die Identifikation FDC-spezifischer Gene zu bekommen und um wichtige Faktoren für die Prionen-replikation, zu identifizieren, wurde eine unvoreingenommene Analyse des FDC-Transkriptoms durchgeführt. Ein interessanter Kandidat, der dabei gefunden wurde, war das Phosphatidlyserin (PS)-bindende Protein Mfge8, was hier genauer untersucht wurde.

Die Entdeckung, dass FDCs von *Mfge8*$^{-/-}$ Mäuse kein FDC-M1 produzieren, das einer der spezifischten FDC-Markern darstellt, aber dessen Identität bis dahin unbekannt war, hat zur Identifikation von FDC-M1 als Mfge8 geführt. Diese Entdeckung wird neue Methoden der Erforschung von FDCs ermöglichen.

Es ist bekannt, dass Mfge8 an der Beseitigung von apoptotischen Zellen beteiligt ist. Mfge8 bindet an PS, dass sich an der Oberfläche von apoptotischen Zellen befindet, was dann wiederum von Integrinen, die auf Makrophagen exprimiert werden erkannt wird. Diese Interaktion induziert die Internalisierung der apoptotischen Zelle durch den Makrophagen. Folglich zeigen Tingible-Body Makrophagen (TBMϕs) von *Mfge8*$^{-/-}$ Mäusen einen Phagozytose-Defekt, was eine gestörte Beseitigung von apoptotischen Zellen zur Folge hat und schliesslich zu der systemischen

Autoimmunerkrankung Lupus Erythematodes (SLE) führt. In dieser Studie wurde allerdings berichtet, dass Mfge8 von TBMϕs und nicht von FDCs produziert wird.

Diese Ansicht konnte hier durch eine detaillierte Analyse der *Mfge8*-Expression in der Milz von Knochenmarkschimären zwischen Wildtyp und *Mfge8*$^{-/-}$ Mäusen widerlegt werden. *Mfge8*-Expression konnte in diesen Chimären nur in den strahlungsresistenten FDCs gefunden werden. In strahlungssensitiven TBMϕs konnte dagegen keine *Mfge8*-Expression nachgewiesen werden. Das Mfge8-Protein war allerdings in TBMϕs präsent, wenn FDCs *Mfge8* exprimierten. Diese Entdeckung führte zu einer neuen Hypothese zur Beseitigung apoptotischer Zellen im Keinzentrum. Diese Hypothese besagt, dass Mfge8, das von FDCs produziert wird, apoptotische Zellen opsonisiert um sie für die Beseitigung durch TBMϕs zu markieren. Im Keimzentrum ist Apoptose häufig, TBMϕs sind dagegen aber ein seltener Zelltyp, was auf die Beseitigung apoptotischer Zellen limitierend wirken könnte. Um trotzdem eine effiziente und schnelle Beseitigung der apoptotischen Zellen zu gewährleisten, teilen FDCs den TBMϕs genaue topologische Informationen zur Lage von apoptotische Zellen, durch die Produktion von Mfge8, mit.

Auch die Frage, ob Mfge8 zur Prionen-Pathogenese beiträgt wurde hier behandelt. Dabei wurden keine Hinweise darauf gefunden, dass Mfge8, das von FDCs produziert wird, die Prionenreplikation oder -anreicherung in lymphatischen Organen beeinflusst. Im Gegensatz dazu war die Prionen-Pathogenese in *Mfge8*$^{-/-}$ Mäusen, die intracerebral inokuliert wurden und damit unabhängig von Prionenreplikation in lymphatischen Organen war, drastisch beschleunigt. Diese Beschleunigung war mit erhöhten Mengen von PrP^{Sc} im Gehirn verbunden. Allerdings war das Auftreten dieses Phänotyps abhänging vom genetischen Hintergrund der untersuchten Mäuse. Ob das Fehlen der *Mfge8*-Expression zu einem gestörten Abbau von Prionen im Gehirn führt und warum die beschleunigte Pathogenese nur in einem bestimmten genetischen Hintergrung auftritt, ist Gegenstand zukünftiger Untersuchungen.

4 Abbreviations

AID	activation-induced cytidine deaminase
ALZ	apical light zone
ANA	anti-nuclear antibody
AP	alkaline phosphatase
APC	antigen-presenting cell
BALT	bronchial associated lymphoid tissue
BCR	B-cell receptor
BLC	B-lymphocyte chemoattractant
BM	bone marrow
BSA	bovine serum albumin
BSE	bovine spongiform encephalopathy
BLZ	basal light zone
CD	cluster of differentiation
cDNA	complementary DNA
CJD	Creutzfeld-Jakob disease
CNS	central nervous system
CWD	chronic wasting disease
DC	dendritic cell
DIG	digoxygenin
dsDNA	double-strand DNA
DZ	dark zone
ELISA	enzyme-linked immunosorbent assay
EM	electron microscopy
FCS	fetal calf serum
FcR	Fc receptor
FDC	follicular dendritic cell
FRC	fibroblastic precursor cell
GALT	gut associated lymphoid tissue
GC	germinal center
GFAP	glial fibrillary acidic protein
GSS	Gerstmann-Sträussler-Scheinker syndrome
H&E	hematoxylin and eosin

HEV	high endothelial venules
HRP	horseradish peroxidase
i.c.	intracerebral
i.p.	intraperitoneal
IC	immune complex
ICAM	intercellular adhesion molecule
IF	immunofluorescence
IFN	interferon
Ig	immunoglobuline
IHC	immunohistochemistry
IL	interleukin
ISH	*in situ* hybridization
LN	lymph node
LPS	lipopolysaccharide
LT	lymphotoxin
LTβR	LTβ receptor
Mϕ	macrophage
MadCAM	mucosal addressin cell adhesion molecule
Mfge8	Milk fat globule-EGF factor 8 protein
MZ	mantle zone
NK cell	natural killer cell
OVA	ovalbumin
PALS	periarteriolar lymphoid sheath
PAS	periodic acid-Schiff
PBS	phosphate buffered saline
PK	proteinase K
PP	Peyer´s patch
PrP^C	cellular isoform of the prion protein
PrP^{Sc}	pathological isoform of the prion protein
PS	phosphatidylserine
qPCR	quantitative PCR
RT	reverse transcriptase
RU	response unit
SD	standard deviation

SLE	systemic lupus erythematosus
SPR	surface plasmon resonance
TBMϕ	tangible body macrophage
TBS	tris-buffered saline
TCR	T-cell receptor
TD	T cell dependent
TNF	tumor necrosis factor
TSE	transmissible spongiform encephalopathy
TUNEL	terminal deoxynucleotidyl transferase mediated dUTP nick end labeling
VCAM	vascular cell adhesion molecule
WT	wild-type

5 Introduction

5.1 Secondary lymphoid organs

The immune system is divided into several functionally different compartments. The two major compartments are the primary and secondary lymphoid organs. In mice and humans primary lymphoid organs, the sites where lymphocyte development and maturation take place, comprise the bone marrow (BM) and the thymus, The BM is the site of B-cell maturation. After successful rearrangement of the B-cell receptor (BCR) genes, B cells expressing a functional BCR on their surface leave the BM and home to the periphery (Benschop and Cambier, 1999). The thymus, on the other hand, is the main site for T-cell development. After rearrangement of the T-cell receptor (TCR) genes, T cells undergo positive and negative selection, which ensures tolerance to host-specific antigens and helps preventing autoimmunity. Thereafter, T cells expressing a functional non-self reacting TCR are released into the periphery (Strasser, 1995).

The secondary lymphoid organs include the spleen, lymph nodes (LN) and various lymphoid tissues that are located in mucosal surfaces, such as gut-associated lymphoid tissue (GALT), bronchial-associated lymphoid tissue (BALT), tonsils and Peyer´s Patches (PPs). Their function is to monitor the lymph and the blood for the presence of pathogens. The location of these lymphoid organs - mucosal surfaces and skin - is optimized in such a way that allows accessory cells of the immune system to rapidly encounter and trap pathogens at their main entry sites and thus elicit an adaptive immune response. In other organs, where lymphoid structures are typically absent, ectopic tertiary lymphoid follicles can form upon chronic inflammations (Fu and Chaplin, 1999).

5.1.1 Structural organization of secondary lymphoid organs

Although secondary lymphoid organs share several common features, they differ in their microarchitecture and organization, as will be described here for LNs and spleen.

Essentially, LNs are supplied by two vascular systems: the lymph vasculature which delivers antigen and antigen-presenting cells (APCs) to the LN, and the blood

vasculature which transports lymphocytes to the LN. LNs are surrounded by the marginal sinus which is connected to the afferent lymphatic vessels that empty into the subcapsular sinus. Lymph leaves the LN via efferent lymphatic vessels in the medullary region. LNs are subdivided into three regions: cortex, paracortex and medulla. The cortex comprises the outermost layer of the LN and contains the primary lymphoid follicles. The paracortex lying just beneath the cortex consists mainly of T cells and APCs. High endothelial venules (HEVs) where lymphocytes from the blood enter the LN are also located in the paracortex. The medulla, the innermost region of the LN, contains medullary cords with plasma and T cells. The medullary cords are separated by vessel-like structures called medullary sinuses, which contain macrophages and plasma cells (Witmer and Steinman, 1984, Castenholz, 1990) (Figure 1.1).

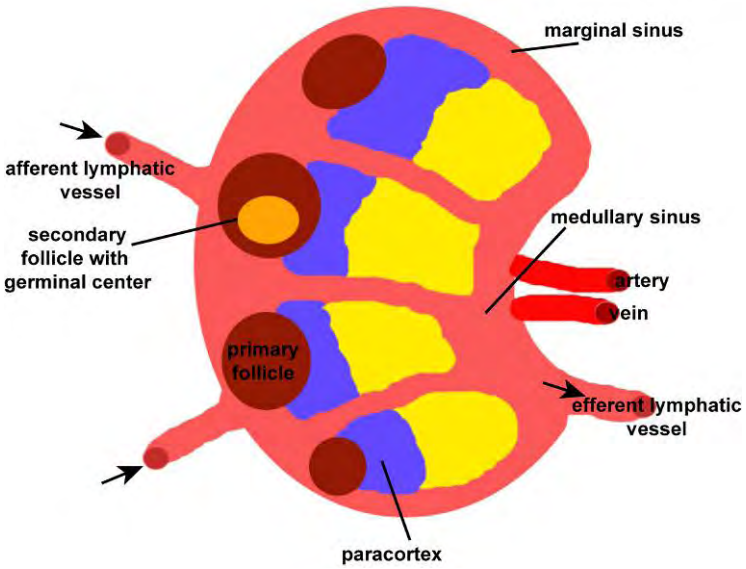

Figure 1.1 Organization of a lymph node.
Afferent lymphatics transport pathogens and APCs to the LN. Lymphocytes enter the LN via the blood stream and leave it again via efferent lymphatic vessels.
The cortex of the LN contains primary and secondary follicles. The paracortex, which is located deeper in the LN consists mainly of T cells and dendritic cells. The innermost area, the medulla mainly contains macrophages and plasma cells.
Adapted from Janeway et al., 2001.

The spleen, on the contrary, is subdivided into red and white pulp, the majority comprising red pulp, which mainly contains erythrocytes targeted for destruction. Furthermore, it also includes a reticular network of stromal cells, macrophages and plasma cells. The lymphocytes in the spleen are mainly located in the white pulp, the site of activation and maturation of B and T cells during an immune response.
The white pulp is surrounded by the marginal zone containing cells that are optimized for antigen trapping such as the marginal zone B cells and specialized macrophages that are thought to regulate the delivery of antigen to the white pulp (Groeneveld et al., 1986). The inner region of the white pulp is divided into B cell zone and T cell zone or periarteriolar lymphoid sheath (PALS) surrounding the central arteriol.

In contrast to the LNs the spleen is not supplied by afferent lymphatics. Blood-borne antigen is delivered to the spleen through the splenic artery which empties into the marginal zone, where the antigen is efficiently trapped (Witmer and Steinman, 1984, Timens, 1991) and further transported into the follicle.

The structural organization of the mucosa-associated lymphoid tissues (including PPs, BALT and GALT) compares to the LNs, in contrast to the antigen delivery pathway: antigen is transported through the mucosal epithelium rather than via afferent lymphatics. Specialized cells, called M cells have been shown to transport pathogens from the lumen to the mucosa (Neutra and Kraehenbuhl, 1992). On the abluminal side, lymphocytes re-enter the blood via efferent lymphatic vessels.

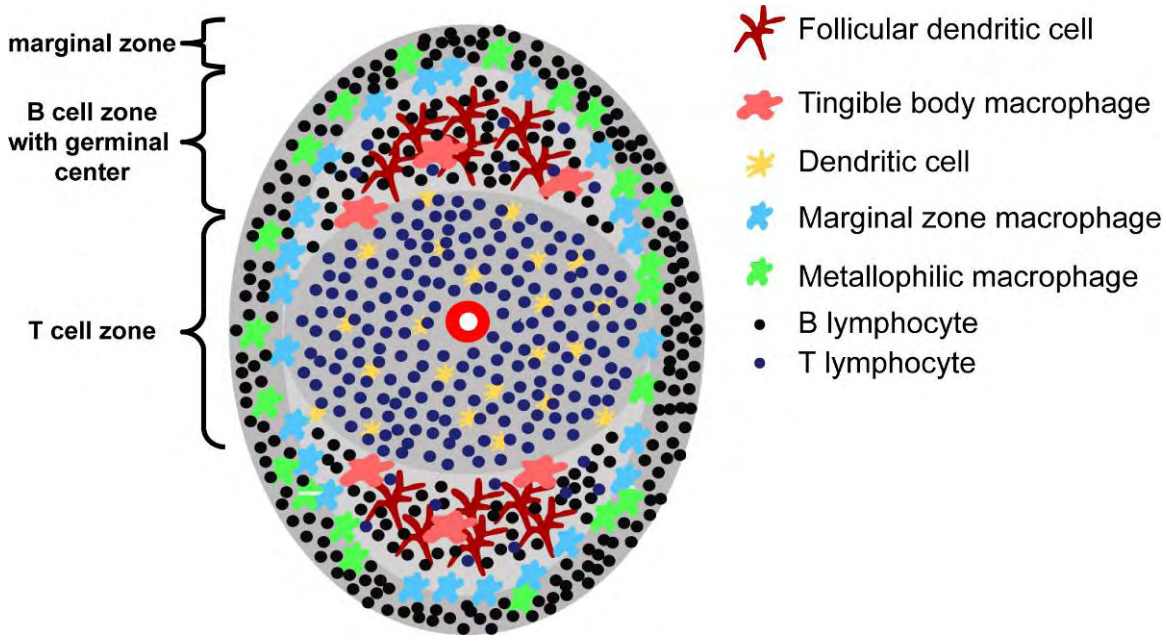

Figure 1.2 Organization of a splenic secondary follicle with its major cell types.
The outer-most layer separating the white pulp follicles from the red pulp is the marginal zone, which contains $CD21^{high}$ marginal zone B cells, $MOMA1^{+}$ metallophilic macrophages and $ER\text{-}TR9^{+}$ marginal zone macrophages. GCs arise in the B cell zone of the follicle. Apart from B cells, this area is populated by GC T cells, follicular dendritic cells (FDCs) and tingible body macrophages (TBMϕs). The T cell zone mainly contains T cells and APCs like dendritic cells (DCs).

5.1.2 Germinal centers

Germinal centers (GC) arise in primary follicles. Follicles that contain a GC are called secondary follicles. GCs are divided into different compartments referred to as mantle zone (MZ), outer zone (OZ), apical light zone (ALZ), basal light zone (BLZ) and dark zone (DZ). The MZ contains mainly recirculating B cells, while the OZ comprises a very heterogenous population of different lymphocytes. In the ALZ small centrocytes are predominantly found, and large centrocytes reside mainly in the BLZ and

centroblasts in the DZ (MacLennan, 1994) (Figure 1.3). GC generation occurs in response to a T-cell dependent (TD) antigen and is established by very few founder B cells. The limiting factor for the GC generation in a primary response to TD antigen is T cell help. Because an activated antigen-specific T cell has to get in contact with a B cell carrying the cognate BCR, it can take up to several days from the initial infection with TD antigen to the first activation of B cells (Liu et al., 1991). Initially, B cells interact with active CD4+ T-cells outside the GC in the T cell zone (Gray, 1988). These B cells then migrate into the GC where they proliferate in the dark zone of the GC (clonal expansion). These highly proliferating B cells, known as centroblasts, downregulate their expression of surface immunoglobuline (Ig), especially IgD. The progeny of these centroblasts are the centrocytes, which upregulate their surface Ig-expression. They do not proliferate and are located in the light zone of the GC (MacLennan, 1994). The light zone also contains the follicular dendritic cells (FDCs), which display antigen in its native form as immune-complexes (ICs) bound to complement- and Fc-receptors on their surface. The survival of the centrocytes is dependent on their ability to react with the antigen presented by FDCs. Only

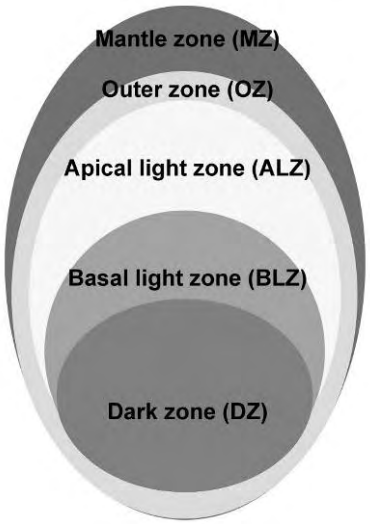

Figure 1.3 Scheme of a GC.
The GC is subdivided into five different compartments. The MZ, which contains mainly recirculating B cells, the OZ with a very heterogenous lymphocyte population, the ALZ containing small centrocytes, the BLZ with large centrocytes and the DZ, which contains centroblasts.
Adapted from Imai and Yamakawa, 1996.

previously activated B cells have the ability to react with antigen displayed by FDCs (Burton et al., 1993). The centrocytes are also suggested to take up the antigen from FDCs, process it and present it to T cells in order to get T cell help and to start another round of clonal expansion. This interaction is crucial for somatic hypermutation, a process in which B cells in the GC undergo a site-directed hypermutation that introduces point mutations in their Ig-variable region genes. This process is dependent on a protein called activation-induced cytidine deaminase (AID), which also regulates class-switching of Igs (Muramatsu et al., 2000). To

prevent generation of self-reactive autoimmune antibodies by this process, B cells have to continuously compete not only for the binding to ICs presented by the FDCs, but also for T cell help. This process leads to generation only of B cells bearing high-affinity receptors for the cognate antigen. Cells that fail to express a high-affinity receptor, either because affinity-maturation resulted in a non-functional B cell receptor (BCR) or their receptor displayed lower antigen affinity, undergo apoptosis, when they fail to interact with FDCs or T cells and therefore to receive essential survival signals. Not all of these survival signals have been identified so far, but one of them is signaling through the BCR. Also binding of T cell derived CD40L which is the ligand of CD40, a member of the TNF-receptor superfamily expressed by B cell has been shown to play a central role (Guzman-Rojas et al., 2002) in GC B cell survival. The high number of apoptotic B cells is removed by a specialized highly phagocytic macrophage population called tingible body macrophages (TBMϕ) (Swartzendruber and Congdon, 1963). The surviving cells differentiate either into memory B cells or plasmablasts that leave the follicle and migrate to sites of high antibody production, like the red pulp of the spleen or the medullary cords of LNs where they differentiate into non-dividing plasma cells (MacLennan, 1994). Plasma cells migrate further to the BM, where they can sustain for long periods. The Ig isotype produced by plasma cells varies and is dependent on the origin of the plasma cell. While plasma cells that originate from the spleen or peripheral LNs mainly produce IgG, plasma cells originating from the PPs or mesenteric LNs produce mainly IgA (Kraal et al., 1986, Weinstein and Cebra, 1991, Weinstein et al., 1991). The class-switch occurs already in the GC, before centrocytes are committed to become a plasmablast or memory B cell. The switch-decision is controlled by several cytokines, for example IL-4 promotes the switch to IgE and IL-5 is important for IgA production. In contrats, IL-1 controls the switch to IgG1 and IgE. IFN-γ is important for the switch to IgG3 and IgG2a while TGF-β is needed for the switch to IgG2b and IgA (Lorenz and Radbruch, 1996).

Memory B cells can be found in follicles long after the initial immune response, when the GC is not present any more. Memory B cells proliferate in response to native antigen displayed by FDCs. They can give rise to plasma cells and memory B cells without inducing a GC (Liu et al., 1991).

5.2 Follicular Dendritic Cells

5.2.1 Origin and Development

Follicular dendritic cells (FDCs) are found in peripheral lymphoid tissues where they reside in primary B cell follicles and GCs (Chen et al., 1978). Until today the cellular origin of FDCs remains enigmatic although most evidence points to a mesenchymal and not to a hematopoietic origin of FDCs. First of all, during postnatal development several transitional states between FDCs and fibroblastic precursor cells (FRC) have been described (Heusermann et al., 1980, Dijkstra et al., 1982, Dijkstra et al., 1984, Imai et al., 1986). Furthermore, FDCs share many morphological and phenotypical features with fibroblasts and stromal cells (Lindhout and de Groot, 1995, Bofill et al., 2000, Lee and Choe, 2003). More support for a stromal origin comes from BM-reconstitution experiments, in which after BM-transfer following lethal irradiation FDCs where always shown to be of host origin (Humphrey et al., 1984). However, in one study where mice homozygous for the severe combined immunodeficiency (*prkdc*^{scid}) mutation that lack FDCs were reconstituted with rat BM or with BM from mice expressing a lacZ transgene, FDCs of donor genotype were found (Kapasi et al., 1998). This experiment does not exclude a stromal origin, since mesenchymal progenitor cells presumably originating from BM can circulate in the blood (Campagnoli et al., 2001, Roufosse et al., 2004). The study of Imazeki *et al*, in which genetically marked spleen slices were grafted into mice, strongly supports a local tissue origin of FDCs. When host and donor spleens were analyzed six months after the engraftment, FDCs in host spleens were of host phenotype, whereas FDCs in grafted spleens were of donor phenotype (Imazeki et al., 1992). These results indicate that once the FDC-population is established, it is not replaced and remains stable for months, even after irradiation with lethal doses. Only if mature FDCs are absent, BM-derived cells can populate the FDC-compartment.

It is well established that the maturation of FDCs requires signaling pathways of the TNF superfamily (Figure 1.4). Analysis of knockout mice deficient for distinct members of the TNF superfamily clarified the importance of these members in FDC-maturation (Table 1.1). The most important factors identified are the lymphotoxin β receptor (LTβR) and the tumor necrosis factor receptor 1 (TNFR1) and their membrane bound heterotrimeric ligands $LT\alpha_1/LT\beta_2$ as well as the soluble ligands $LT\alpha_3$ and TNF (De Togni et al., 1994, Rennert et al., 1996, Rennert et al., 1997, Koni and Flavell, 1998, Fu and Chaplin, 1999). Expression of LTβR and TNFR1 by stromal cells is required for FDC-maturation, while the source of LT and TNF is hematopoietic (Ware et al., 1995). B cells are particularly important for FDC-maturation as source of membrane bound $LT\alpha_1/LT\beta_2$ (Figure 1.4). Consequently, mice that lack B cells also lack mature FDCs. T cells are also a source of secreted LT and TNF, but are dispensable for FDC-maturation, as was shown by BM-reconstitution of SCID mice. If SCID mice were reconstituted with T cells alone, no FDC-maturation took place, whereas after transfer of B cells only, generation of FDCs was restored (Kapasi et al., 1993). Signaling via LTβR and TNFR is not only involved in FDC-maturation but also in lymphoid organogenesis. *Ltβr*$^{-/-}$ as well as *Ltα*$^{-/-}$ mice not only lack FDCs, but also all LNs and PPs and are characterized with disrupted splenic microarchitecture. This is also the case for *Ltβ*$^{-/-}$ mutants, however, mesenteric LNs can be found in these mice. Peripheral LNs but no PPs are observed in *Tnf*$^{-/-}$ and *Tnfr1*$^{-/-}$ mice and their

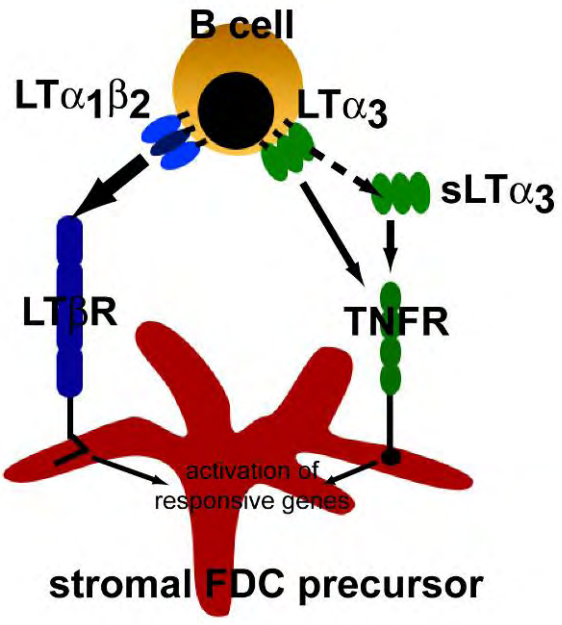

Figure 1.4 LT-signaling in FDC-maturation.
The most important source of lymphotoxins needed for FDC-maturation is B cells. They produce the membrane bound $LT\alpha_1\beta_2$ heterotrimer which signals through the LTβR. B cells also produce the membrane bound homotrimer $LT\alpha_3$, which can be cleaved to its soluble form $sLT\alpha_3$. Both membrane-bound and soluble $LT\alpha_3$ signal through the TNFR.

spleens are more organized, in spite of a disrupted marginal zone. The latter contains cells that express CD21 and FDC-M2, which might resemble immature FDCs that are trapped there (Pasparakis et al., 2000)(Table 1.1). While signaling via the LT-LTβR axis is crucial for development and homeostasis of lymphoid tissue, the TNF-TNFR1 signaling axis has its main function in promoting inflammatory responses (Ware et al., 1995).

Gene deletion	LN	PP	FDCs	Architecture
LTα	-	-	-	Disrupted
LTβ	- (MLN present)	-	-	Disrupted
TNF	+	-	FDCs trapped in MZ	Disrupted MZ
LIGHT	+	+	+	+
LTβR	-	-	-	Disrupted
TNFR1	+	-	FDCs trapped in MZ	Disrupted MZ
TNFR2	+	+	+	+

Table 1.1 Deletions of LT-signaling components and their consequences for lymphoid organogensis.

5.2.2 Morphological and phenotypic characterization of FDCs

FDCs are a very heterogenous cell type in regard to their ultrastructural morphology. Imai and Yamakawa presented a detailed morphological study of FDCs based on electron microscopical (EM) analyses (Imai and Yamakawa, 1996). They compared FDCs in relation to their localization in different areas of the GC. The mantle zone (MZ) contains IgM^+IgD^+ small resting B cells and some intermingled FDCs. The FDCs connect to each other via desmosome-like junctions and only few FDC-lymphocyte clusters, with lymphocytes encircled by smooth and slender extensions of the FDCs are present. These FDCs lack long branching cytoplasmic processes and do not form labyrinth-like structures.

The outer zone (OZ) contains a heterogenous cell population, including centrocytes, plasma cells and T cells, among which the FDC network is rather loose. The FDCs lack FcγRII (CD23) expression, but are ultrastructurally similar to FDCs in the MZ.

The dark zone (DZ) containing activated B cells and some TBMϕs represents the site of centroblast proliferation. The distribution of the FDC network is expanded, but loose. Also in this area of the GC cytoplasmic extensions are not well developed and

labyrinth-like structures are absent. No FDC-lymphocyte clusters are formed, although some centroblasts are loosely encircled.

In the basal light zone (BLZ) many apoptotic cells along with many centrocytes and TBMϕs can be detected. The FDCs express complement receptor 2 (CD21) and intercellular adhesion molecule 1 (ICAM-1), but no CD23. They are well-organized and show characteristic labyrinth-like structures. The prominent cytoplasmic extensions form tight clusters with centrocytes, suggesting an involvement of FDCs in the selection of centrocytes that have undergone successful somatic hypermuation.

Also the apical light zone (ALZ) contains centrocytes and some apoptotic bodies. The FDCs are very similar to those in the BLZ: high CD21 expression and presence of CD23 and ICAM-1. Here they form a very dense meshwork with their cytoplasmic

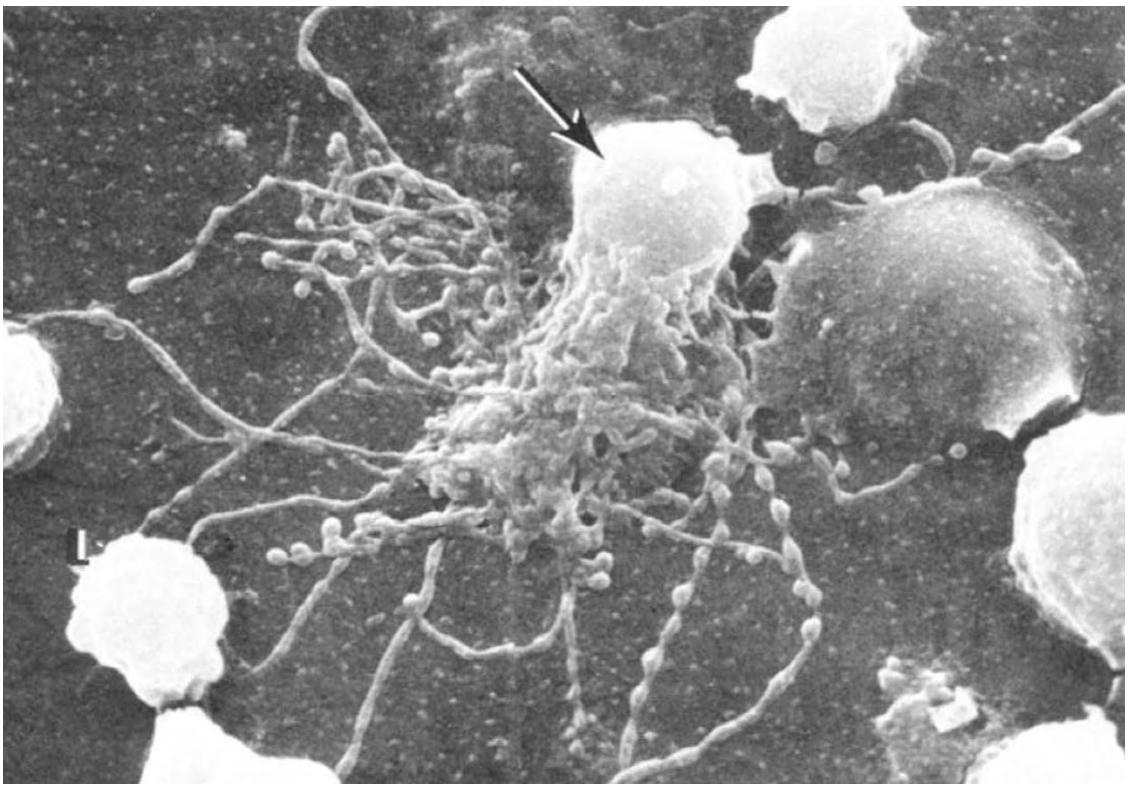

Figure 1.5 Iccosome-bearing FDC.
Scanning electron micrograph illustrating an isolated FDC bearing iccosomes. FDCs were isolated from popliteal LNs 24h after passive immunization into the footpad. Magnification 2.500x.
From Szakal et al., 1985.

extensions. The ALZ is the site where centrocytes differentiate into plasmablasts or memory B cells and it is believed that FDCs play a central role in this decision.

In 1985, Szakal *et al*. described FDCs with beaded dendrites (Szakal et al., 1985). Since these beads were then shown to contain immune-complexes, they were

termed iccosomes (immune-complex coated bodies). Iccosomes are arranged periodically on the dendrites and believed to facilitate the interaction of ICs with B cells.

Iccosome-bearing FDCs can only be found early in GC development (Szakal et al., 1989). The edema around day three of GC development might facilitate iccosome dispersion. The free iccosomes are taken up by B cells via endocytosis. By day five most iccosomes are gone, but the majority of B cells contain endocytosed ICs. Therefore, it seems that iccosomes are important for Ag-presentation to GC B cells, which in turn endocytose and degrade the Ag and potentially present it to T cells in a processed form (Kosco et al., 1988b, Szakal et al., 1988).

Apart from ultrastructural analysis, a useful tool to characterize FDCs is the expression analysis of certain surface antigens, although none of these antigens is exclusively expressed by FDCs. Most surface antigens can be grouped in few functional categories such as cell adhesion molecules (ICAM-1, VCAM-1 or MadCAM-1), complement and complement receptors C1q, C4 (FDC-M2), CR1 (CD35), CR2 (CD21), CR3 (CD11b), Fc-receptors FcεRII (CD23), FCγRII (CD32), and cytokine receptors (LTβR, TNFR1). Another very useful marker is FDC-M1, whose identity is currently unknown. Expression so far has only been shown in FDCs and TBMϕs. The anti-FDC-M1 antibody (4C11) was developed by immunizing rats with enriched murine FDC fractions (Kosco et al., 1992). The obtained antibodies were screened by immunohistochemistry for binding to FDCs. Another antibody obtained by this method recognized FDCs and was termed FDC-M2. The antigen of this antibody was later identified as complement C4. In the study presented here, the antigen recognized by the anti-FDC-M1 antibody was identified and is described in chapter 6.1.

5.2.3 Functions of FDCs

As mentioned above, FDCs play a central role in the GC reaction. One of their most important features is the trapping of native antigen in form of ICs (Tew et al., 1982). However, it is still not entirely clear how ICs reach the FDCs and which cell types are involved in this transport. It is known that most antigen that arrives in the LNs is degraded by medullary macrophages, while only small amounts arrive in the follicle where they are displayed by FDCs (Fossum, 1980, Szakal et al., 1983). Further, ICs

are known to be transported actively to the follicle and not to travel freely (Gretz et al., 2000). It has been shown that subcapsular sinus (SCS) macrophages are able to capture ICs without degrading them. Whether these macrophages also deliver the antigen to the FDCs remains controversial. A recent study has shown by two-photon microscopy that B cells can take over ICs from macrophages and then migrate with it to FDCs, where they transfer the ICs onto the FDCs (Phan et al., 2007). The authors also demonstrated that this process is dependent on the expression of complement receptor CD21 by B cells, via which ICs are bound. They further suggest that the higher expression of CD21 by FDCs is needed to successfully compete with the IC-transporting B cells for the binding to ICs. Once the IC is bound by an FDC, it will be retained for very long periods. Trapping of ICs not only occurs via complement receptors, but also via Fc-receptors like CD23 and CD32. The retention of ICs is thought to drive B cell proliferation and selection of B cells bearing high affinity BCRs. B cells in the GC are prone to undergo apoptosis and it is believed that FDCs supply B cells with survival signals as long as the B cell is able to bind to ICs displayed by FDCs. This hypothesis is supported by a variety of *in vitro* experiments. When GC B cells are cultured alone, they rapidly undergo apoptosis. However, when FDCs are added to the cultures together with T cells, FDCs form clusters with B cells and promote their stimulation up to 20-fold (Burton et al., 1993). This effect can be further increased by adding specific antigen (Kosco et al., 1992). Although the signals provided by FDCs that prevent the death of GC B cells are still unknown, it has become clear that FDCs inhibit apoptosis by inducing high levels of the cellular form of FAS-associated death-domain-like IL-1 converting enzyme inhibitory protein (cFLIP) in B cells (van Eijk et al., 2001).

Also T cell help is important for GC B cells' survival. If T cells are depleted from the co-culture system, the cluster-formation and B-cell proliferation are drastically inhibited. Therefore, FDCs and T cells promote the survival of GC B cells synergistically. To assure T cell help, it is thought that B cells take up the iccosomes that are shed by the FDCs, process the antigen and display it to T cells (Burton et al., 1991).

5.2.4 Adhesion molecules expressed by FDCs

Expression of adhesion molecules is crucial for the FDC-GC B cell interaction and cluster formation. Lymphoid cells can be entirely ensheathed by FDC processes, which also becomes apparent when primary FDC cultures are prepared. Enriched

FDC preparations are always obtained as FDC clusters. If fresh lymphocytes are added to cultured FDCs that have lost their lymphocytes, they readily form new clusters (Tsunoda et al., 1992). Several adhesion molecules have been identified on FDCs and are proposed to play a central role in the FDC-lymphocyte interaction. Among these are intercellular adhesion molecule 1 (ICAM-1) and vascular adhesion molecule 1 (VCAM-1) on FDCs and their ligands leukocyte function-antigen-1 (LFA-1) and very late activation antigen 4 (VLA-4) on B cells (Koopman et al., 1991, Kosco et al., 1992, Ree et al., 1993, Tanaka et al., 1994). Indeed, when either the ligands or the receptors were blocked by antibodies, cluster formation *in vitro* was severely reduced (Koopman et al., 1991). Another adhesion molecule proposed to be important in the clustering between B cells and FDCs was mucosal addressin cell adhesion molecule 1 (MadCAM). If MadCAM was blocked by antibodies, lymphocyte adherence to FDCs in frozen section was impaired (Szabo et al., 1997).
Expression of both fibronection and laminin receptors on FDCs was detected by immunohistochemistry. These factors are needed to bind to extracellular matrices and to reticulin and laminin fibers, respectively (Ogata et al., 1996). Interactions between the cytoplasmic extensions of FDCs and fibres may be crucial to build up the three-dimensional framework in the lymphoid follicle (Imai and Yamakawa, 1996).

5.2.5 Chemotactic attraction of lymphocytes by FDCs

The discovery that FDCs express B-lymphocyte chemoattractant (BLC, CXCL13), a chemokine that binds to the chemokine receptor CXCR5 and therefore attracts CXCR5 expressing cells, lead to the view that FDCs play a central role in attracting B and T cells that are involved in the GC reaction. BLC expression is found in primary and secondary lymphoid follicles in LNs, spleen and PPs. In the spleen BLC is also expressed in cells lining the follicular sinus (Cyster, 1999, Ngo et al., 1999). Its target molecule CXCR5 is expressed by all mature B cells and *in vitro* studies have shown that they all respond to BLC (Forster et al., 1994, Cyster, 1999). However, *in vivo* only a subset of B cells migrates to BLC-positive areas, indicating that additional factors are involved in B cell positioning (Forster et al., 1994, Ansel et al., 1999). CXCR5 expression was also found in memory and some activated T cells. Activation of $CD4^+$ T cells leads to strong CXCR5 upregulation *in vivo* suggesting that BLC also promotes the migration of T cells into the follicle. Consistent with the notion that production of BLC by FDCs strongly regulates GC organization is the phenotype of

mice deficient for BLC or CXCR5: disorganized GC with B cell accumulation around the central arteriol (Ansel et al., 2000).

5.3 Tingible body macrophages

TBMϕs are defined as a subset of mononuclear macrophages, that are highly phagocytic and reside in GCs of secondary lymphoid tissues. They were first described by Flemming in 1885 (Flemming, 1885). They contain many phagocytosed apoptotic cells in various stages of degradation, so called tingible bodies. These tingible bodies have been shown, mainly by EM studies, to originate primarily from phagocytosed lymphocytes. TBMϕs can become very large and their size ranges typically between 20-30 μm (Swartzendruber and Congdon, 1963). Histologically TBMϕs can be best identified by their localization in the GC and by their expression of FDC-M1 and typical macrophage-markers like MOMA-2 (Kraal et al., 1987), Mac-2 (Smith et al., 1991) and CD68 (macrosialin) and by their lack of F4/80 expression (Rabinowitz and Gordon, 1991), although one report claimed that some TBMϕs express F4/80 under certain conditions. The same study reported that they express Thy-1 in a cell cycle dependent manner (Smith et al., 1988).

The kinetics of TBMϕ appearance in the developing GC was investigated by Smith *et al*. This study showed that the increase in TBMϕ-number was proportional to the increase of the GC-size, while the TBMϕ : B cell ratio remained relatively constant at 1:350 – 1:400. It has been proposed that TBMϕs are involved in the initiation of GCs (Kamperdijk et al., 1978), but the fact that TBMϕs are not found in GCs before day three after antigen challenge and that GCs in old mice can develop without TBMϕs strongly contradicts this notion. When the GCs start to decline, the number of TBMϕs starts to reduce drastically. Therefore it is believed that TBMϕs are not resident macrophages of the spleen, but are recruited to the follicle upon GC generation, which is also supported by the finding that no macrophages with TBMϕ-chararcteristics can be found in primary follicles (Smith et al., 1991) .

Apart from their scavenging function, it has been proposed that TBMϕs are involved in the regulation of GC reactions (Smith et al., 1998). The fact that some TBMϕs contain endocytosed iccosomes (Szakal et al., 1988) and express MHC class II raises the possibility that they present FDC-derived antigen to T cells (Kosco et al., 1988a). However, a study by Smith *et al*. investigating TBMϕs enriched cultures for their ability to present antigen to T cells revealed that TBMϕs are poor antigen-presenters, but lead to suppression of IL-2 production by T cells. This suppression

was mediated by prostaglandins, lipids with a immuno-modulatory function. These results indicate that TBMϕs are involved in the downregulation of GC reactions by suppressing IL-2 production in T cells (Smith et al., 1998).

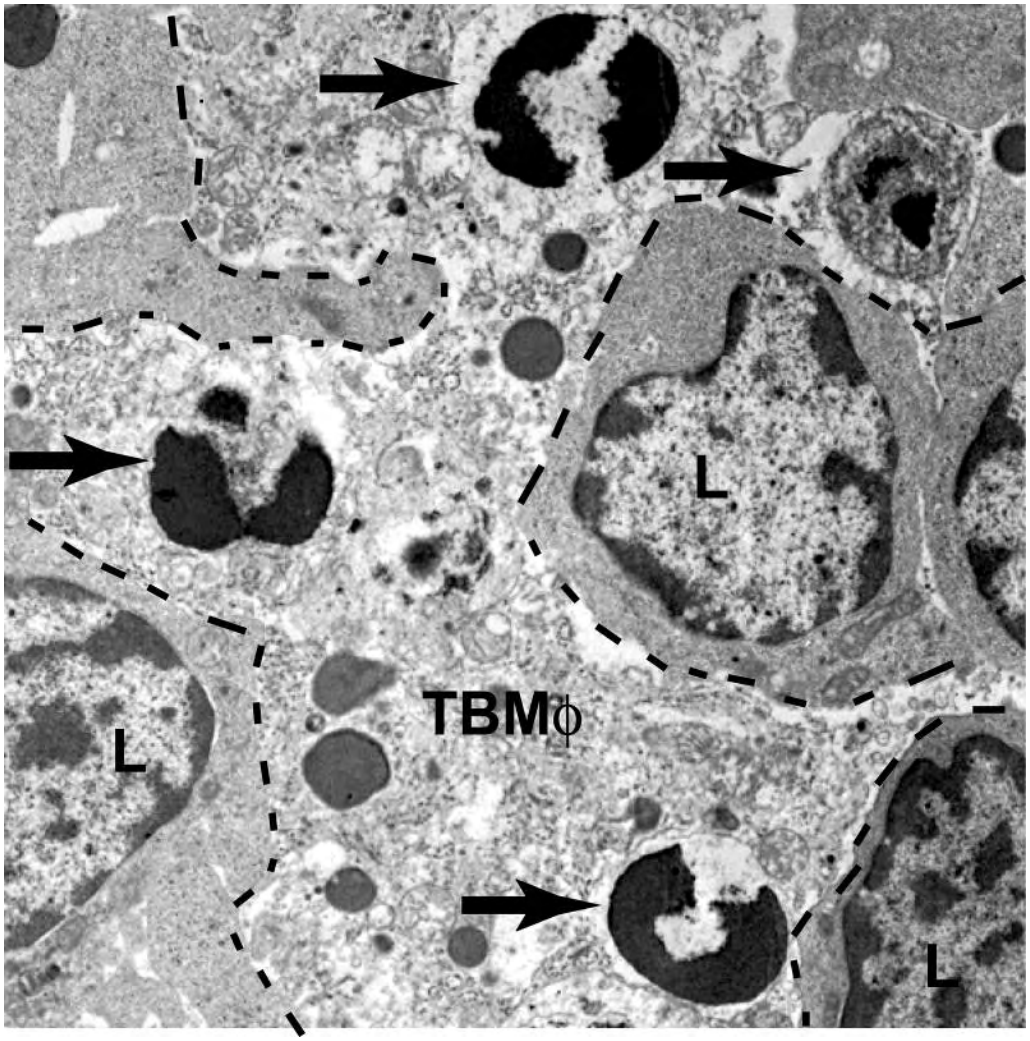

Figure 1.6 Tingible body macrophage.
Electron micrograph showing a TBMϕ (dotted line) with several engulfed apoptotic lymphocytes in different degradation stages (arrows).

5.4 Milk-fat globule epidermal growth factor 8 (Mfge8)

Mfge8 (also known as lactadherin) is a secreted glycoprotein that is involved in the clearance of apoptotic cells. It has a signal sequence, two epidermal growth factor (EGF) domains, a proline/threonine (PT)-rich domain and two factor-VIII-homologous domains, termed C1 and C2 (Figure 1.7).

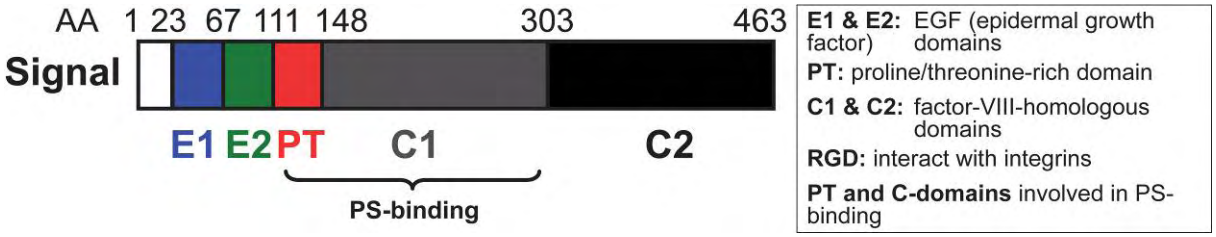

Figure 1.7 Functional domains of the Mfge8 protein.

Originally Mfge8 has been found in milk fat globules that carry fat secreted from mammary epithelial cells into the lumen during lactation (Patton and Keenan, 1975). In the mammary gland Mfge8 is produced by mammary epithelial cells, where it is needed to remove dying cells during involution of the mammary gland (Hanayama and Nagata, 2005).

More recently Mfge8 was found to be expressed by immature dendritic cells, thioglycollate elicited peritoneal macrophages (Hanayama et al., 2002) and also expression by TBMϕs was reported (Hanayama et al., 2004b).

Mfge8 is able to bind apoptotic cells by recognition of phosphatidylserine (PS) which is displayed on the surface of apoptotic cells. PS is a component of the plasma membrane and is kept on the intracellular side in a healthy cell by an ATP-dependent aminophospholipid translocase (Balasubramanian and Schroit, 2003). During apoptosis PS becomes rapidly exposed on the outer side of the cell membrane. The interaction of Mfge8 with PS is mediated via a RGD (arginine-glycine-aspartate) motif (Figure 1.7). This PS-Mfge8 complex, when bound through $\alpha_v\beta_3$ or $\alpha_v\beta_5$-integrins by macrophages induces the internalization of the apoptotic cell by the macrophage and its further degradation (Hanayama et al., 2002) (Figure 1.8).

Mfge8$^{-/-}$ mice show an impaired removal of apoptotic cells from the GC by TBMϕs. EM-analysis revealed that the TBMϕs have several unengulfed apoptotic cells bound on their surface indicating an impaired internalization and degradation of these cells. Therefore it seems that *Mfge8*$^{-/-}$ TBMϕs can recognize and bind apoptotic cells, but

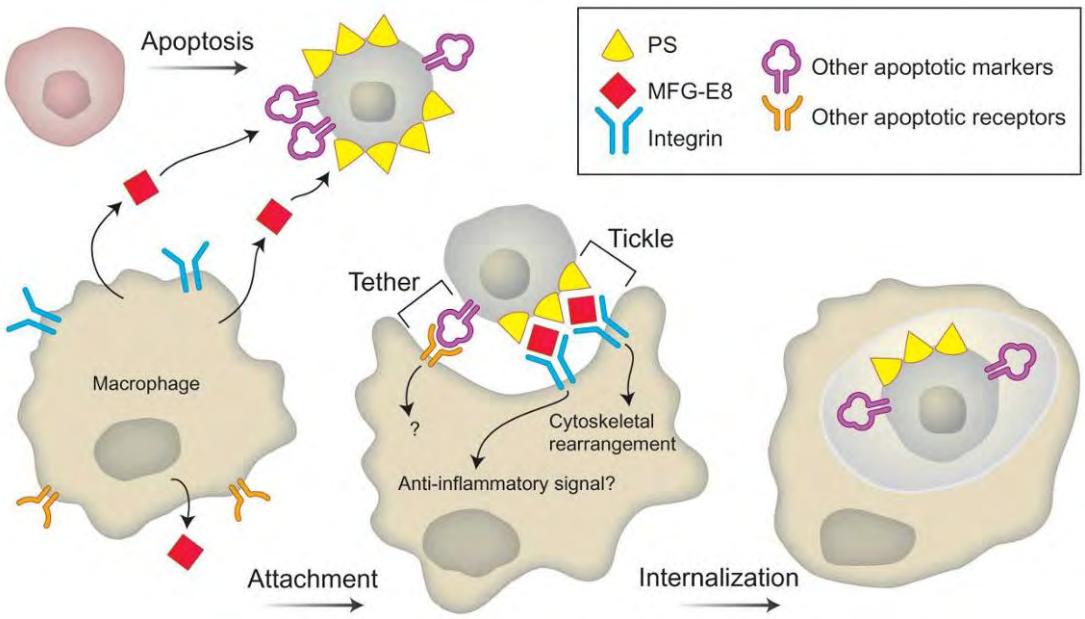

Figure 1.8 Model of Mfge8-dependent engulfment of apoptotic cells.
Upon apoptosis the dying cell displays PS on its surface. Mfge8 secreted by macrophages recognizes PS on the apoptotic cell and opsonizes it for engulfment. Mfge8 is dispensable for the attachment (tethering) of the apoptotic cell to the macrophage, but it is essential for the tickling (engulfment) of the apoptotic cell. The tickling is mediated by binding of Mfge8 to integrins on the macrophage.
From Zullig and Hengartner, 2004.

are unable to engulf them (Figure 1.9). Futhermore, these mice were reported to have more of GCs and enlarged follicles in the spleen. They also develop splenomegaly at old age. The impaired removal of apoptotic cells from the GC of *Mfge8*$^{-/-}$ mice results in systemic lupus erythematosus (SLE) with increased levels of anti-doublestrand DNA (dsDNA) and anti-nuclear antibodies (ANA), as well as Ig-deposits in the glomeruli of the kidney and proteinuria with increased urinary albumin-levels. This phenotype is rather mild, since it only can be observed in mice of approx. 40 weeks of age. However, the onset of the disease in *Mfge8*$^{-/-}$ mice can be accelerated by immunization. This induces GCs and therefore increases the appearance of apoptotic cells (Hanayama et al., 2004b). The genetic background of the *Mfge8*$^{-/-}$ mice raised some concerns, since the development of the lupus-like autoimmunity was described in mice on a B6x129sv mixed background, which often develop a spontaneous lupus-like disease. But importantly, it was later claimed that the phenotype could be reproduced in mice on a pure C57BL/6 background. Interestingly, the autoimmune phenotype was more severe in female than in male mice (Hanayama et al., 2006).

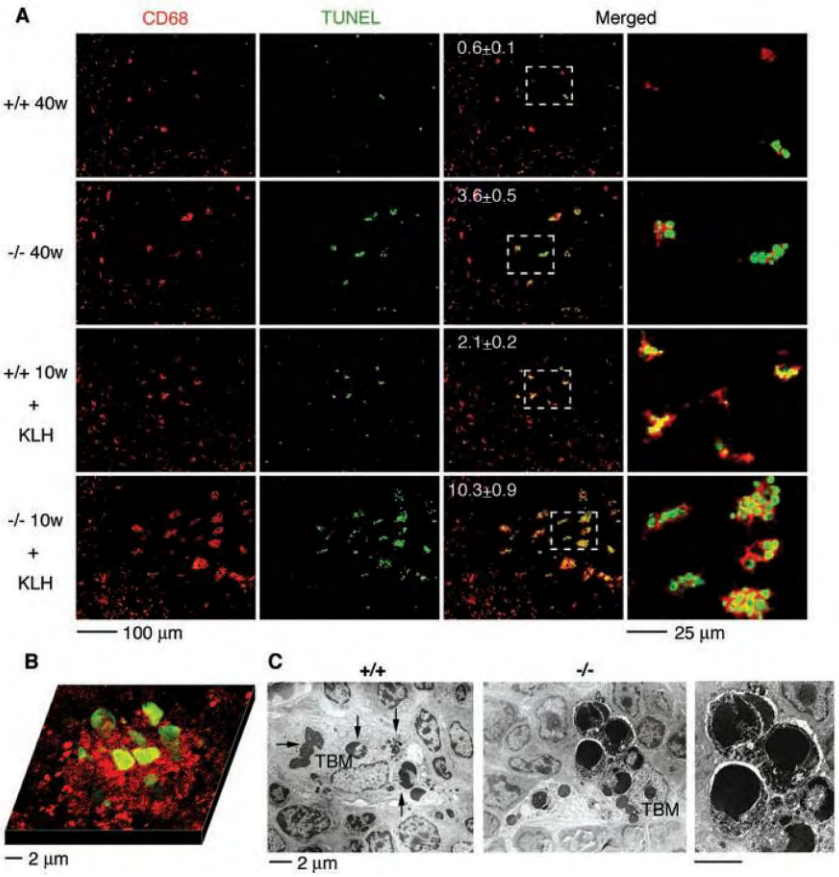

Figure 1.9 Impaired engulfment of apoptotic cells in *Mfge8*$^{-/-}$ mice.
(A) CD68^{+} TBMϕs of aged or immunized *Mfge8*$^{-/-}$ mice show increased numbers of attached TUNEL^{+} apoptotic cells. **(B)** Confocal microscopy and **(C)** EM shows that the majority of TUNEL^{+} cells that are bound by TBMϕs are located on the surface of the macrophage and not inside. This indicates impaired engulfment of apoptotic cells in the absence of Mfge8.
From Hanayama *et al*., 2004b.

5.5 Systemic Lupus Erythematosus (SLE)

SLE is an autoimmune disease that affects several organs, unlike organ-specific autoimmune diseases, such as diabetes. Therefore, SLE is classified as a systemic autoimmune disease. Consistently, the autoantibodies causing this disease are themselves systemic. SLE is characterized by the occurance of autoantibodies that target proteins that are present in each cell, such as components of the RNA-splicing machinery or chromatin. These autoantibodies are generally referred to as dsDNA antibodies or ANA antibodies (Janeway et al., 2001).

A number of genes have been identified that are involved in the development of SLE. Most of these genes can be grouped in four categories. The first category comprises genes involved in removal of apoptotic cells from the body, such as C1q (Botto, 1998, Walport et al., 1998, Gaipl et al., 2004) or Mfge8 (Hanayama et al., 2004b). Also the absence of secreted IgM, which is needed for complement induced clearance of dead cells, or the deletion of DNase I, which digests extracellular chromatin, results in SLE (Boes et al., 2000, Napirei et al., 2000, Zwart et al., 2004). In line with this, patients with SLE caused by an impaired uptake of apoptotic cells by TBMϕs have been reported (Baumann et al., 2002).

To the second category belong genes that control B and T cell activation. Among these are Fas and Fas ligand (Nagata and Suda, 1995), FcγRIIB, a inhibitory Fc receptor on B cells (Bolland et al., 2002) or the cell-cycle inhibitor p21 (Balomenos et al., 2000). Genes of the third category control IC-mediated inflammation in affected organs. The polymorphic genes FcγRIIa and FcγRIII have different IC-binding affinities and are linked with the occurrence of glomerulonephritis (Gibson et al., 1999). The last category is the hormonal status. Many autoimmune diseases show a strong sex bias, what has also been shown for female *Mfge8*$^{-/-}$ mice, which exhibit a more severe disease phenotype (Whitacre et al., 1999, Hanayama et al., 2004b, Hanayama et al., 2006).

While it is clear, that impaired removal of apoptotic cells can lead to SLE, the precise mechanism that leads to generation of autoimmune antibodies is not clear, but following model has been proposed: When an apoptotic cell is not removed by macrophages it undergoes secondary necrosis which is linked with the release of chromatin and other nuclear proteins. Secondary necrosis causes inflammation and complement activation and possibly opsonization of nuclear debris by complement components. The consequences of this might be that opsonized nuclear antigens are

taken up and processed by APCs and presented to histone-specific T cells, which in turn activate autoreactive dsDNA-specific B cells (Fig. 1.10). Protein-free DNA is poorly immunogenic. DNA however, released from necrotic cells is complexed with proteins, such as histones, which can be processed and presented to T cells (Moens et al., 1995, Rekvig, 1997). Indeed, histone-specific T cells were found in patients suffering from SLE (Desai-Mehta et al., 1995, Voll et al., 1997, Mohan et al., 1993). In addition to this, FDCs might bind nuclear antigens as ICs and therefore drive selection of high affinity antibodies against nuclear antigens (Baumann et al., 2002, Gaipl et al., 2005), resulting in the development of a lupus-like autoimmune disease.

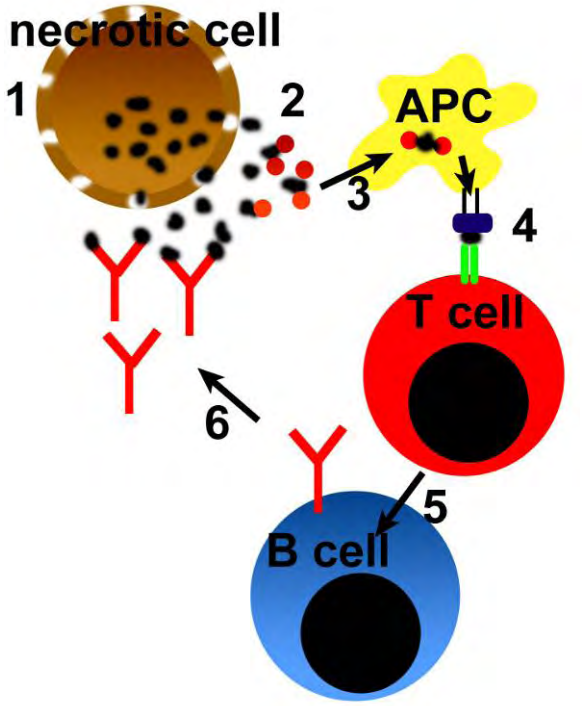

Figure 1.10 Model for generation of auto-antibodies during SLE.

1) An apoptotic cell that is not removed by macrophages undergoes secondary necrosis and releases nuclear proteins.
2) This induces an inflammatory response during which the complement system is activated and opsonizes the released nuclear proteins.
3) The opsonized antigens are taken up by APCs, processed and displayed via MHC molecules.
4) APCs then activate autoreactive T cells bearing a TCR specific for nuclear antigens.
5) Activated T cells then in turn activate B cells that carry a BCR recognizing nuclear antigen.
6) After affinity maturation B cells release high affinity antibodies directed against nuclear antigens.

5.6 Prion diseases

5.6.1. General aspects of prion diseases

Prion diseases are fatal transmissible neurodegenerative disorders and are termend transmissible spongiform encephalopathies (TSEs). They comprise human diseases like Kuru, Creutzfeld-Jakob disease (CJD), fatal familiar insomnia and Gerstmann-Sträussler-Scheinker syndrome (GSS) (Aguzzi and Polymenidou, 2004, Aguzzi, 2006), ovine forms like scrapie, bovine spongiform encephalopathy (BSE) in cattle (Hope et al., 1989) and chronic wasting disease (CWD) in elk and deer (Sigurdson and Aguzzi, 2007). The neuropathological features of TSEs are extensive spongiosis, astrogliosis and microgliosis as well as neuronal loss with deposition of large extracellular amyloid-like aggregates (Prusiner et al., 1983, Weissmann, 2004).

The nature of the infectious agent still remains enigmantic. But observations that the infectious agent is resistant to UV irradiation, high temperature and formaldehyde treatment has led to the protein-only hypothesis which claims that the infectious agent consist of protein only and can replicate without nucleic acids. This infectious agent has been termed prion (for proteinaceous infectious particle) (Prusiner, 1982). The prion is a proteinase-resistant glycoprotein designated PrP^{Sc} (for scrapie). PrP^{Sc} is a postranslationally modified form of the normal cellular prion protein PrP^{C} (for cellular) (Bolton et al., 1982, Prusiner et al., 1982). The proteinase-resistancy is a useful tool to discriminate between PrP^{Sc} and PrP^{C}, but it is questionable that all forms of the infectious particle are proteinase-resistant. Indeed, there is evidence suggesting that a significant fraction of the infectious particles is proteinase-sensitive (Lasmezas et al., 1997).

PrP^{C} is encoded by the *Prnp* gene. Strong evidence in favour for the protein-only hypothesis was found when this gene was knocked out in mice: $Prnp^{0/0}$ mice are resistant to infection with prions (Sailer et al., 1994). The hope that *Prnp*-knockout mice would also reveal the answer to the question what the physiological function of PrP^{C} is, was unfortunately not fulfilled. Although many physiological functions, like for example involvement in copper binding and copper metabolism (Brown et al., 1997a, Brown et al., 1997b) have been attributed to PrP^{C}, none of these could be convincingly demonstrated (Hutter et al., 2003). However, the fact that it is present on the cell surface and attached to the cell membrane by a glycophosphatidlyinositol-(GPI) anchor might hint to a role in cell adhesion and recognition, ligand binding or

transmembrane signaling. The ubiquitous expression of PrP^C suggests a rather general function with significance to many cell types. In the brain PrP^C is expressed mainly by neurons, but also by astrocytes and microglia. Outside the CNS PrP^C expression was found in heart, skeletal muscle, lung, intestines, testis, ovaries and lymphoid tissue. The main PrP^C expressing cell type in lymphoid tissue are FDCs, but also hematopoietic cells express low levels of PrP^C (McBride et al., 1992).

6.6.2 Conversion of PrP^C to PrP^{Sc}

The conversion of PrP^C to PrP^{Sc} is incompletely understood. At present there are two major models describing the mechanistic features of the PrP^C to PrP^{Sc} conversion: The “refolding” or “template assistance” model (Fig. 1.11A) suggests that the spontaneous conversion of PrP^C to PrP^{Sc} is prevented by an energy barrier. Only if PrP^C interacts with an existing PrP^{Sc} molecule the conversion process can be initiated. Once a PrP^C:PrP^{Sc} heterodimer is formed the catalytic activity of PrP^{Sc}

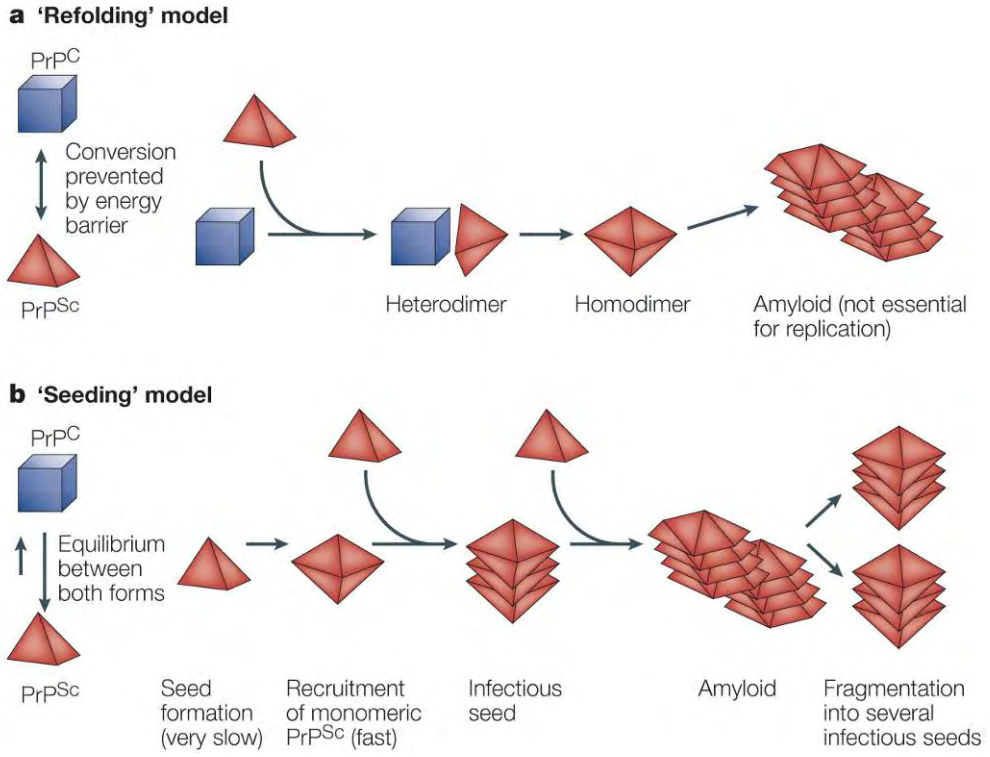

Figure 1.11 “Refolding” and “Seeding” models for the conversion of PrP^C into PrP^{Sc}.
(A) The `refolding' or “template assistance” model postulates that PrP^C interacts with PrP^{Sc} introduced from outside. PrP^{Sc} induces the conversion of PrP^C into new PrP^{Sc} molecules. Spontaneous conversion of PrP^C to PrP^{Sc} is prevented by a high energy barrier.
(B) The `seeding' model postulates that PrP^C and PrP^{Sc} form a reversible thermodynamic equilibrium. Only after several monomeric PrP^{Sc} molecules are organized into a highly ordered seed, further monomeric PrP^{Sc} molecules can be recruited to the seed, resulting eventually in amyloid. PrP^{Sc} becomes stabilized in such a seed. Fragmentation of PrP^{Sc} aggregates results in new seeds. From Aguzzi and Sigurdson, 2004.

reduces the energy needed for the conversion of PrP^{C} to PrP^{Sc} (additional enzymes or chaperones might be required for this process). Therefore, the formation of a PrP^{Sc} homodimer is now possible. The newly formed PrP^{Sc} can then function itself as template resulting in an exponential increase of PrP^{Sc}. The slowest step in this model is the conversion itself, which might require extensive unfolding and refolding of the protein (Gajdusek, 1988, Prusiner and DeArmond, 1990, Prusiner, 1991).

The “seeding model” (Fig. 1.11B) claims that the conversion is reversible and controlled thermodynamically. The transition of PrP^{C} to PrP^{Sc} occurs spontaneously but the thermodynamically favoured form is PrP^{C}. After spontaneous formation of monomeric PrP^{Sc}, the newly formed PrP^{Sc} can be stabilized when it interacts with a crystal-like seed or aggregates of PrP^{Sc}. In this model the rate limiting step is the seed-formation (Come et al., 1993, Jarrett and Lansbury, 1993, Lansbury and Caughey, 1995).

Both models are not mutually exclusive and can be applied to both inherited or infectious forms of prion diseases. In inherited forms, a mutation in the *Prnp* gene may change the ability of spontaneous formation of infectious PrP^{Sc} or PrP^{Sc} aggregates that function as a seed for polymerization. In infectious prion diseases the incoming PrP^{Sc} might resemble either the PrP^{Sc} catalyzing the transition from the heteordimer to the PrP^{Sc} homodimer or the polymerization-seed.

6.6.3 Prions and the immune system

In natural scrapie infections the infectious prions are normally not directly transmitted to the CNS. Typical entry of prions occurs rather through the oral route via food intake or via skin (scarification). Before prions reach the brain they have to travel from the entry site to the CNS, in a process called neuroinvasion (Aguzzi, 2003). During the first stage in their travel prions have to leave the gut and enter the lymphoid system. In sheep that where orally inoculated with prions to mimic the natural situation, prions were first recovered from the distal ileum after oral challenge (Wells et al., 1994, van Keulen et al., 1996). It was further observed that PPs were able to accumulate large amounts of prions. Prinz *et al*. could show that the susceptibility of mice to oral inoculation correlated with their number of PPs (Prinz et al., 2003b). Furthermore, Heppner *et al*. were able to show that M cells play a central role in transporting prions to PPs (Heppner et al., 2001). M cells are located in the follicle-associated epithelium of the PPs and are specialized in the uptake and

transcytosis of macromolecules and microorganisms (Hathaway and Kraehenbuhl, 2000). Once prions have entered the lymphoid system, they spread to all lymph nodes and the spleen, where they are replicated efficiently. High titres of prions can be recovered from the lymphoid organs long before they can be detected in the brain (Kimberlin and Walker, 1979, Mabbott et al., 1998). Several cell types of the immune system might be involved in replication and transport of prions in lymphoid organs. B cells, macrophages and dendritic cells might be important for prion transport, but less important for prion replication. One major cell type has been identified that is responsible for prion replication and accumulation in lymphoid organs. This cell type is the FDC. FDCs express high levels of PrP^C, much higher levels than any other cell type of the lymphoid system (Jeffrey et al., 2000). Mice devoid of FDCs are resistant to prion disease after peripheral administration of prions. Also a temporary depletion of FDCs by injection of soluble LTβR-Ig treatment during the time of infection renders mice resistant to peripherally administered prions. Initially, it was believed that B cells are the most important cell type for peripheral prion replication, since mice devoid of B cells where unable to replicate prions in their lymphoid organs (Klein et al., 1997). But now all evidence points towards an indirect role of B cells in prion replication. B cells provide essential survival and differentiation signals to FDCs via LT and TNF. Their presence is indispensable for normal FDC maturation and therefore for efficient peripheral prion replication (Aguzzi, 2003).

FDCs can even render the organ tropism of prions, when they appear ectopically in tertiary follicles. Normally liver and kidney are free of prions, but Heikenwälder *et al*., could show that upon transgenic expression of LTα and LTβ in these organs FDC-containing tertiary follicles arise. When these mice were inoculated with prions, high titres of prions were recovered from liver and kidney (Heikenwalder et al., 2005). Visualization of prion accumulation in lymphoid organs by histoblot, (a technique where tissue is blotted onto a membrane, digested with proteinase K to remove cellular PrP^C and then incubated with anti-PrP antibodies) shows that all detectable PrP^{Sc} perfectly colocalizes with FDCs (Fig. 1.12).

Why are FDCs such efficient prion replicators? There are several possible reasons. Their high expression of PrP^C is certainly of importance. But apart from that FDCs exhibit several other features that might make them so unique in their ability to replicate prions. One such feature is their expression of complement receptors. There is a large body of evidence that the complement system has a key role in enabling

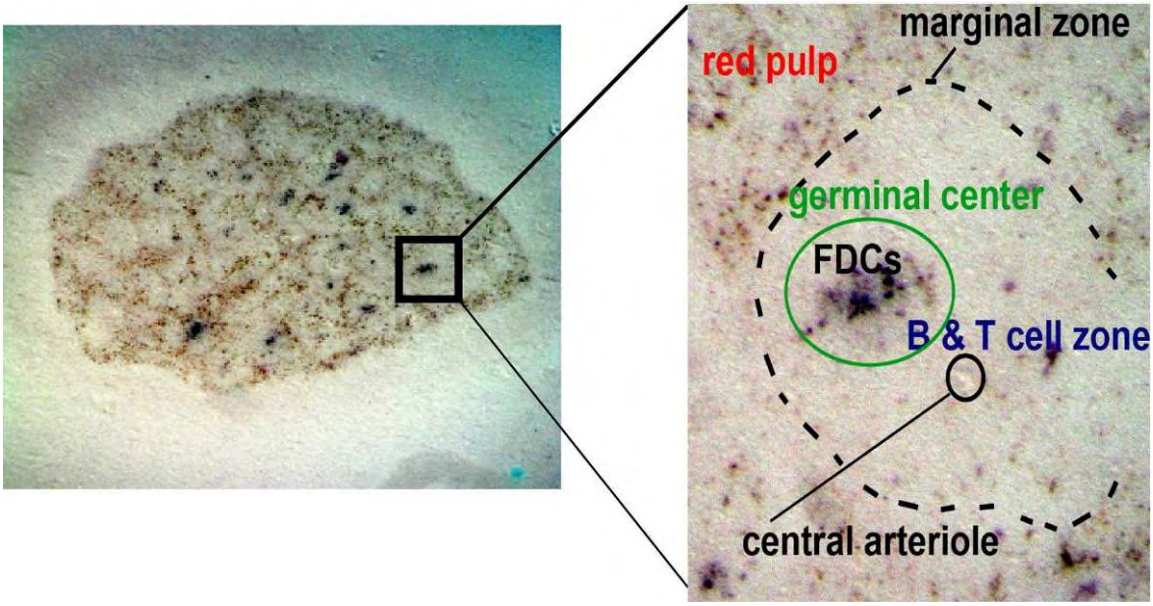

Figure 1.12. Histoblot of a prion infected spleen.
A splenic cryosection was blotted onto a nitrocellulose membrane, digested with proteinase K and incubated with anti-PrP antibodies. Disease associated PrP^{Sc} can only be detected in white pulp follicles and colocalizes with FDCs.

peripheral prion replication. Mice deficient of components of the complement system, like C1q, C3 or C4 knockout mice, or mice deficient of complement receptors (like CD21/35 knockout mice) all show substantially impaired peripheral prion replication (Klein et al., 2001). Also temporary inactivation of complement C3 by cobra venom significantly impaired peripheral prion replication and delayed the onset of the disease in mice (Mabbott et al., 2001). Recently, Zabel *et al.*, where able to show by reciprocal BM-chimeras that only the depletion of CD21/35 on FDCs, but not on B cells significantly impaired prion replication in lymphoid organs, underlining the importance of complement receptor expression by FDCs (Zabel et al., 2007). These results suggest that once prions enter the body they activate the complement system and become opsonized by soluble complement factors and can then be bound by FDCs through their complement receptors.

One additional feature of FDCs that might contribute to their ability to replicate prions is their longevity and the fact that they do not undergo extensive cell division. Recent results from the lab of Charles Weissmann indicate that *in vitro* prions are mainly transmitted horizontally from the parental cell to the daughter cell rather than to neighboring cells. *In vitro* replication is most efficient if cell division is slowl, because after each division the prion load in each cell is reduced by 50%. If the rate of cell division is too fast, the prion load in each cell is continuously decreased with each

round of cell division until the prions are completely cleared from the cell. It is likely that this also holds true for the *in vivo* situation. This might also explain why neurons are also very efficient prion replicating cells, they are also very long-lived and hardly undergo cell division.

But how do prions travel from lymphoid organs to neurons located in the CNS? Substantial evidence suggests that prions migrate along peripheral nerves from the lymphoid system to the CNS. This migration is dependent on PrP^C expression by peripheral nerves (Aguzzi, 2003). Lymphoid organs are highly innervated with sympathetic nerves (Felten and Felten, 1988). Denervation or sympathectomy significantly delayed the onset of prion pathogenesis by impairing the transport of prions from the lymphoid organs to the CNS (Glatzel et al., 2001). A study conducted by Prinz and Heikenwälder *et al*. showed that the distance between FDCs and peripheral nerves determines the velocity with which prions are able to enter the CNS (Prinz et al., 2003a).

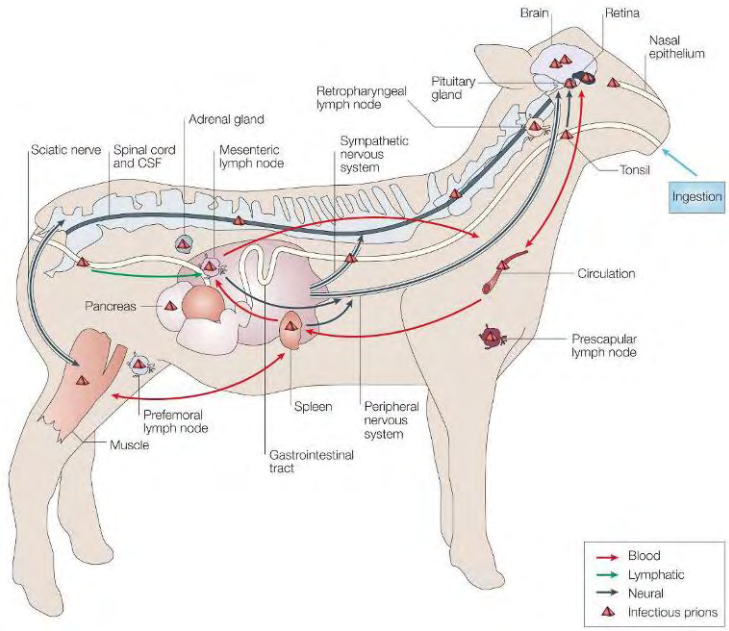

Figure 1.13 Prion accumulation in an infected animal. After ingestion of prions, they travel along the gastrointestinal tract to pancreas, lymphoid organs and muscle, then continue their travel along peripheral nerves to the CNS. From Aguzzi and Sigurdson, 2004.

5.7 Outline of this study

A detailed understanding of FDC biology is not only important because FDCs are a central component of the GC reaction and therefore for adaptive immunity in general, a detailed understanding of FDC development and function is also needed, because they are involved in diseases like prion diseases as described above. But prion diseases are not the only situation where FDCs play a noxious role: Upon infection with HIV, FDCs trap large numbers of infectious virions for months if not years (Tenner-Racz et al., 1988). Hence, FDCs represent a viral reservoir in close contact to $CD4^+$ T cells that can become subsequently infected. Therefore, FDCs render the GC conducive to HIV replication, thereby contributing to the pathogenesis of AIDS.

Due to the central role of FDCs in the replication of prions, Huber *et al.* performed a transcriptomic mircroarray analysis in order to identify FDC-specific genes. For this, isolated FDCs were compared to spleens that were devoid of FDCs due to treatment with soluble LTβR-Ig fusion protein (Huber et al., 2005).

The aim of this unbiased transcriptomic screen was to identify new genes that were important to FDC biology and that would give new insights into the function of FDCs in health and disease. One interesting candidate that was identified by this screen was Mfge8.

The aim of the study presented here was to determine the function of Mfge8 in FDCs. The first step was to clarify the origin of Mfge8 in the spleen, since Hanyama *et al.*, claimed TBMϕs rather than FDCs as the source of splenic Mfge8.

In order to solve this, FDCs of *Mfge8*$^{-/-}$ mice were first analysed histologically. FDCs from *Mfge8*$^{-/-}$ mice seemed to be morphologically normal despite the fact that they lacked expression of the FDC-marker FDC-M1. This raised the possibility that Mfge8 and FDC-M1 are identical, which was then confirmed by several independent techniques.

In the second part of this study the question whether FDCs, TBMϕs or both cell types express *Mfge8* was addressed by generating BM-chimeric mice between wild-type (WT) and *Mfge8*$^{-/-}$ mice and *in situ* hybridization (ISH) techniques. This approach identified FDCs as the sole source of Mfge8 in the spleen.

Next, the question whether the phenotypes observed in the *Mfge8*$^{-/-}$ mice, like impaired removal of apoptotic cells from the GC and the development of SLE can be

attributed to lack of *Mfge8* expression by FDCs was addressed by using BM chimeric mice.

The last part of this study deals with the question, whether Mfge8 produced by FDCs is involved in prion replication or accumulation by these cells.

6 Results

6.1 Mfge8 and FDC-M1 are identical

6.1.1 FDC-M1$^+$ networks are absent in spleens of Mfge8$^{-/-}$ mice

The results of the microarray screen performed by Huber *et al.* suggested that FDCs express *Mfge8* (Huber et al., 2005). This could be confirmed by immunofluorescence (IF) using an anti-Mfge8 antibody (Figure 6.1). The dense reticular network formed by FDCs clearly stained positive for Mfge8. Furthermore, some cells lining the marginal zone were weakly positive for Mfge8. Within the follicle all staining was restricted to the B-cell zone, the T-cell zone in the center of the follicle and also the red pulp did not show any Mfge8$^+$ cells by IF (Fig. 6.1).

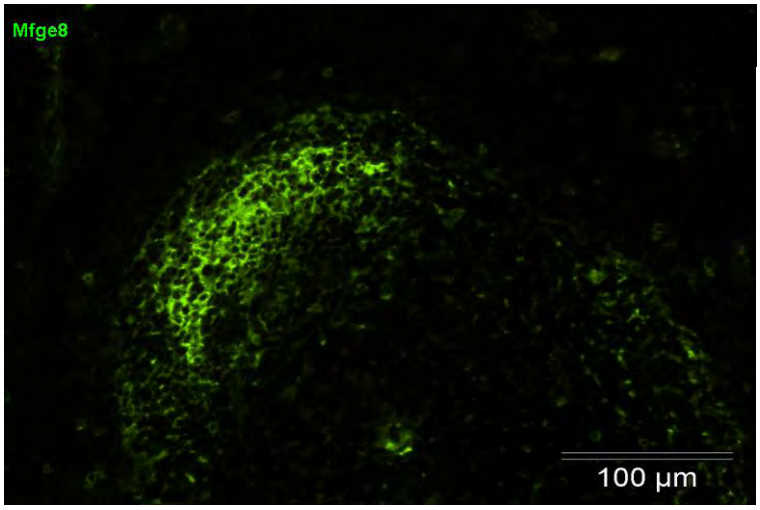

Figure 6.1 Immunofluorescent staining of FDCs using an anti-Mfge8 antibody.
High Mfge8 expression can be found on FDC networks. Some single cells around the FDC network stain weakly positive for Mfge8. These cells could resemble TBMϕs. Also cells lining the marginal zone stain weakly positive for Mfge8. Almost no Mfge8$^+$ cells can be found in the T-cell zone of the follicle or the red pulp.

Since Mfge8 was so abundantly expressed on FDCs, *Mfge8*$^{-/-}$ mice were analyzed in order to define the role of FDC-borne Mfge8. Although the splenic microarchitecture of *Mfge8*$^{-/-}$ mice was altered with enlarged TBMϕs, progressive splenomegaly, and hyperplastic follicles with increased numbers of PNA$^+$ GCs, FDC abnormalities were not reported (Hanayama et al., 2004b). However, a complete absence of FDC-M1$^+$ networks from splenic cryosections of *Mfge8*$^{-/-}$ mice was observed when stained with the anti-FDC-M1 antibody 4C11 (Figure 6.2A). Expression of other FDC markers, including CD21/35 (Fig. 6.2A) or FDC-M2 (data not shown), did not differ between *Mfge8*$^{-/-}$ and WT mice.

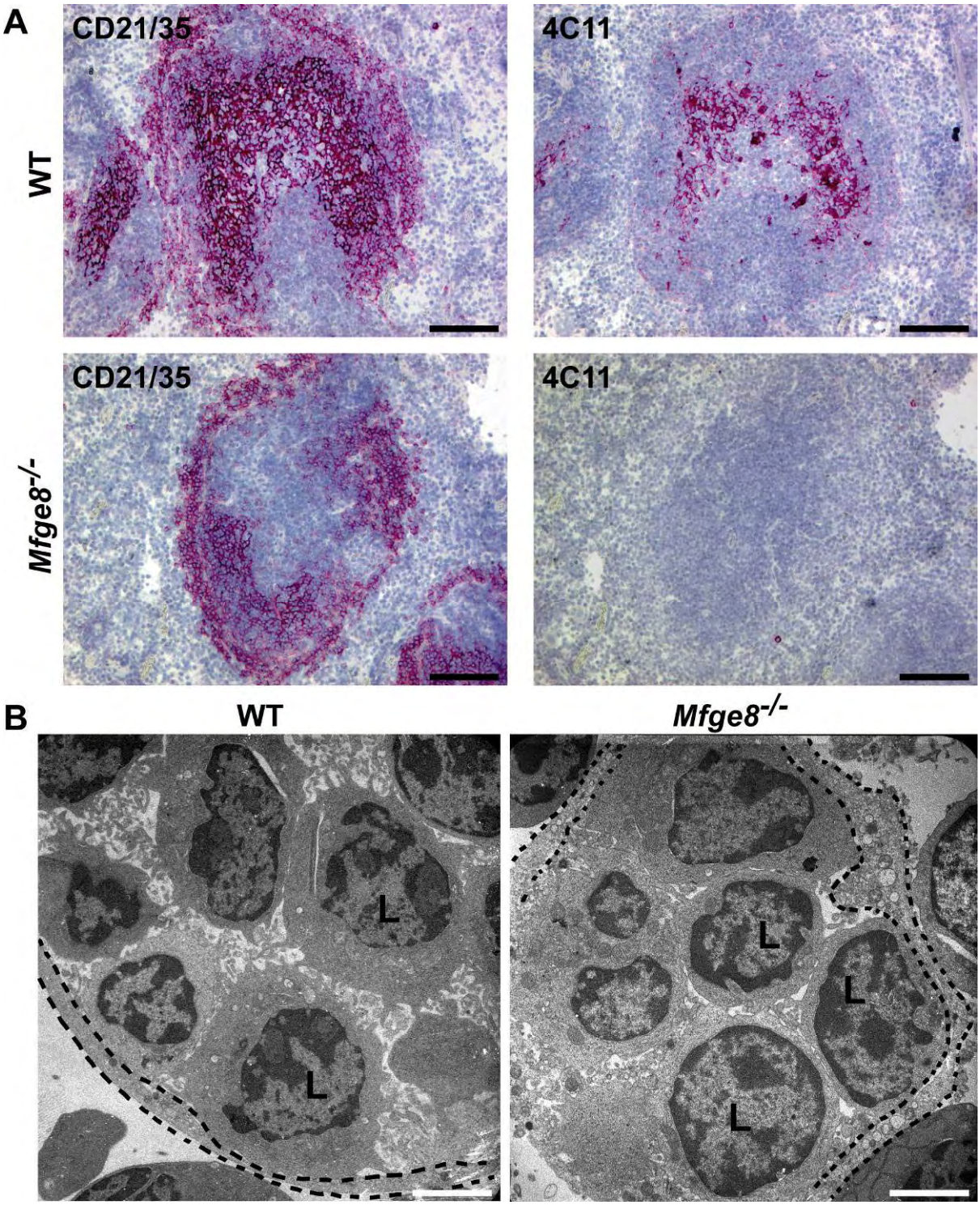

Figure 6.2 FDCs are present in *Mfge8*$^{-/-}$ mice but do not express FDC-M1.
(A) IHC of spleens from WT and *Mfge8*$^{-/-}$ mice were analyzed for CD21/35 and FDC-M1 expression by light microscopy. FDC-M1^{+} networks are absent in *Mfge8*$^{-/-}$ mice. Scale bar: 100 μm. **(B)** EM of isolated FDC-enriched clusters showing an FDC (dotted line) surrounding lymphocytes (L). There are no obvious morphological differences between FDC-lymphocytes aggregates from WT and *Mfge8*$^{-/-}$ mice. Scale bar: 2.90 μm

This lack of 4C11 immunoreactivity in *Mfge8*$^{-/-}$ spleens could result either from absence of mature FDCs, or from FDC-M1 antigen in FDCs. Therefore, FDC-enriched clusters of WT and *Mfge8*$^{-/-}$ mice were analyzed by EM. FDC clusters were identified as multicellular aggregates with FDCs encircling lymphocytes by long dendritic cytoplasmic extensions. WT and *Mfge8*$^{-/-}$ FDCs were ultrastructurally indistinguishable in isolated FDC-enriched clusters (Fig. 6.2B). Therefore, Mfge8 ablation abrogates 4C11 immunoreactivity but does not eliminate mature FDCs, either because Mfge8 and FDC-M1 are identical, or because Mfge8 is involved in the regulation of FDC-M1 expression.

6.1.2 Mammary epithelial cells express FDC-M1

If FDC-M1 and Mfge8 are the same antigen, then FDC-M1 immunoreactivity might be expected in all tissues known to express *Mfge8*, including the mammary gland which upregulates *Mfge8* expression after weaning (Nakatani et al., 2006). Mfge8 is localized on the membrane of mammary epithelial cells and in the alveolar lumen where milk fat globules accumulate (Nakatani et al., 2006). Hence, mammary glands of lactating WT or *Mfge8*$^{-/-}$ mice were examined by IF with 4C11 or the anti-Mfge8 antibody 18A2-G10 (Miyasaka et al., 2004). Membranes of mammary epithelial cells were 4C11^{+} and showed a high degree of colocalization with Mfge8 (Fig. 6.3A). Importantly, 4C11 immunoreactivity was absent in *Mfge8*$^{-/-}$ mammary glands.

6.1.3 4C11 immunolabeling of spleen and mammary gland is blocked by recombinant Mfge8

To investigate whether the staining of FDC-M1 and Mfge8 can be abrogated by pre-incubation of antibodies with recombinant Mfge8 (rMfge8), 18A2-G10 and 4C11 were pre-incubated with an excess of rMfge8 before applying them to mammary-gland cryosections obtained from lactating WT mice (Fig. 6.3B). Pre-incubation with rMfge8, but not with rEGF (epidermal growth factor), completely abolished staining of both 18A2-G10 and 4C11. The results of this competition assay provided evidence that the FDC-M1 antigen is Mfge8.

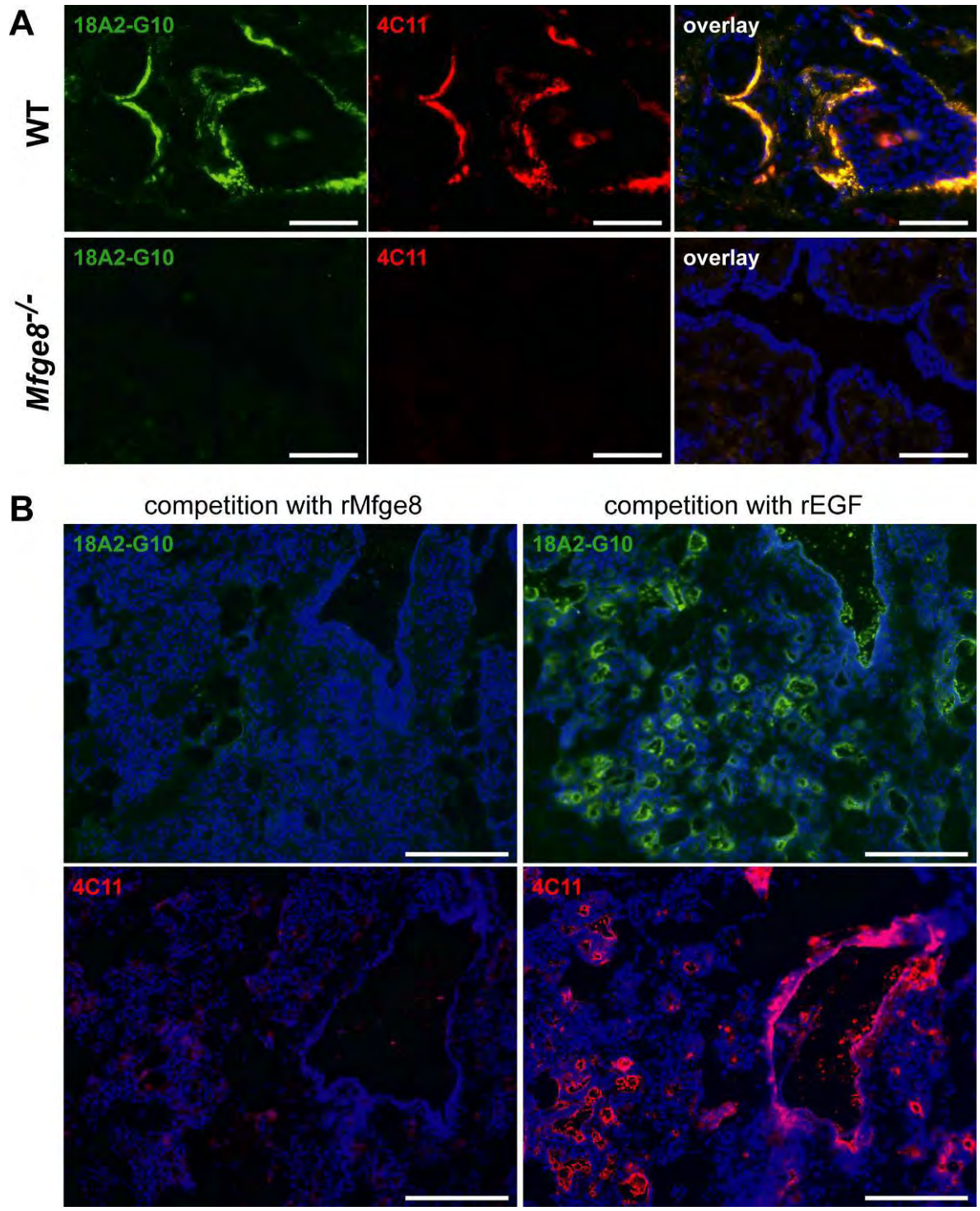

Figure 6.3 Mammary epithelial cells express FDC-M1.
(A) Cryosections of involuting mammary glands from lactating WT and *Mfge8*$^{-/-}$ mice were analyzed for Mfge8 and FDC-M1 expression by IF. Two-color stains of WT mammary glands with 18A2-G10 (green) and 4C11 (red) were performed. Immunoreactivity for both antibodies was observed on the membrane of mammary epithelial cells and within the alveolar lumen. The overlay shows high degree of colocalization. Scale bar: 50 μm. **(B)** Pre-incubation of 18A2-G10 or 4C11 with 25 μg/ml rMfge8, but not rEGF, blocked the staining. Scale bar: 200 μm.

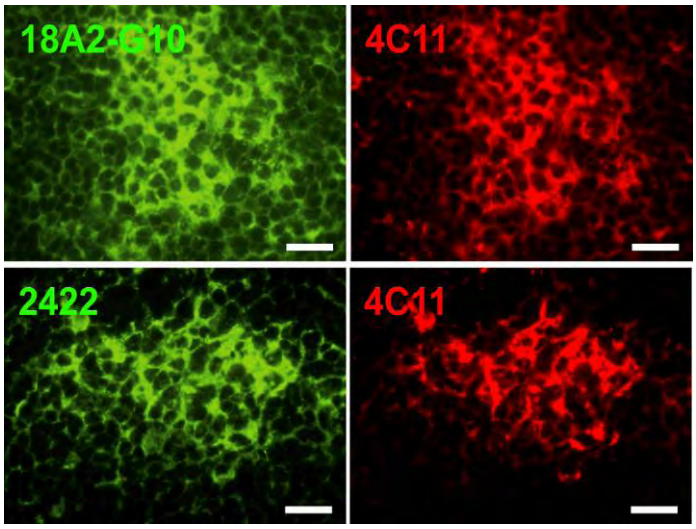

Figure 6.4 FDC-M1 and Mfge8 show a high degree of colocalization.
Spleens from WT mice were analyzed by IF. The upper panel shows double-staining of the same section with either 18A2-G10 (green) and 4C11 (red) and the lower panel double-staining with 2422 (green) and 4C11 (red). Both anti-Mfge8 antibodies show a high degree of colocalization with 4C11.

Next, immunofluorescent analysis of Mfge8 expression in the spleen was performed. Two-color labeling of splenic cryosections revealed a very high degree of colocalization between 4C11 and anti-Mfge8 antibodies (18A2-G10 or 2422) (Hanayama et al., 2004b) on FDCs (Fig. 6.4).

To assess whether rMfge8 would compete with 4C11 in spleen 18A2-G10 or 4C11 antibodies were pre-incubated with rMfge8. Only pre-incubation with rMfge8, but not

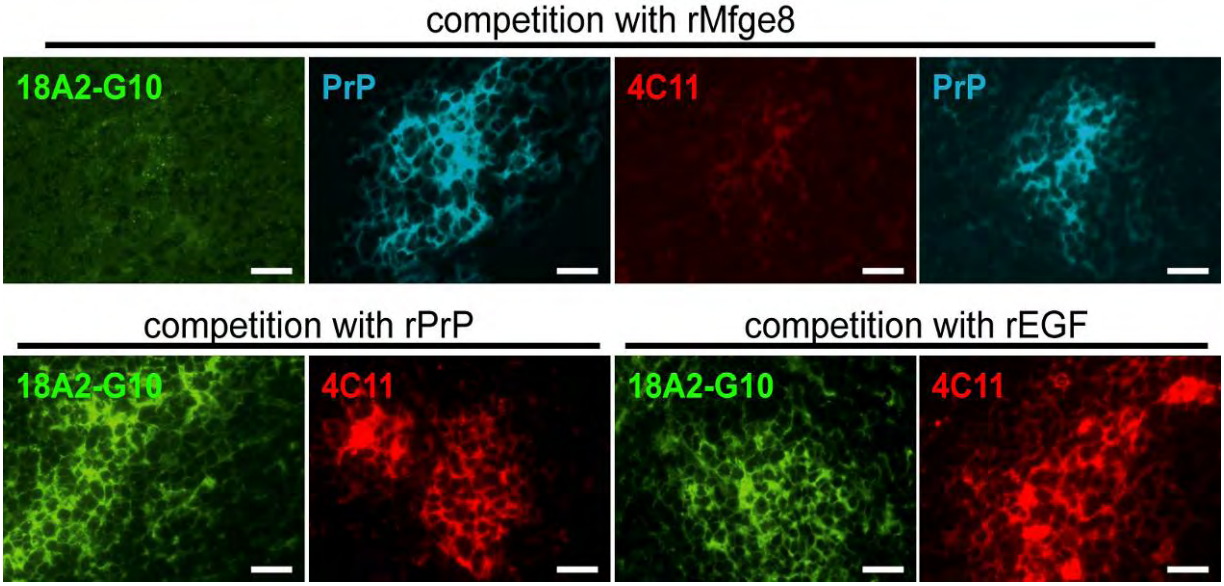

Figure 6.5 rMfge8 competes with 4C11 for binding to FDCs.
Pre-incubation of 18A2-G10 or 4C11 with 25 μg/ml rMfge8 blocks the staining of FDCs by these antibodies. To visualize FDCs, sections were stained with the anti-PrP antibody POM2 directly conjugated to Cy5. When 18A2-G10 antibody and 4C11 were pre-incubated with rEGF or rPrP, the staining of FDCs was not affected. Scale bar: 100 μm.

with rPrP (which was chosen, because PrP is a protein also abundantly present on FDCs) or rEGF (which was chosen because Mfge8 contains an EGF domain), significantly reduced their ability to stain splenic FDCs (Fig. 6.5), providing further

evidence that Mfge8 is the FDC-M1 antigen. Since rMfge8 binds to PS (Hanayama et al., 2002), the observed increase in background signal may be a result of binding of rMfge8-antibody immunocomplexes to PS globally exposed on membranes.

PrP^C is abundantly expressed on FDCs (McBride et al., 1992) and was therefore used to visualize the presence of FDCs. In contrast to FDC-M1, pre-incubation of FDC-M2 with rMfge8 did not impair the immunolabeling of FDCs (data not shown). Although binding of 4C11 to FDCs was abolished by competitive pre-incubation with rMfge8, its affinity may be lower than that of 18A2-G10, since 10 μg/ml rMfge8 only partially inhibited the FDC staining by 4C11 yet completely inhibited that of 18A2-G10 (data not shown).

6.1.4 The anti-Mfge8 antibody 2422 and 4C11 compete for binding to FDCs

When spleen sections were pre-incubated with anti-Mfge8 antibody 2422 and then stained with fluorescently labeled 4C11, the 4C11 signal was completely abolished (Fig. 6.6, upper panel). Conversely, after pre-incubation of the sections with an excess of 4C11, FDC staining by 2422 was reduced (Fig. 6.6, middle panel). When both antibodies were applied simultaneously onto the section, both antibodies

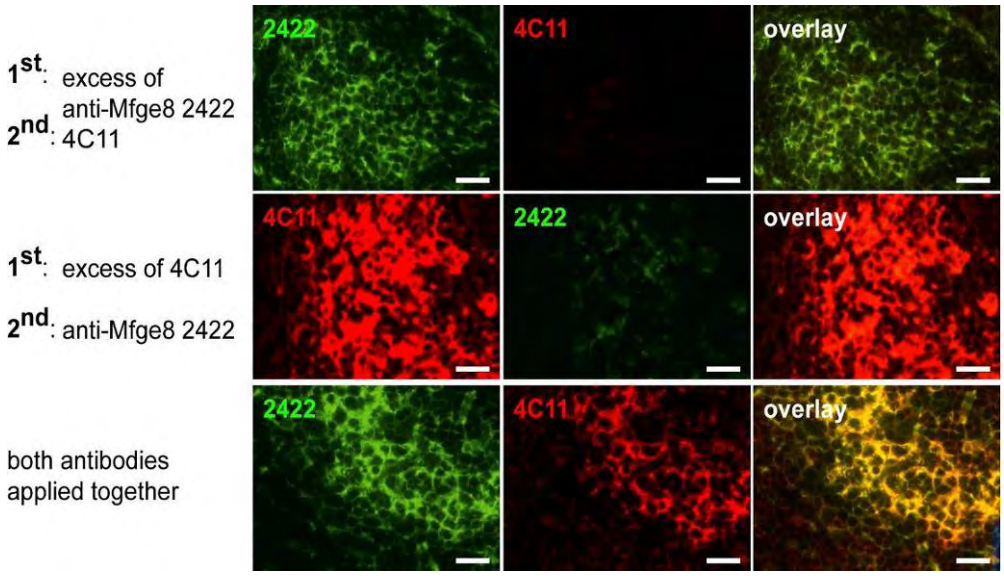

Figure 6.6 rMfge8 competes with FDC-M1 for the binding to FDCs.
Spleen-cryosections were first stained with 2422 (green). When after washing sections were incubated with 4C11 (red) no binding was observed (upper panel). When an excess of 4C11 was applied before 2422, binding of the latter was abolished (middle panel). When the two antibodies were applied onto the sections concomitantly, both antibodies were able to stain FDCs (lower panel). Scale bar: 20 μm.

recognized FDCs (Fig. 6.6, lower panel). This observation indicates that the antibodies 2422 and 4C11 compete with each other for Mfge8, possibly because they recognize the same epitope, or sterically incompatible epitopes.

6.1.5 The anti-Mfge8 antibody 2422 and FDC-M1 compete for binding to rMfge8

The molecular details of the competition between 2422 and 4C11 for rMfge8 were analyzed by surface plasmon resonance (SPR). First, 4C11, or rat IgG2c isotype control antibody were covalently immobilized on the sample and control flow cell of a sensor chip surface, respectively. Then recombinant proteins (rEGF, rPrP, rMfge8, 50 µg/ml each) were injected into both flow cells, and association and dissociation sensograms for each recombinant protein were recorded after subtraction of the respective interactions with the isotype control-coupled surface. No deviation from the baseline was observed after injection of rEGF or rPrP (indicated by black arrows) on the 4C11-coated chip (Fig. 6.7, panels A and B), indicating that no interaction occurred between these proteins and the coated 4C11 antibody. Conversely, injection of rMfge8 resulted in a rapid increase of resonance units (RU) in the 4C11-coated flow cell during the injection phase, suggesting specific interactions.

To test whether the association could be confirmed in a reverse orientation (interaction of 4C11 with a rMfge8-coated surface), rMfge8, or rPrP for control, were covalently conjugated to two continuous flow cells (data not shown). In four subsequent injections an interaction of 4C11 with the immobilized rMfge8 was observed, as evidenced by an increase in RUs (Fig. 6.7, panel C). No RU increase was observed between the third and the fourth 4C11 injection, indicating that binding of 4C11 to rMfge8 had reached saturation. When 2422 was subsequently injected onto the chip, binding was minimal (Fig. 6.7, panel C, arrow “2422”). 18A2-G10 was then injected, and resulted in a strong RU increase, indicating an interaction with the rMfge8-coated flow cell (Fig. 6.7 panel C, arrow). As expected, rat IgG2c did not bind to immobilized rMfge8 (data not shown).

After regenerating the chip with 100 mM HCl, the antibodies were re-injected on the rPrP- and rMfge8-coated flow cells in a different order. 2422 was injected first in two consecutive injections, allowing saturation of rMfge8 binding (Fig. 6.7 panel D). When 4C11 was then injected onto the 2422-covered flow cell, it did not bind to rMfge8 (Fig. 6.7 panel D, 4C11-indicated injection). In contrast, 18A2-G10 always bound to rMfge8 regardless of any previously bound 2422 or 4C11 (Fig. 6.7 panel C and D). Hence, the 18A2-G10 epitope is distinct from those of the other two antibodies. Along

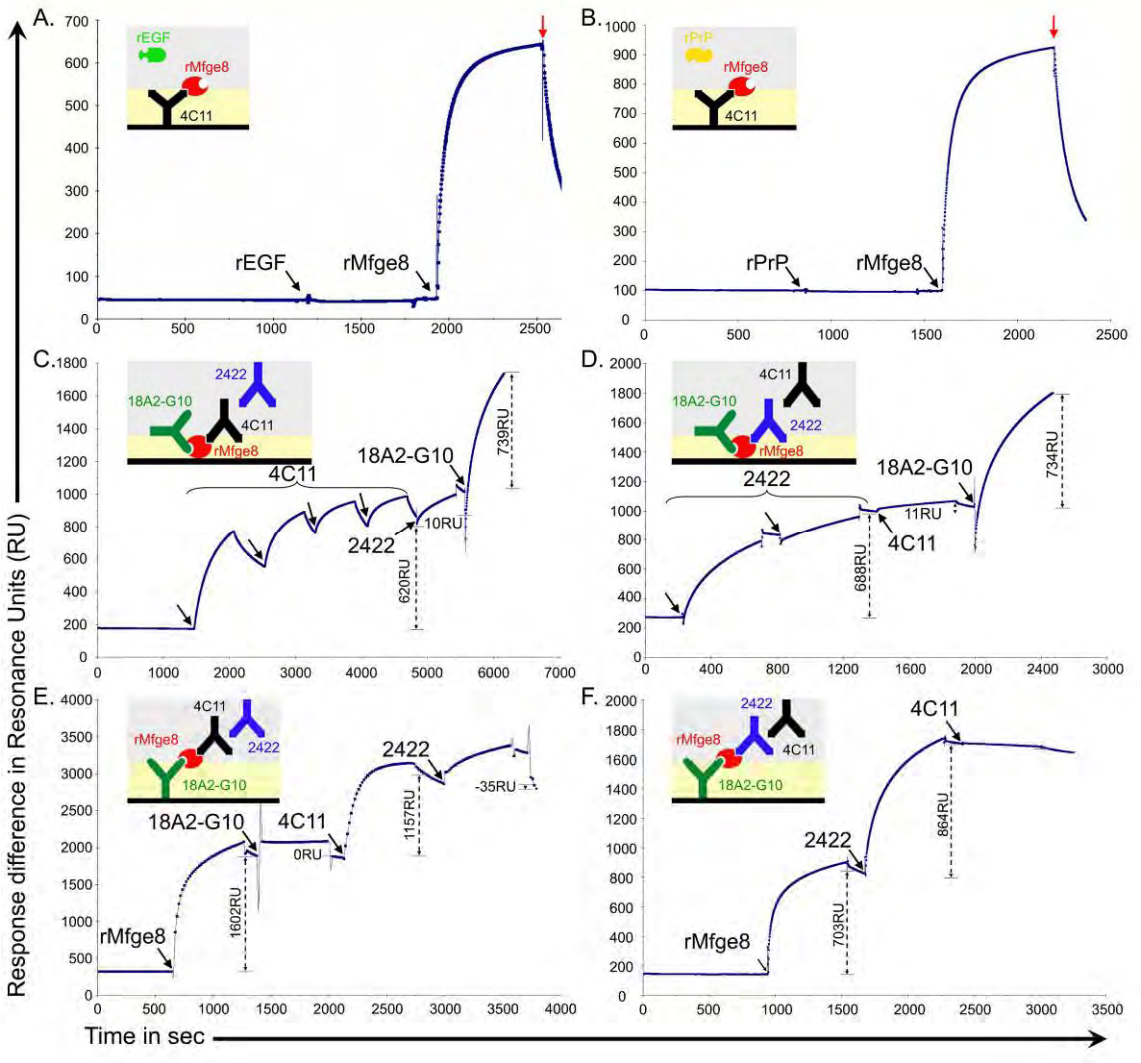

Figure 6.7 Anti-Mfge8 antibody 2422 competes with FDC-M1 for binding to rMfge8 in SPR experiments.
In panels (A) and (B) sensograms show binding of rMfge8, but not rEGF or rPrP respectively, to immobilized 4C11, covalently bound on CM5 Biacore chip. Red arrows indicate the end of rMfge8 injection. In panels (C) and (D) rMfge8 and rPrP (as negative control) were covalently coupled to sample and control flow cell, respectively. (C) In four subsequent injections, 4C11 bound to immobilized rMfge8 until an apparent saturation level. 2422 was subsequently injected on the rMfge8-covered surface, resulting in minor increase in resonance units (RUs). The following injection of 18A2-G10 shows a strong interaction with rMfge8. (D) After regeneration with 100mM HCl (not shown), 2422 was injected onto the chip showing a strong interaction in two successive injections. Subsequent injection of 4C11 resulted in minimal binding to rMfge8. In contrast, 18A2-G10's binding to rMfge8 was not affected by previous injections. (E) 18A2-G10 was covalently bound to the chip surface and was able to capture rMfge8. When 18A2-G10 was then injected, no binding was observed, since all of its epitopes on rMfge8 are occupied by the immobilized moiety. In contrast, 4C11 could efficiently bind to the rMfge8 captured surface. Next, 2422 was injected onto the chip, but showed no binding to rMfge8, due to a competition effect of 4C11. (F) After regeneration (not shown), and capture of rMfge8 on the chip surface, 2422 was injected, this time showing a strong interaction. 4C11, which was injected next did no longer bind to Mfge8.
For control, injections of all proteins were made on two flow cells, where the first flow cell was coated with control protein or antibody and the second with the protein/antibody of interest. Sensograms show binding of each recombinant protein/antibody after subtraction of their binding to control antibody/protein-coupled surface. Black arrows indicate the beginning of the indicated injection. Inserts are schematic representations of binding and competition events of the sensogram in the respective panel.

with the immunofluorescent competition experiments (Fig. 6.6), these results indicate that 4C11 and 2422 abrogate each other's binding to Mfge8. Thus, 4C11 and 2422 share a common or overlapping epitope, or recognize Mfge8 epitopes which sterically hinder each other.

Further evidence for this hypothesis came from the next setup, where 18A2-G10 was immobilized on a new flow cell. rMfge8 readily bound to the non-competing antibody. A third injection was performed with one of the three antibodies 18A2-G10, 2422, and 4C11 in a sandwich-like design. Under these conditions, injected 18A2-G10 did not bind to the surface decorated with 18A2-G10-captured rMfge8, confirming that 18A2-G10 binds to a single non-repeating epitope on Mfge8 (Fig. 6.7 panel E). Subsequent injection of 4C11 resulted in a strong interaction with captured rMfge8. When 2422 was injected, no binding occurred. Then the order of injection was reversed. After capturing of rMfge8 by immobilized 18A2-G10, 2422 was injected first, followed by injection of 4C11. In this case, the first antibody 2422 interacted with 18A2-G10-captured rMfge8, but not 4C11 due to competition with the former antibody (Fig. 6.7, panel F).

6.1.6 The antibody 4C11 immunoprecipitates Mfge8

2422 has been previously reported to be able to immunoprecipitate Mfge8 (Hanayama et al., 2002). In order to assess whether 4C11 immunoprecipitates Mfge8, 4C11, 2422, or rat IgG2c isotype control antibodies were conjugated to tosylactivated paramagnetic beads. These were then exposed to protein extracts of WT or *Mfge8*$^{-/-}$ spleens. Precipitated proteins were analyzed by Western blotting with anti-Mfge8 antibody 18A2-G10. Following immunoprecipitation with 2422-coated beads, two Mfge8-specific bands were detected with molecular weights of approximately 45 and 55 kDa (Fig. 6.8). In the immunoprecipitates derived using 4C11 beads, two Mfge8-specific signals were obtained with molecular weights matching those of the 2422-immunoprecipitation (Fig. 6.8). These signals were absent in spleens from *Mfge8*$^{-/-}$ mice, confirming the specificity and identity of bands observed in immunoprecipitates from WT protein extracts.

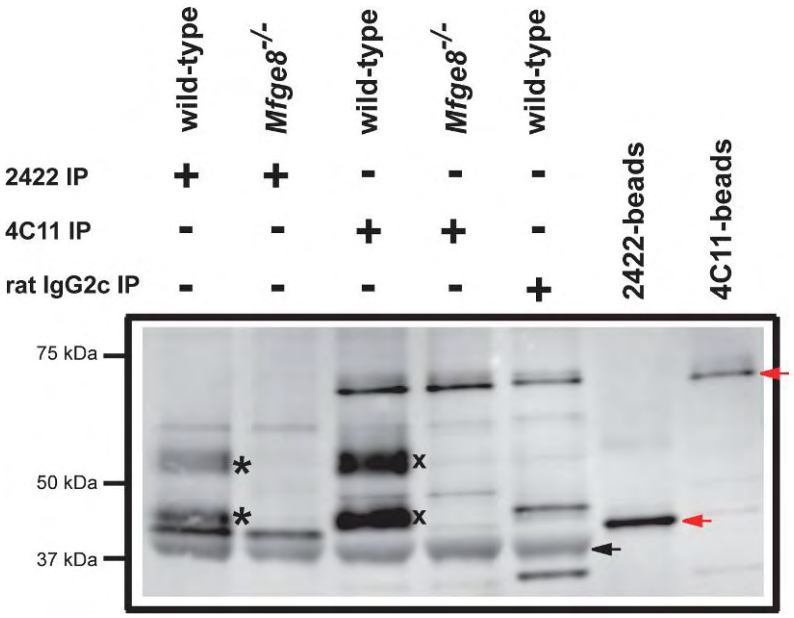

Figure 6.8 FDC-M1 immunoprecipitates Mfge8 from mouse spleen homogenates.
Splenic protein extracts from WT and *Mfge8*$^{-/-}$ mice were immunoprecipitated with paramagnetic beads conjugated to anti-Mfge8 antibody 2422, 4C11 or to a rat IgG2c isotype control antibody. Beads coupled with 2422 or 4C11, but not exposed to splenic protein extracts were included as controls. The Western blot was probed with anti-Mfge8 antibody 18A2-G10. In WT, but not in *Mfge8*$^{-/-}$ samples immunoprecipitated with either 2422 or 4C11, two Mfge8-specific signals were visible (marked with * and x). Additional non-Mfge8-specific bands possibly representing hamster and rat immunoglobulin fragments (red arrows), and a 37 kDa band of unknown identity (black arrow), reacted with the secondary antibody only (data not shown).

6.2 FDCs and not TBMϕs are the major source of Mfge8 in the spleen

6.2.1 Analysis of Mfge8 expression in BM chimeric mice

In contrast to the above findings, it has previously been reported that within splenic follicles Mfge8 is exclusively produced by TBMϕs (Hanayama et al., 2004b). To address this discrepancy, and to investigate whether Mfge8 might be secreted by TBMϕs and trapped by FDCs or vice versa, reciprocal BM chimeras between *Mfge8*$^{-/-}$ and WT mice were used. FDCs are stromal and radiation resistant (Kapasi et al., 1998), whereas TBMϕs are mononuclear phagocytes of hematopoietic origin and are thought to be radiation sensitive (Flemming, 1885, Humphrey et al., 1984), therefore, analysis of these BM-chimeric mice should enable to determine the origin of Mfge8 in lymphoid organs. To provide an independent marker of histogenesis, lethally irradiated *Mfge8*$^{-/-}$ mice expressing the CD45.2 allele were reconstituted with BM from CD45.1 congenic WT mice, and vice versa (Fig. 6.9).

In case both cell types express Mfge8, then WT mice reconstituted with *Mfge8*$^{-/-}$ BM (*Mfge8*$^{-/-}$→WT) should only show *Mfge8* expression by FDCs, while the hematopoietic TBMϕs are expected to lack *Mfge8* expression. In the reverse situation (WT→*Mfge8*$^{-/-}$) only the BM derived TBMϕs should express *Mfge8*, but not the stromal FDCs (Fig. 6.9).

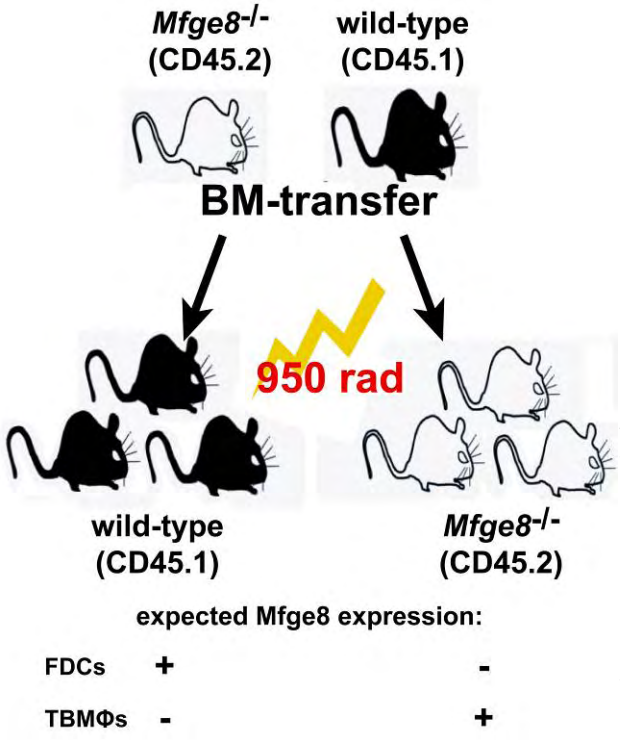

Figure 6.9 Scheme of BM-reconstitutions.
BM of *Mfge8*$^{-/-}$ or CD45.1 congenic WT donors was isolated and injected into lethally irradiated WT (*Mfge8*$^{-/-}$→WT) or *Mfge8*$^{-/-}$ (WT→*Mfge8*$^{-/-}$) hosts, respectively. WT→WT and *Mfge8*$^{-/-}$→*Mfge8*$^{-/-}$ chimeras served as controls.
In case both cell types express Mfge8, following phenotype was expected:
In *Mfge8*$^{-/-}$→WT mice only FDCs, but no TBMϕs are expected to express *Mfge8* and in WT→*Mfge8*$^{-/-}$ mice only TBMϕs, but not FDCs should express *Mfge8.*

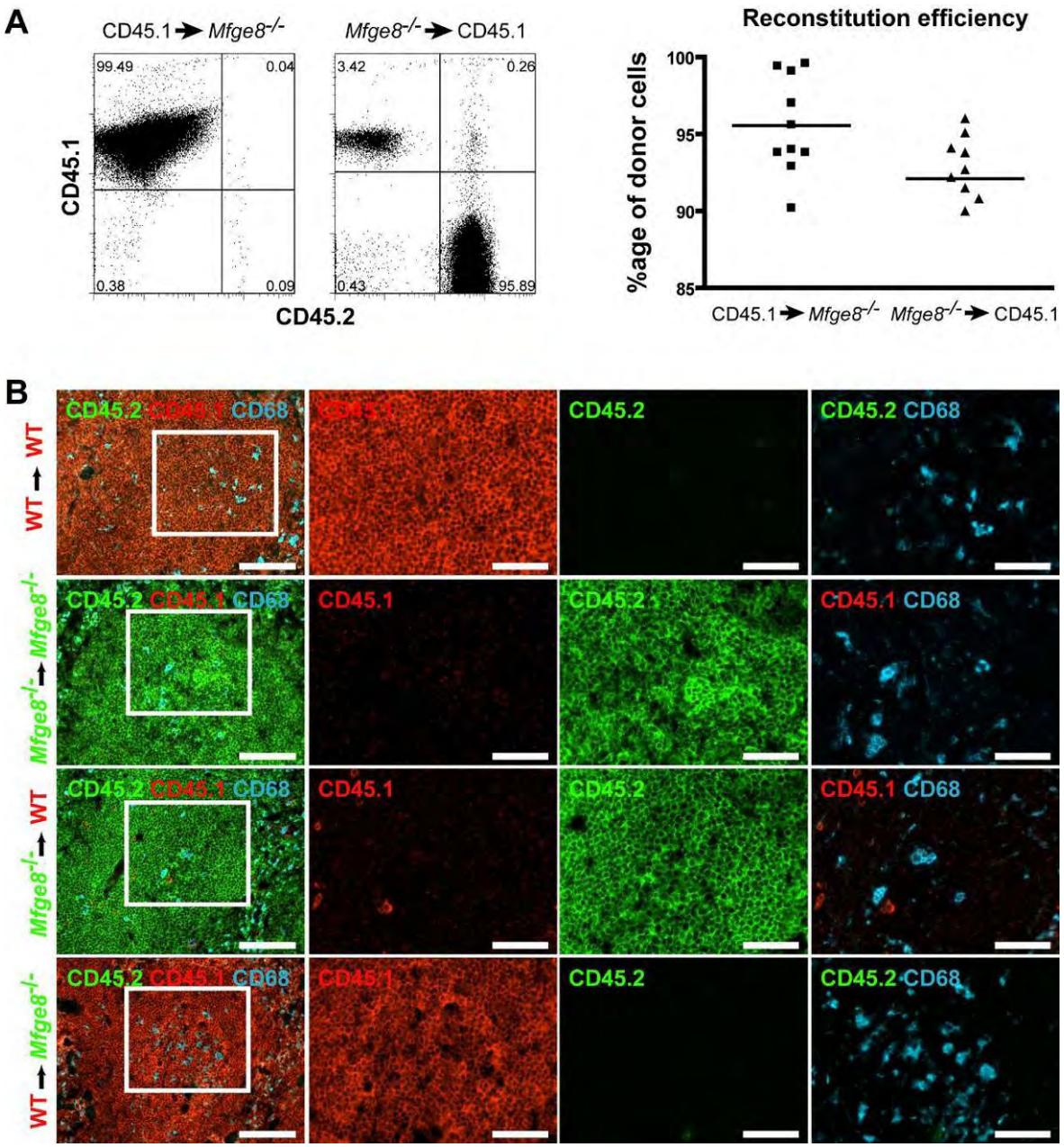

Figure 6.10 Assessment of reconstitution efficiency.
(A) Efficiency of the BM-transfer was assessed by FACS-analysis on peripheral blood collected five weeks after BM-transfer. Cells were stained with antibodies against CD45.1 and CD45.2. Dot plots show the frequency of $CD45.1^+$ and $CD45.2^+$ cells. Percentage of cells within the different quadrants is given in each quadrant. Dot plots shown are representative for ten CD45.1→*Mfge8*$^{-/-}$ and nine *Mfge8*$^{-/-}$→CD45.1 mice. Reconstitution efficiency for all reconstituted mice is shown as percentage of donor cells. Average efficiency for CD45.1→*Mfge8*$^{-/-}$ was 95.5% ± 3.2% and for *Mfge8*$^{-/-}$→CD45.1 92.1% ± 3.2%. Values are given as mean ± SD.
(B) Spleen-cryosections were subjected to three-color immunolabeling with antibodies against CD45.2 (green), CD45.1 (red) and CD68 (cyan). Specificity and background levels of the CD45.2 and CD45.1 immunostains were determined on WT→WT and *Mfge8*$^{-/-}$→*Mfge8*$^{-/-}$ spleen sections (panel 1 and 2). $CD68^+$ TBMϕs did not colocalize with the few observed host-derived $CD45.1^+$ (*Mfge8*$^{-/-}$→WT) or $CD45.2^+$ (WT→*Mfge8*$^{-/-}$) cells. White squares outline the area shown in higher magnification. Scale bar column 1: 100 μm, column 2-5: 20 μm**.**

Five weeks after reconstitution the average efficiency was 93.8±3.6% as assessed by flow-cytometric analysis of CD45.1^{+} and CD45.2^{+} cells in peripheral blood confirming a successful reconstitution (Fig. 6.10A). The donor origin of TBMϕs was confirmed by multi-color IF using antibodies against CD45.1, CD45.2 and CD68 to rule out the possibility that they had survived the lethal irradiation (Fig. 6.10B). The specificity of the CD45.1 and CD45.2 antibodies was determined by staining *Mfge8*$^{-/-}$→*Mfge8*$^{-/-}$ (all CD45.2^{+}) and WT→WT (all CD45.1^{+}) spleens with anti-CD45.1 (red) and anti-CD45.2 (green) antibodies, respectively. No cross-reactivity was observed (Fig. 6.10B, 1st and 2nd panel). Two-color immunolabeling of *Mfge8*$^{-/-}$→WT spleens with anti-CD68 (cyan) and the host-cell marker CD45.1 (red) confirmed that TBMϕs were not host-derived (Fig. 6.10B 3rd panel). Consequently, TBMϕs of WT→*Mfge8*$^{-/-}$ spleens did not express the host-cell marker CD45.2 (Fig. 6.10B 4th panel). Therefore, in all chimeras TBMϕs originated from donor BM and were not of host origin, although occasionally few host-derived cells were present in some follicles.

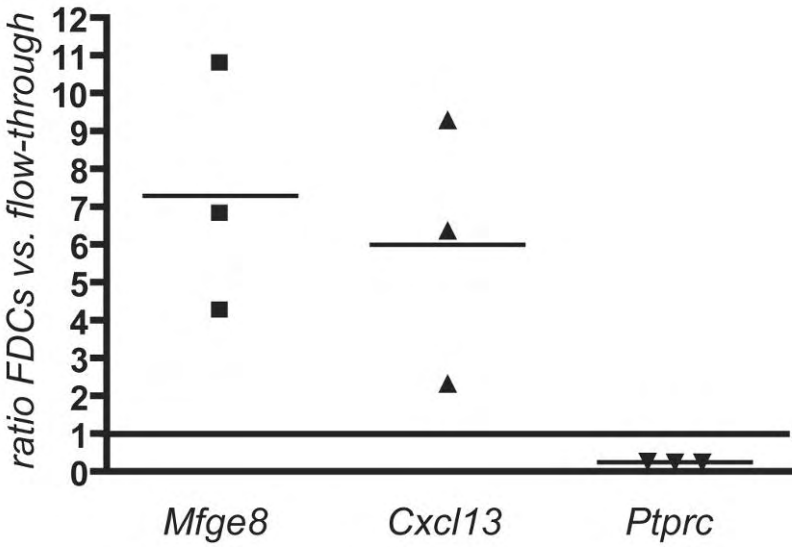

Figure 6.11 Quantitative PCR expression analysis of *Ptprc* in FDC-enriched cell clusters.
FDC-enriched clusters were co-isolated with GC B cells by MACS-sorting using biotinylated 4C11 antibody and anti-biotin magnetic beads. After RNA isolation cDNA of the FDC-enriched and the flow-through fraction was synthesized. *Mfge8*, *Cxcl13* and *Ptprc* expression levels in cell-fractions of three independent isolations (using lymph nodes of 5 mice per isolation) were determined by quantitative RT-PCR (qPCR). Expression levels are shown as ratio of FDCs vs. flow-through. Mfge8 expression in FDCs was increased 7.3 ± 2.7 fold, *Cxcl13* expression was increased 6.0 ± 2.9 fold and *Ptprc* levels were reduced 4.1 ± 0.2 fold as compared to the flow-through fraction. Values are given as mean ± SD.

Early analyses of BM chimeras were taken to suggest a hematopoietic derivation of FDCs (Kapasi et al., 1998), but most evidence favors a stromal origin (Groscurth, 1980, Dijkstra et al., 1984, Humphrey et al., 1984, Yoshida et al., 1995). Therefore, FDCs may not express CD45, which is a strictly hematopoietic marker (Ledbetter and Herzenberg, 1979). This may be the reason why FDCs failed to show expression of the host CD45 allele in these BM chimeras. To support this idea, FDC-enriched versus FDC-depleted fractions were analayzed after MACS-sorting of FDCs as described previously (Sukumar et al., 2006). Expression of *Ptprc* (the gene encoding for CD45) was markedly reduced in the FDC-enriched fraction, whereas FDC-specific genes like *Mfge8* and *Cxcl13* were increased (Fig. 6.11). The residual CD45 expression probably resulted from B cells that were co-isolated with the FDC-clusters. These results support the hypothesis that FDCs do not express CD45 and explain why they were not identifiable as host-derived cells in CD45.1/CD45.2 immunolabelings.

Prior to the analysis, the BM-chimeric mice were immunized with ovalbumin (OVA) in alum six and eight weeks after reconstitution to induce GC formation. Nine weeks post reconstitution, splenic Mfge8 and CD68 expression was analyzed by IF of cryostat sections. Surprisingly, *Mfge8*$^{-/-}$ mice receiving WT BM (WT→*Mfge8*$^{-/-}$)

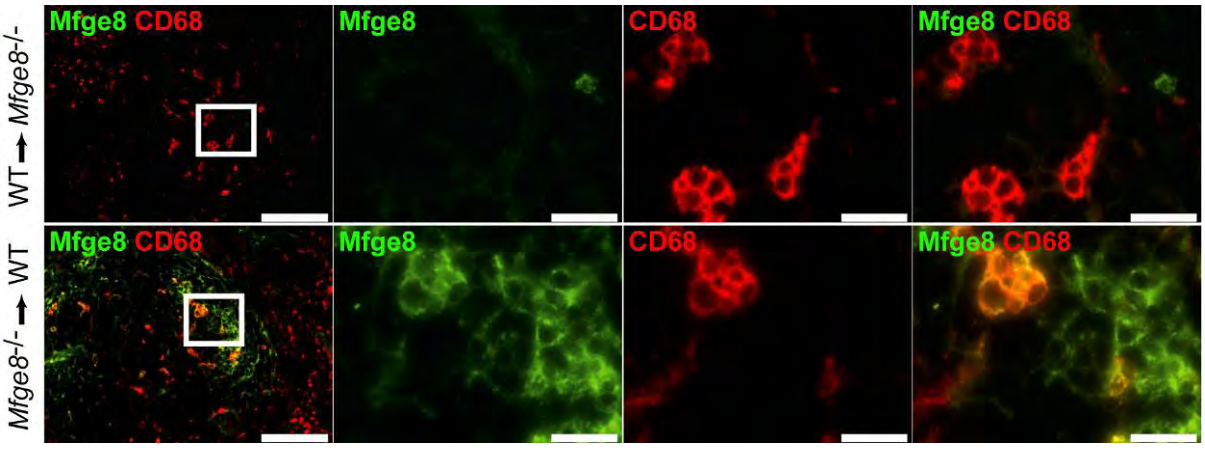

Figure 6.12. Analysis of splenic Mfge8 expression by IF.
Splenic cryosections from *Mfge8*$^{-/-}$ mice reconstituted with WT BM (upper panel) and from WT mice reconstituted with *Mfge8*$^{-/-}$ BM (lower panel) were immunostained with anti-Mfge8 antibodies (clone 2422, green) and anti-CD68 antibodies (red). Immunoreactivity of the Mfge8 antibody on FDCs and CD68^{+} TBMϕs was only observed when FDCs were of WT origin. Figures show areas inside follicles. White square marks the area shown in higher magnification. Scale bar: 20 μm.

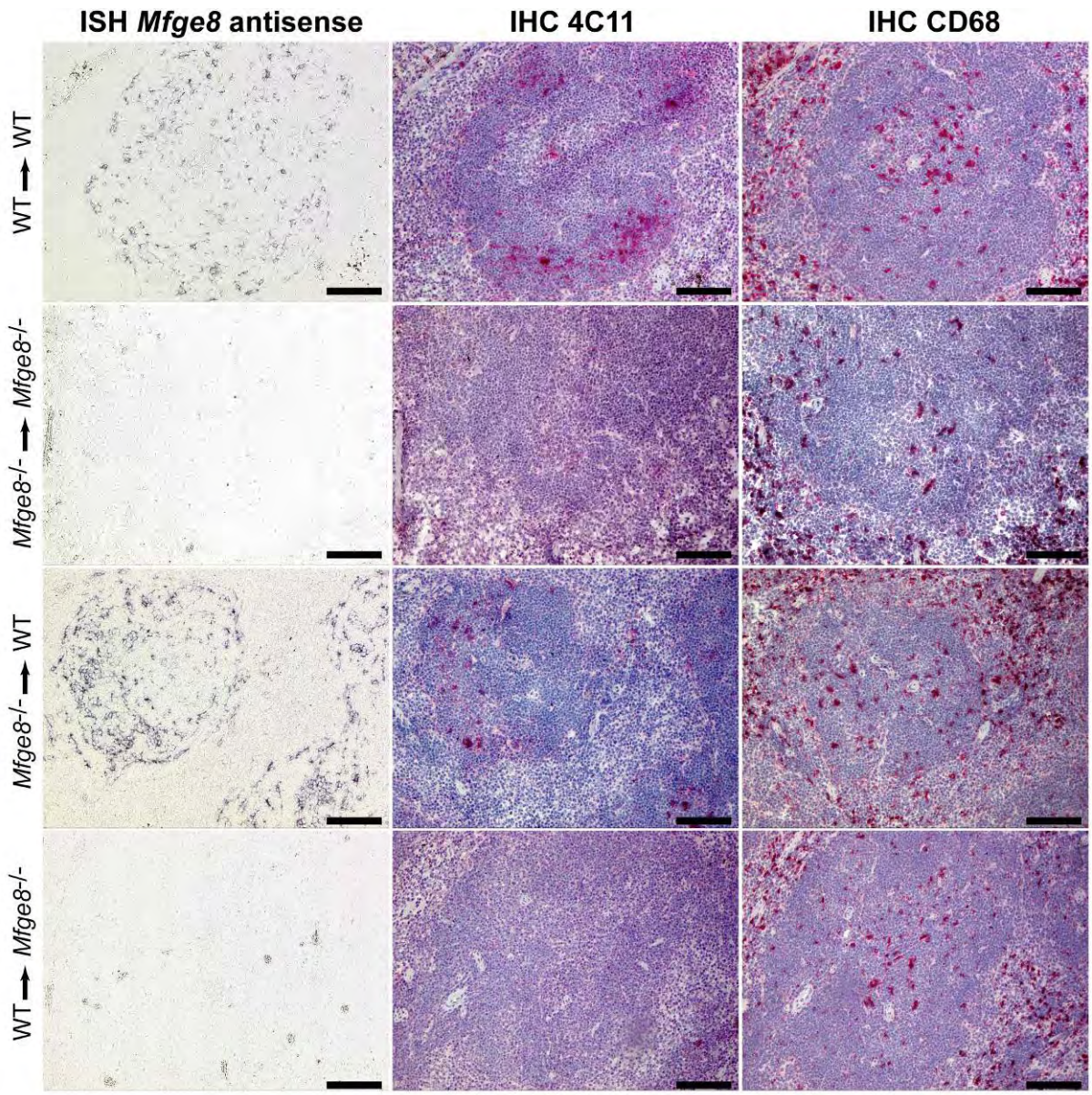

Figure 6.13. Analysis of splenic Mfge8 expression by ISH.
Splenic *Mfge8* expression was assessed using ISH (left column). Adjacent sections were immunolabeled with 4C11 (middle column) and anti-CD68 antibodies (right column). *Mfge8* expression and 4C11 immunostaining was only found in WT mice irrespective of the BM genotype (panel 1 and 3). *Mfge8*$^{-/-}$ mice that received BM from either *Mfge8*$^{-/-}$ mice or from WT mice showed no *Mfge8*-specific signal after ISH and no 4C11 immunostaining. Presence and localization of TBMϕs is shown by the CD68 immunostaining. Scale bar: 100 μm.

lacked all Mfge8 immunoreactivity in spleens. Not only radiation resistant FDCs, but also BM-derived CD68$^+$ TBMϕs were negative for Mfge8, although they had clearly originated from WT donors (Fig. 6.12 upper panel). In contrast, spleens of WT mice reconstituted with *Mfge8*$^{-/-}$ BM (*Mfge8*$^{-/-}$→WT) contained not only Mfge8$^+$ FDCs, but also Mfge8-immunostained TBMϕs originating from *Mfge8*$^{-/-}$ donors (Fig. 6.12 lower panel). In all samples, Mfge8$^+$ TBMϕs were visible whenever FDCs expressed Mfge8, yet were always Mfge8$^-$ whenever FDCs did not express Mfge8.

Next, the transcriptional pattern of splenic Mfge8 was determined by RNA ISH. In WT→WT mice, *Mfge8* transcription was restricted to follicles (Fig. 6.13, upper panel). The strongest expression was found in the GC, where FDCs reside. Some Mfge8$^+$ cells surrounded follicles. These cells were radiation resistant, and may represent immature FDC precursor cells, as proposed previously (Pasparakis et al., 2000). Overall, the ISH visualized more *Mfge8*$^+$ cells than the FDC-M1 IHC, probably due to the higher sensitivity of the riboprobe.

Adjacent sections were immunostained with 4C11 and anti-CD68 antibodies. However, both Mfge8 immunostains and *Mfge*8 ISH visualized characteristic FDC networks, confirming that Mfge8 is indeed produced by FDCs, rather than being secreted by other cell types and taken up by FDCs (Fig. 6.13 upper panel). No signal was detected after ISH on *Mfge8*$^{-/-}$→*Mfge8*$^{-/-}$ spleens, confirming the specificity of the *Mfge8 in situ* riboprobe (Fig. 6.13, 2nd panel).

The *Mfge8* expression pattern in *Mfge8*$^{-/-}$→WT chimeras was identical to that of WT mice (Fig. 6.13, 3rd panel). Conversely, *Mfge8* expression was completely absent from WT→ *Mfge8*$^{-/-}$ chimeras (Fig. 6.13 4th panel). These results indicate that only

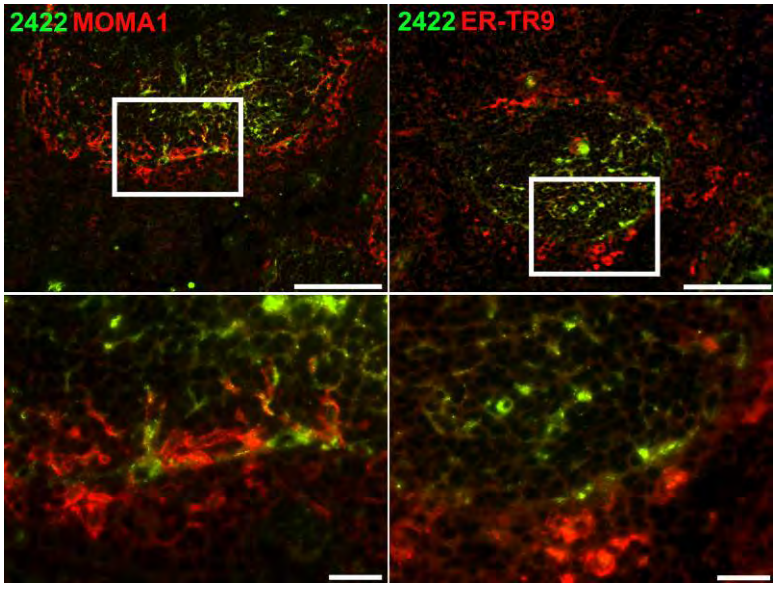

Figure 6.14. Mfge8$^+$ cells do not express MOMA1 or ER-TR9. Cryosections of WT spleens were immunostained with 2422 antibodies (green) and anti-MOMA1 (left panel) or anti-ER-TR9 antibodies (right panel). 2422$^+$ cells (green) residing at the border of the marginal zone were not positive for MOMA1 or ER-TR9 (both red). These cells are therefore neither MOMA1$^+$ metallophilic nor ER-TR9$^+$ marginal zone macrophages. White squares outline the area shown in higher magnification. Scale bar upper panel: 100 μm, lower panel: 20 μm.

radiation resistant cells, such as FDCs, but not radiation sensitive cells, such as TBMϕs, are the source of Mfge8 in the spleen.

To exclude that the Mfge8$^+$ cells encircling the follicle around the marginal zone are either ER-TR9$^+$ marginal zone macrophages or MOMA1$^+$ metallophilic macrophages dual-color IF was performed with anti-Mfge8 antibodies (green) together with either anti-ER-TR9 or anti-MOMA-1 antibodies (both red). Mfge8$^+$ cells in the marginal zone did not colocalize with ER-TR9$^+$ or with MOMA-1$^+$ macrophages and are therefore a different cell population (Fig. 6.14).

To deternibe whether in other lymphoid tissues *Mfge8* expression is also exclusively stromal, inguinal lymph nodes from BM-chimeric mice were analysed by ISH (Fig. 6.15). The results obtained from the lymph nodes coincided with the results observed in the spleen. All detectable *Mfge8* originated from stromal cells, since only in inguinal lymph nodes from *Mfge8*$^{-/-}$→WT an *Mfge8* specific signal was detected by ISH. In lymph nodes obtained from WT→ *Mfge8*$^{-/-}$ chimeras no *Mfge8* expression was found (Fig. 6.15)

To further corroborate the above findings, fluorescent ISH for *Mfge8* in combination with IF for CD68 was performed. This method allows to directly visualize whether CD68$^+$ TBMϕs contain *Mfge8* RNA. For this, splenic cryosection of previously immunized WT mice were prestained with a biotinylated anti-CD68 antibody before the same section was hybridized with the *Mfge8* riboprobe. Analyses of the follicles clearly showed that none of the observed CD68$^+$ cells contained

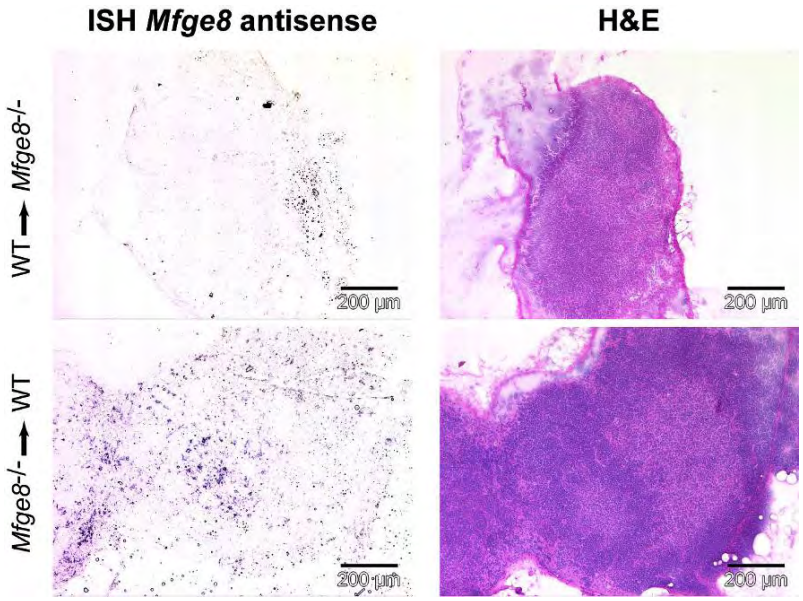

Figure 6.15. Analysis of Mfge8 expression in inguinal lymph nodes by ISH. *Mfge8* expression in inguinal lymph nodes from WT→*Mfge8*$^{-/-}$ and *Mfge8*$^{-/-}$→WT mice was assessed using ISH (left column). Adjacent sections were counterstained with H&E (right column). Mfge8 expression was only detectable when stromal cells were of WT origin. The observed background signal in the WT→*Mfge8*$^{-/-}$ lymph node orginates from co-isolated fat tissue and does not represent *Mfge8* RNA expression. Scale bar: 200 µm.

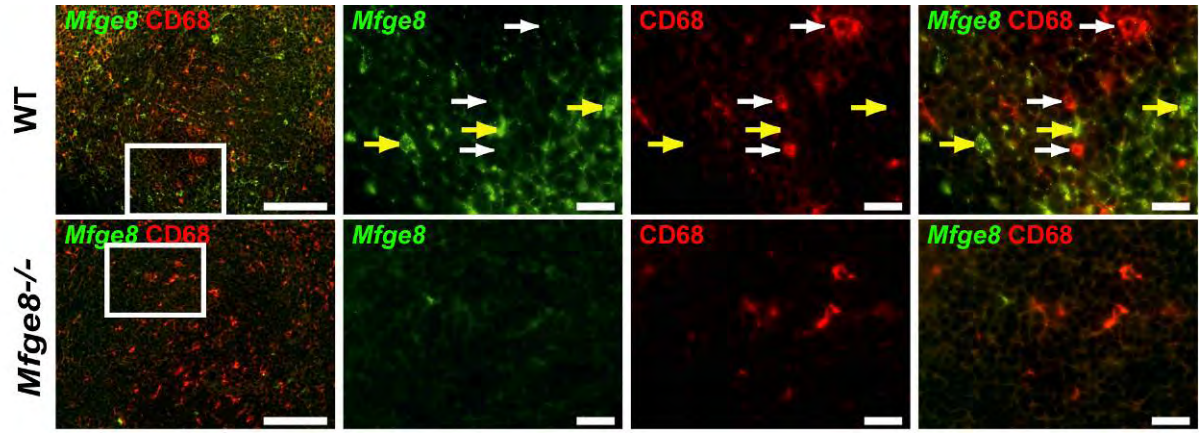

Figure 6.16 CD68$^+$ TBMϕs lack *Mfge8* RNA.
Cryosections from WT and *Mfge8*$^{-/-}$ spleens were first immunolabeled with biotinylated CD68 antibody (red) and then subsequently subjected to fluorescent ISH using an *Mfge8*-specific RNA probe (green). Yellow arrows indicate *Mfge8* positive cells; white arrows indicate CD68$^+$ cells. The green *Mfge8* RNA specific signal failed to colocalize with CD68$^+$ TBMϕs. White squares outline the area shown in higher magnification. Scale bar in 1st column is 100 μm and in columns 2-4, 20 μm.

Mfge8 RNA (Fig. 6.16, upper panel, white arrows). Consequently, non of the cells expressing *Mfge8* RNA were CD68$^+$ (Fig. 6.16, upper panel, yellow arrows). No *Mfge8* specific signals could be detected in the *Mfge8*$^{-/-}$ spleen confirming the specificity of the riboprobe (Fig. 6.16 lower panel).

To confirm the ISH results with a more sensitive method to exclude that TBMϕs express *Mfge8* at low levels, *Mfge8* expression in the chimeric mice was determined by RT-PCR on cDNA synthesized from RNA isolated from splenocytes. In WT→*Mfge8*$^{-/-}$ chimeric spleens *Mfge8* expression was below the detection limit of RT-PCR (<0.25% WT splenocyte RNA spiked into *Mfge8*$^{-/-}$ splenocyte RNA, data not shown), whereas *Mfge8*$^{-/-}$→WT spleens showed expression levels similar to WT→WT spleens (Fig. 6.17). Therefore, >99.75% of *Mfge8* mRNA in chimeric spleens originated from radiation resistant cells. Since RT-PCR is highly sensitive, these results strongly suggest that radiation resistant stromal cells are the only source of Mfge8 in the spleen.

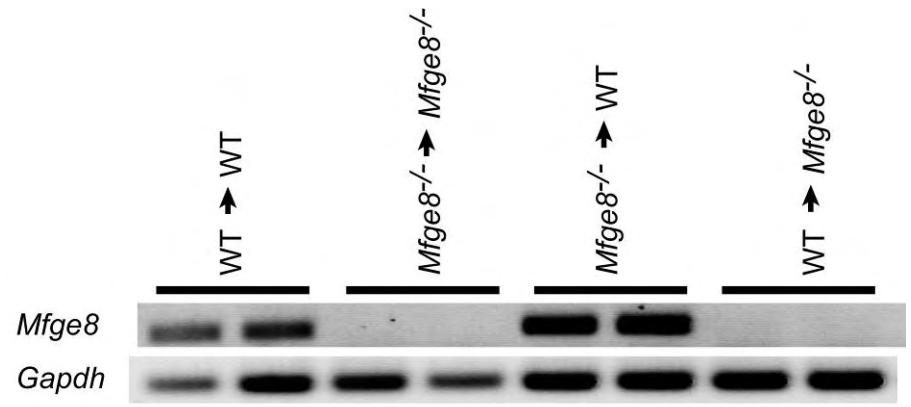

Figure 6.17 RT-PCR analysis of chimeric mice.
PCR (40 cycles) with *Mfge8*-specific primers was performed on cDNA from splenocytes from two different mice per group. In spleen *Mfge8* expression was only observed in WT mice that received either WT or *Mfge8*$^{-/-}$ BM. No *Mfge8* expression was found in *Mfge8*$^{-/-}$ mice that received WT BM or *Mfge8*$^{-/-}$ BM. Therefore only the stromal non-hematopoietic compartment showed *Mfge8* expression.

6.3 Does restriction of *Mfge8*-deficiency to FDCs suffice to impair phagocytosis and cause SLE?

6.3.1 Lack of Mfge8 expression by FDCs results in splenomegaly and increased binding of apoptotic cells by TBMϕs

Mfge8$^{-/-}$ mice have splenomegaly and exhibit a phagocytosis defect of TBMϕs and develop SLE resulting in glomerulonephritis (Hanayama et al., 2004b). To answer which of these phenotypes are caused by the lack of *Mfge8* expression by FDCs and/or other stromal cells, the different BM-chimeras where analyzed.

The splenomegaly in aged mice could clearly be ascribed to lack of *Mfge8* expression by stromal cells. Only *Mfge8*$^{-/-}$→*Mfge8*$^{-/-}$ and WT→*Mfge8*$^{-/-}$ mice with spleen weights of 125.7 mg ± 24.14 and 130.5 mg ± 16.44, respectively, developed splenomegaly. WT→WT and *Mfge8*$^{-/-}$→WT mice had normal spleen sizes with weights of 66.73 mg ± 5.22 and 67.9 mg ± 7.6, respectively. Therefore, hematopoietic Mfge8 did not influence the spleen size (Fig. 6.18).

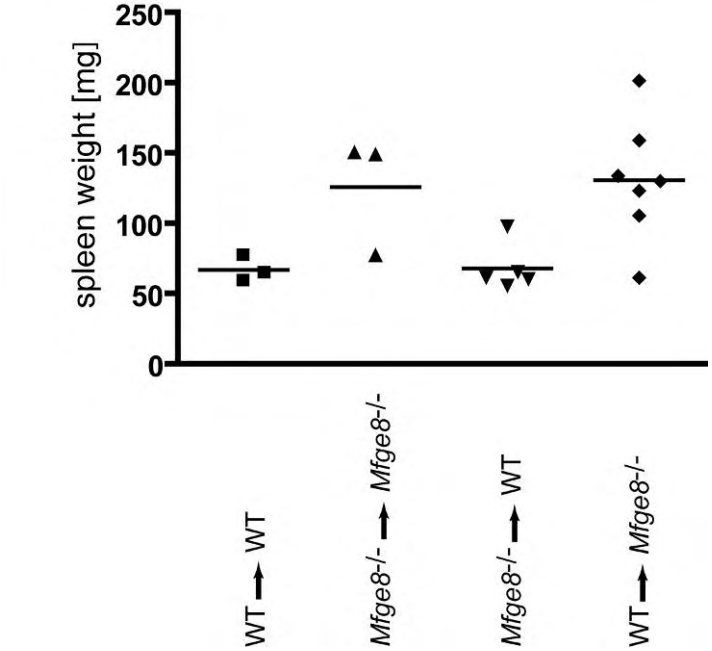

Figure 6.18 Stromal *Mfge8*-deficiency causes splenomegaly. Spleen weights of BM-chimeric mice were determined 41 weeks post BM-reconstitution after repeated immunization with OVA in alum. *Mfge8*$^{-/-}$→*Mfge8*$^{-/-}$ and WT→*Mfge8*$^{-/-}$ mice showed markedly increased spleen weights compared to WT→WT and *Mfge8*$^{-/-}$→WT mice.

Hanayama *et al*. showed, that TBMϕs in *Mfge8*$^{-/-}$ mice were enlarged. This was caused by an accumulation of apoptotic cells on the macrophage´s surface due to impaired engulfment of apoptotic cells. To assess whether the phagocytosis defect of TBMϕs can be attributed to the absence of FDC-produced Mfge8, the number of TUNEL^{+} cells per TBMϕ was determined in the BM-chimeras. To this end, TUNEL assays combined with immunofluorescent stainings for CD68 were performed on spleens from previously immunized chimeric mice. All TUNEL^{+} cells associated with

CD68$^+$ TBMϕs residing within splenic follicles were counted and the average number of TUNEL$^+$ cells per TBMϕ was determined. TBMϕs of *Mfge8*$^{-/-}$→*Mfge8*$^{-/-}$ mice bound in average 2.55 ± 0.15 TUNEL$^+$ cells, while TBMϕs of WT→WT mice bound 2.00 ± 0.17. TBMϕs of WT→*Mfge8*$^{-/-}$ mice bound slightly more TUNEL$^+$ cells (2.35 ± 0.18) than TBMϕs of *Mfge8*$^{-/-}$→WT mice (2.14 ± 0.11) (Fig. 6.19). TBMϕs of non-

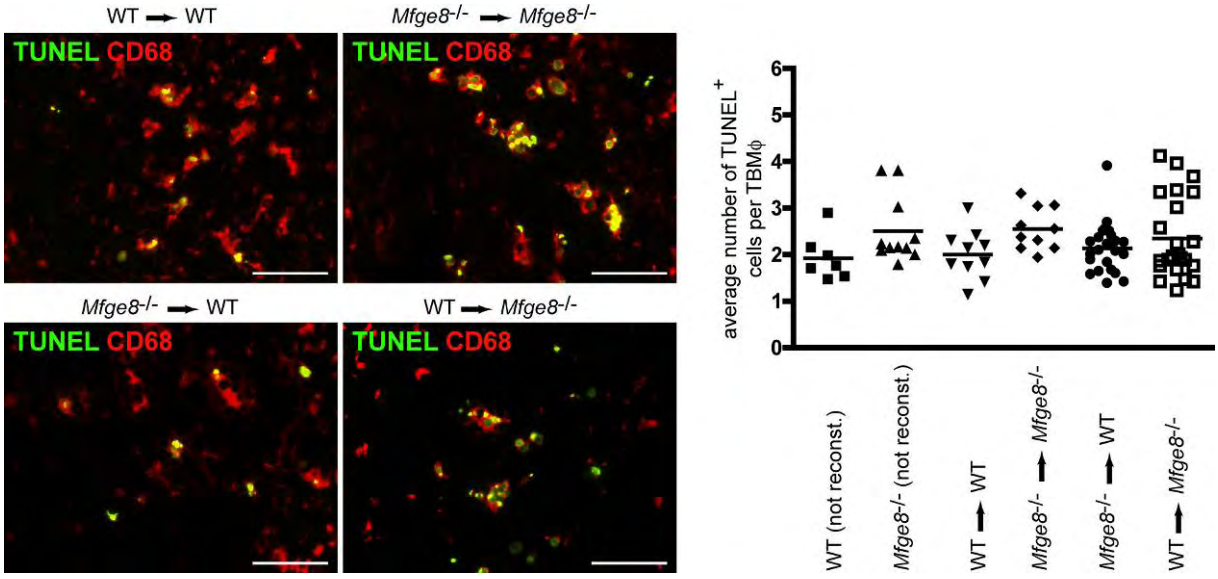

Figure 6.19 Lack of *Mfge8* expression by FDCs results in increased binding of apoptotic cells by TBMϕs.
9 weeks after BM-reconstitution (after previous immunization with OVA in alum 6 and 8 weeks after BM-reconstitution) apoptotic cells were visualized by TUNEL assay on splenic cryosections. A CD68-staining was included to visualize TBMϕs. >300 TUNEL$^+$ cells per group were counted and the average number of TUNEL$^+$ cells per TBMϕs determined. *Mfge8*$^{-/-}$→*Mfge8*$^{-/-}$ and WT→*Mfge8*$^{-/-}$ showed a slightly higher number of TUNEL$^+$ cells per TBMϕ than WT→WT and *Mfge8*$^{-/-}$→WT mice. For control unreconstituted WT and *Mfge8*$^{-/-}$ mice were included.

reconstituted WT mice bound 1.92 ± 0.45 and of non-reconstituted *Mfge8*$^{-/-}$ mice 2.51 ± 0.71 TUNEL$^+$ cells. Although the observed differences were minor, there was a clear trend towards an increased number of bound TUNEL$^+$ cells in the absence of Mfge8 on stromal cells, which supports the idea that FDC-derived Mfge8 is involved in controlling the engulfment of apoptotic cells. One explanation for the rather small differences could be the time point of analysis. The GC reaction is a very dynamic process and therefore the time point of analysis might be crucial. Furthermore, the fact that the mice analyzed were irradiated and reconstituted might also influence the kinetics of the GC reaction and might introduce further unknown parameters influencing the results.

Hanayama *et al*., showed by EM that apoptotic cells attached to the TBMϕs were not engulfed. To determine whether this observation can be reproduced in BM-chimeric mice, 40 weeks after BM-transfer spleens from mice that were immunized several

times with OVA in alum were prepared for EM-analysis. In every case (WT→WT, *Mfge8*$^{-/-}$→*Mfge8*$^{-/-}$, *Mfge8*$^{-/-}$→WT, and WT→*Mfge8*$^{-/-}$) TBMϕs with incorporated lymphocytes at different stages of degradation were found. (Fig. 6.20). These results strongly suggest, that even in the complete absence of Mfge8 TBMϕs still have the ability to take up and degrade apoptotic cells. Therefore, several redundant mechanisms might exist that ensure the removal of apoptotic cells from the GC.

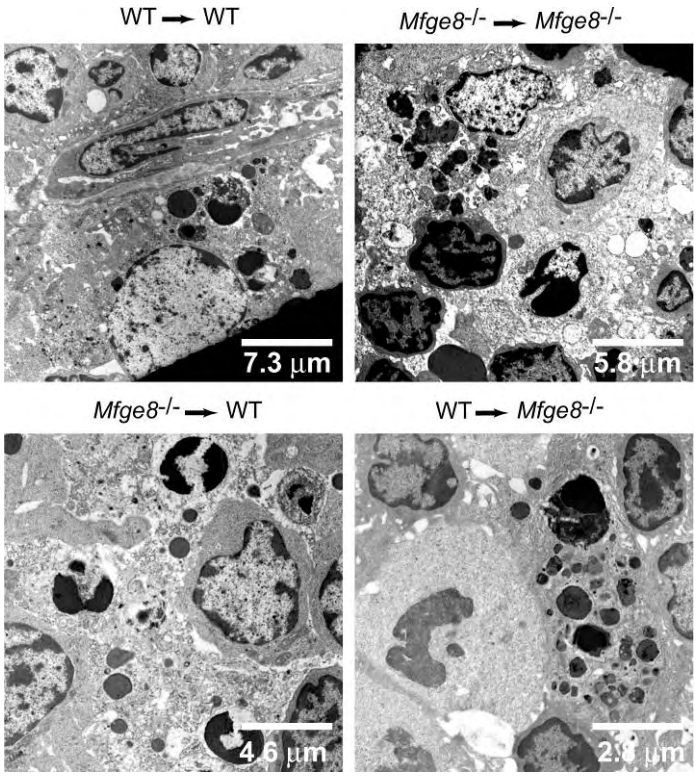

Figure 6.20 Morphological features of TBMϕs of aged BM-chimeric mice. 40 weeks after reconstitution BM-chimeric mice were analyzed by EM. In all chimeric mice (WT→WT, *Mfge8*$^{-/-}$→*Mfge8*$^{-/-}$, *Mfge8*$^{-/-}$→WT, and WT→*Mfge8*$^{-/-}$) apoptotic cells in different degradation stages were observed inside TBMϕs indicating a general ability of TBMϕs to phagocytose dying cells also in the absence of Mfge8.

6.3.2 No proof of SLE can be found in BM-chimeras

The SLE described in *Mfge8*$^{-/-}$ mice was characterized by glomerulonephritis with Ig-deposits in the glomeruli and increased levels of ANA and anti-dsDNA antibodies at 40 weeks of age or at young age after previous immunization (Hanayama et al., 2004b). To assess whether the development of SLE can be attributed to a single compartment (stromal or hematopoietic) serum of the BM-chimeric mice was analyzed for elevated levels of autoantibodies by ELISA. To accelerate the onset of disease, BM-chimeric mice received three immunizations with OVA in alum in two week intervals starting 30 weeks after the BM-transfer. 41 weeks after the BM-transfer serum was taken and the titre of dsDNA and ANA antibodies determined by ELISA. (Fig. 6.21).

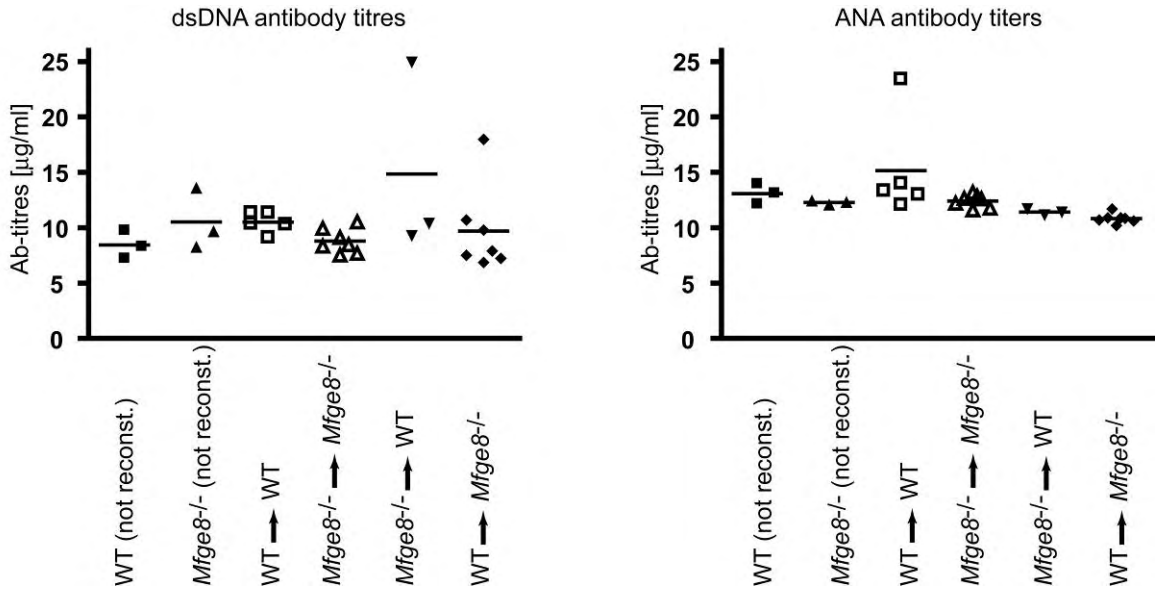

Figure 6.21 Determination of autoantibody titres.
ANA and dsDNA antibody levels were determined by ELISI in serum from unreconstituted WT and *Mfge8*$^{-/-}$ mice and from WT→WT, *Mfge8*$^{-/-}$→*Mfge8*$^{-/-}$, *Mfge8*$^{-/-}$→WT, and WT→*Mfge8*$^{-/-}$ BM-chimeric mice 41 weeks after BM-transfer. All mice showed similar levels of autoantibodies. N=3-6 mice per group. Each symbol represents one mouse.

Surprisingly, no differences between the different BM-chimeric mice were detected, no matter whether the stromal, the hematopoietic or both compartments lacked *Mfge8* expression. Even the antibody levels of non-reconstituted *Mfge8*$^{-/-}$ mice did not show an elevation (Fig. 6.20).

Despite the absence of elevated autoantibody-levels, the kidneys of these mice were analyzed for pathologic alteratiions with periodic acid Schiff (PAS) staining. PAS staining visualizes glycogen and other polysaccharides which are present in basal membranes. This technique enables to detected pathologic alterations of the basal membranes of mesangial cells. Unfortunately, the BM-chimeras turned out to be not useful to determine the contribution of FDCs to SLE, because mice of all groups (WT→WT, *Mfge8*$^{-/-}$→*Mfge8*$^{-/-}$, *Mfge8*$^{-/-}$→WT and WT→*Mfge8*$^{-/-}$) developed a glomerulopathy with signs of mesangial lysis and some dispersed foamy cells, which are typical of a “radiation nephritis” caused by the lethal irradiation prior to the BM-transfer (Fig. 6.22). Because the radiation-induced nephritis overshadowed the glomerulonephritis of *Mfge8*$^{-/-}$ mice, it was not possible to determine the contribution of either the stromal or hematopoietic compartment to the autoimmune glomerulonephritis.

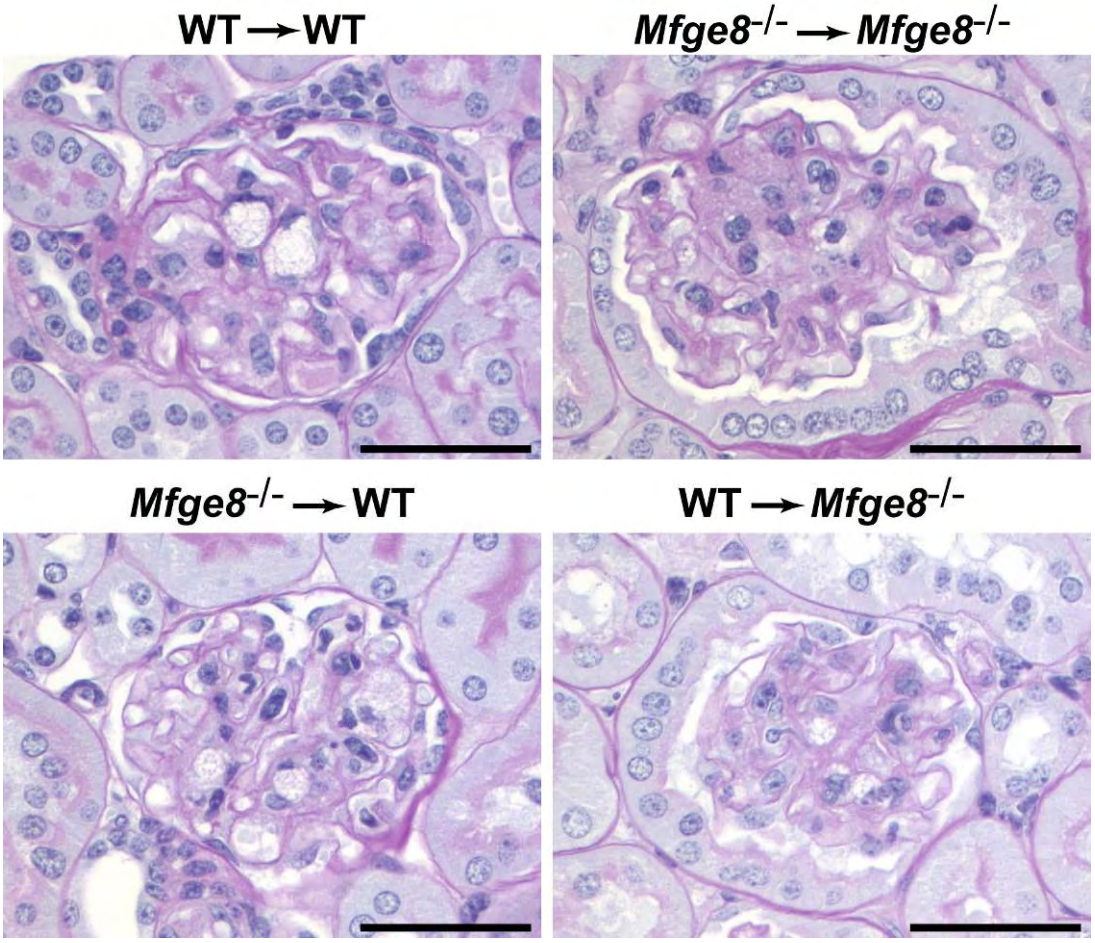

Figure 6.22 PAS staings of kidneys.
PAS stainings were performed on paraffin-sections of kidneys from WT→WT, *Mfge8*$^{-/-}$→*Mfge8*$^{-/-}$, *Mfge8*$^{-/-}$→WT, and WT→*Mfge8*$^{-/-}$ mice 41 weeks after the BM-transfer. All mice showed signs typical of a "radiation nephritis" with mesangial lysis and foamy cells within the glomeruli. Scale bar: 50 μm.

6.4 Putative FDC precursors express *Mfge8*

6.4.1 Mfge8$^+$ cells are present in spleens of Ltbr$^{-/-}$ and Rag1$^{-/-}$ mice

The *Mfge8* ISH detected not only mature FDC networks, but also scattered *Mfge8*$^+$ cells within the follicle and *Mfge8*$^+$ cells lining the marginal sinus (Fig. 6.13). Since up to date no FDC precursor cell has been identified, it is possible that these cells might represent immature FDC precursor cells. In order to assess, whether *Mfge8* ISH hybridization can serve as a tool to detect putative FDC precursors, *Ltbr*$^{-/-}$ and *Rag1*$^{-/-}$ mice that were reported to lack mature FDCs due to the absence of LTβR-signaling or due to the lack of B cells providing LT, respectively were analyzed by *Mfge8* ISH. Indeed, on splenic cryosections of *Ltbr*$^{-/-}$ few *Mfge8*$^+$ were detectable. These cells were rare, but were localized inside splenic follicles and might represent a vey early FDC precursor cell that was arrested in its development due to the absence of LTβR-signaling. (Fig 6.23, upper panel).

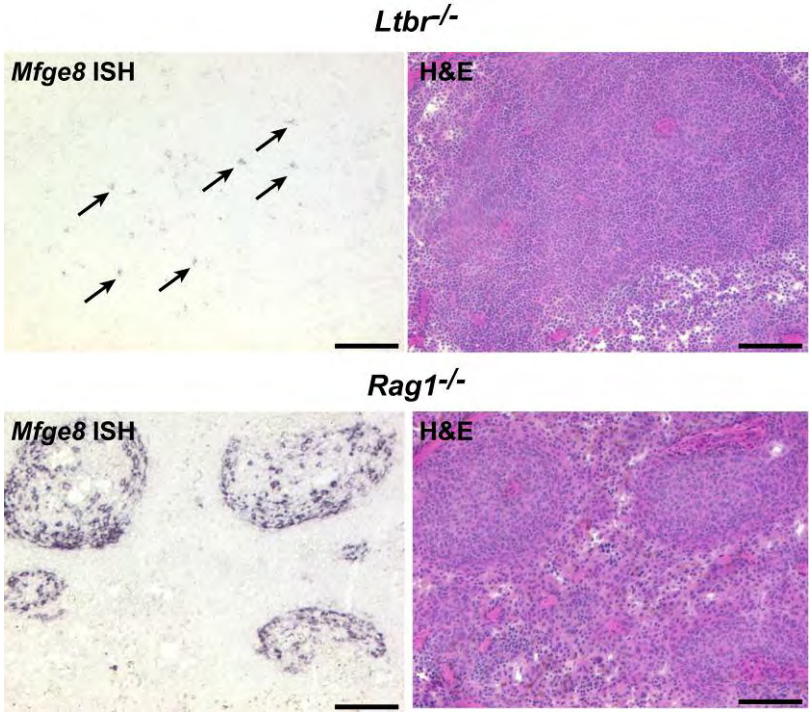

Figure 6.23 *Mfge8*$^+$ cells in spleens of *Ltbr*$^{-/-}$ and *Rag1*$^{-/-}$ mice.
Splenic cryosections of *Ltbr*$^{-/-}$ and *Rag1*$^{-/-}$ mice were stained with an *Mfge8* riboprobe or with H&E. Both, in spleens of *Ltbr*$^{-/-}$ and *Rag1*$^{-/-}$ mice *Mfge8*$^+$ cells were detected by ISH. While only few scattered Mfge8$^+$ cells were present within follicles of *Ltbr*$^{-/-}$ mice, *Rag1*$^{-/-}$ mice showed abundant expression of *Mfge8* in and around small follicle-like structures. Scale bar: 100 μm.

Surprisingly, *Rag1*$^{-/-}$ mice showed very abundant *Mfge8* expression. These mice exhibited rather small follicle-like structures that were surrounded by *Mfge8*$^+$ cells. In addition, many *Mfge8*$^+$ cells were also found within these small follicle-like structures (Fig. 6.23 lower panel). These cells might represent a more advanced stage of FDC-precursor cells. Since *Rag1*$^{-/-}$ mice still have LTα and LTβ expression by natural killer (NK) cells, it is plausible that NK cells can provide LTα and LTβ to FDC precursors and therefore enabling differentiation to a more advanced stage.

6.5 Regulation of *Mfge8* expression in macrophages

6.5.1 Thioglycollate induces Mfge8 expression in macrophages

Peritoneal Mϕs were previously shown to express *Mfge8* upon stimulation with thioglycollate (Hanayama et al., 2002), which induces a peritonitis. To confirm that the *Mfge8* expression in the peritoneum really originates from hematopietic cells, the BM-chimeric mice were stimulated with thioglycollate for 48h. Then peritoneal Mϕs were harvested by peritoneal lavage. RNA was isolated, cDNA synthesized and *Mfge8* expression was analyzed by RT-PCR. In contrary to the observation in the spleen, *Mfge8* expression in the peritoneum originated solely from hematopoietic cells. *Mfge8* expression was only detectable in peritoneal lavage of WT→WT and WT→*Mfge8*$^{-/-}$ chimeras, but not in that of *Mfge8*$^{-/-}$→WT and *Mfge8*$^{-/-}$→*Mfge8*$^{-/-}$ chimeras (Fig. 6.24A). Furthermore, *Mfge8* expression was only detectable upon stimulation with thioglycollate (Fig. 6.24B) and was absent in unstimulated cells. These results are in agreement with previous reports (Hanayama et al., 2002), and suggest that Mϕs do not express *Mfge8* under normal conditions, but only after stimulation.

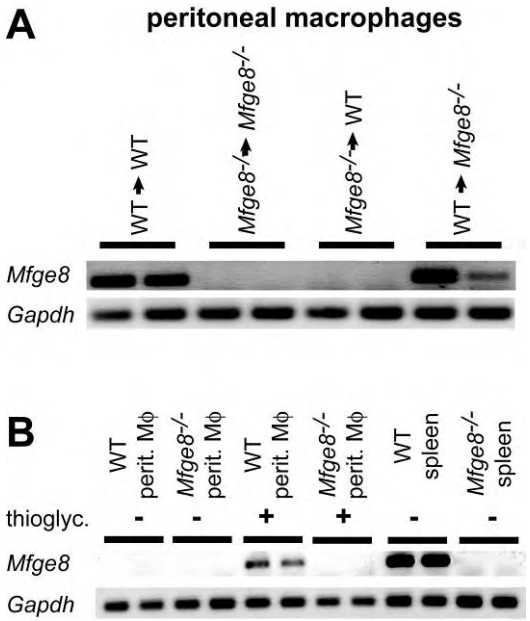

Figure 6.24 *Mfge8* expression in macrophages. **(A)** PCR for *Mfge8* on cDNA from thioglycollate elicited peritoneal Mϕs showed the opposite expression pattern to the spleen: *Mfge8* expression was only found after reconstitution with WT BM (upper panel). All *Mfge8* expression originated from hematopoietic cells **(B)** PCR on cDNA derived from peritoneal Mϕs without previous thioglycollate stimulation showed absence of *Mfge8* expression in these cells (lower panel).

In line with this are results obtained from a screen of several tissues for *Mfge8* expression. In this screen a lung of a mouse suffering from severe pulmonitis was analyzed. While lungs from healthy mice lacked all detectable *Mfge8* expression (Fig. 6.25, upper panel), this inflamed lung showed many large *Mfge8* expressing cells (Fig. 6.25, middle panel). Staining of consecutive section with anti-CD68 antibodies suggested that *Mfge8* expressing cells were alveolar Mϕs (Fig. 25, middle panel). To

control for the specificity of the *Mfge8* riboprobe *Mfge8*$^{-/-}$ lungs were included. There, no signal was detectable showing the specificity of the *Mfge8* ISH (Fig. 6.25, lower panel).

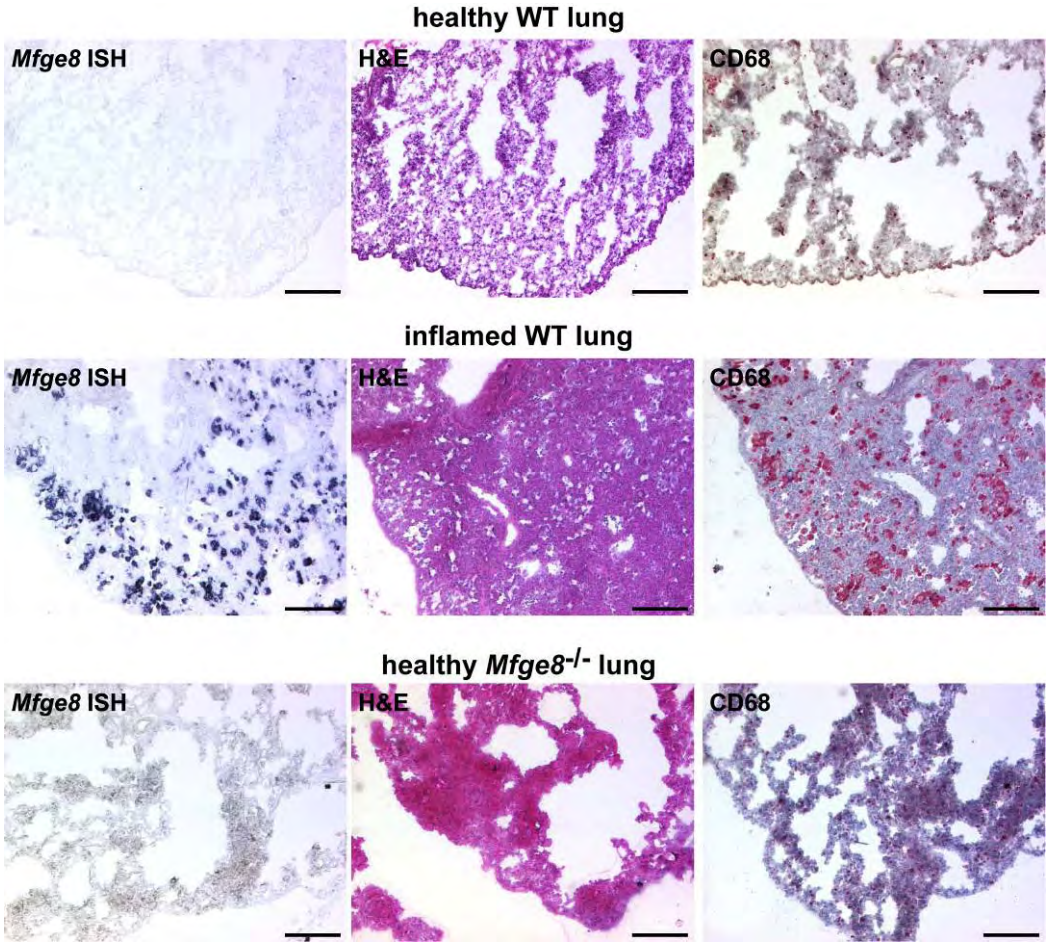

Figure 6.25 *Mfge8* expression in the lung.
Cryosections of lung tissue were subjected to ISH with an *Mfge8* riboprobe (left column). Consecutive sections were stained with H&E (middle column) or anti-CD68 antibodies (right column). No *Mfge8* expression was found in healthy WT lungs (upper panel) or in *Mfge8*$^{-/-}$ lungs. Only an inflamed lung containing many large alveolar Mϕs showed strong *Mfge8* expression. Scale bar: 200 μm.

To gain deeper insight into the stimuli required to induce *Mfge8* expression, isolated peritoneal Mϕ were stimulated with IFNγ and LPS, LPS alone or IL-4, common inducers of the classical, innate or alternative pathway, respectively. In contrast to classically activated Mϕ, via IL-4 alternatively activated Mϕ participate in an anti-inflammatory response, which is associated with increased phagocytosis and antigen presentation (Stein et al., 1992, Goerdt and Orfanos, 1999). *Mfge8* expression was quantified by RT-PCR after 24h of stimulation. Culturing of Mϕs for 24h without stimulation already induced *Mfge8* expression. But treatment with IFNγ and LPS or LPS alone almost completely shut off *Mfge8* expression. IL-4 treatment, however increased *Mfge8* expression 2.6 fold (Fig. 6.26). These results show that *Mfge8*

expression in Mϕs is tightly regulated, whereas FDCs seem to express *Mfge8* in a constitutive manner, since also putative FDC precursors express *Mfge8* (Fig 6.23) and also naïve, non-immunized mice have *Mfge8* expressing FDC networks. The results presented above indicate that TBMϕs do not express *Mfge8* under physiological conditions, not even after thorough immunization when many TBMϕs show high immunoreactivity for *Mfge8* antibodies.

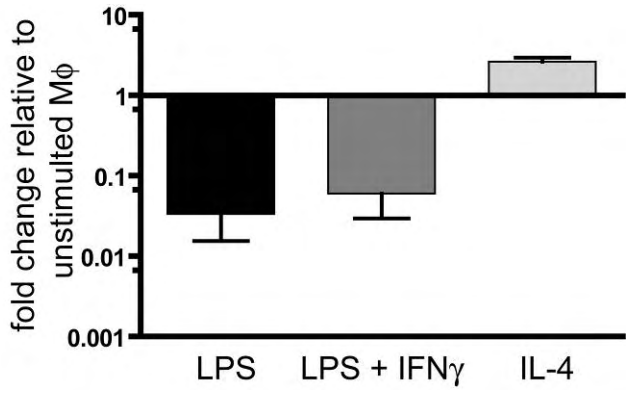

Figure 6.26 IL-4 induces *Mfge8* expression in Mϕs.
Isolated peritoneal Mϕs were stimulated with LPS, LPS and IFNγ or IL-4 for 24h. *Mfge8* expression was quantified by RT-PCR. After treatment with LPS *Mfge8* expression was reduced by 96.6% compared to untreated cells. After treatment with LPS and IFNγ *Mfge*8 expression was reduced by 94.0%. Treatment with IL-4 resulted in a 2.6 fold higher *Mfge8* expression than in untreated cells. Graph shows average ± SD *Mfge8* expression in relation to cultured, unstimulated Mϕs from three independently performed experiments.

6.6 *Mfge8* is dispensable for prion replication by FDCs

6.6.1 Mfge8$^{-/-}$ mice show accelerated disease progression

The initial aim of the microarray screen performed by Huber *et al*. (Huber et al., 2005) was not only to identify FDC specific genes, but also to identify genes expressed by FDCs that are involved in the replication or accumulation of prions. Mfge8 was an interesting candidate for being involved in prion diseases, due to the well established role of *Mfge8* in the removal of apoptotic cells: It was interesting to determine whether *Mfge8* is also capable to regulate the removal of prions. To address this question *Mfge8*$^{-/-}$ and WT mice on a (B6x129sv)$_{F1}$ background were inoculated intraperitoneally (i.p.) and intracerebrally (i.c.) with prion. The disease progression until terminal stage was monitored and indeed differences in incubation times between controls and *Mfge8*$^{-/-}$ mice were found (Fig. 6.27).

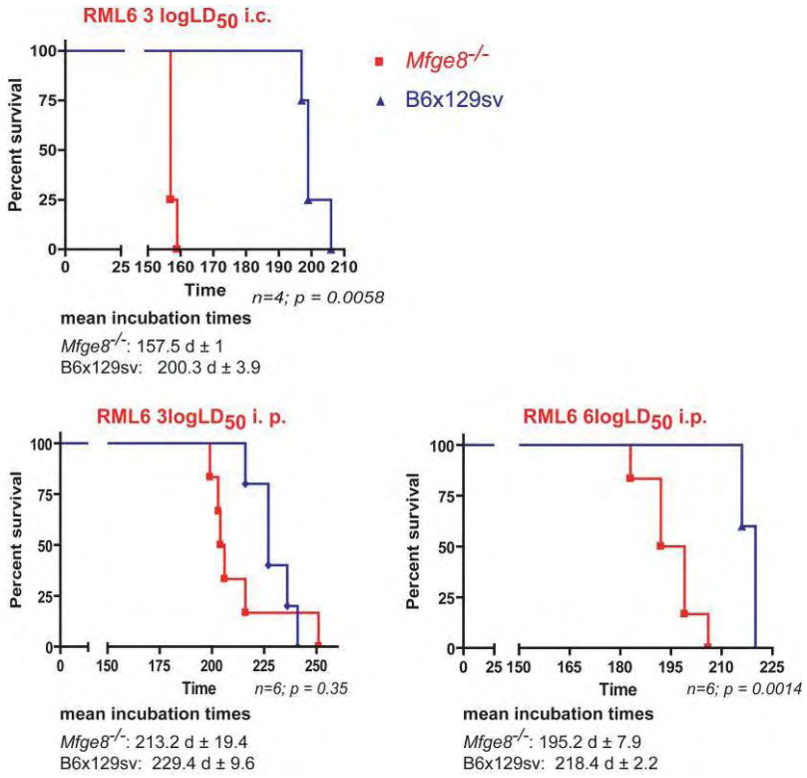

Figure 6.27 *Mfge8*$^{-/-}$ show accelerated disease progression.
WT (B6x129sv)$_{F1}$ and *Mfge8*$^{-/-}$ were inoculated i.c. with 3logLD$_{50}$ (n=4) and i.p. with 6log LD$_{50}$ (n=6) and 3logLD$_{50}$ (n=6) of RML6 prions. The incubation time until terminal disease was monitored. The mean incubation time after low dose (3logLD$_{50}$) i.c. inoculation was drastically accelerated in *Mfge8*$^{-/-}$ mice (157.5 ± 1 in *Mfge8*$^{-/-}$ and 200.3 ± 3.9 in WT mice). The differences in incubation time after low dose i.p. inoculation were minor (213.2 ± 19.4 in *Mfge8*$^{-/-}$ and 229.4 ± 9.6 in WT mice). After high dose (6logLD$_{50}$) i.p. inoculation the differences were still less pronounced as after i.c. inoculation (195.2 ± 7.9 in *Mfge8*$^{-/-}$ and 218.4 ± 2.2 in WT mice).

After low dose (3logLD_{50}) i.c. inoculations the difference in incubation time was most pronounced. *Mfge8*$^{-/-}$ mice succumbed to disease approx. 43 days earlier than the WT controls. After i.p. inoculation the differences were much less distinct (approx. 16 days after low dose and approx. 23 days after high dose inoculation). Since the differences were most pronounced after i.c. inoculation, where the infectious agent is directly admitted to the CNS, without requiring prior replication in lymphoid organs, it is unlikely that *Mfge8* deficiency in FDCs accounted for this effect. To further confirm this notion, accumulation of disease-associated proteinase K (PK) resistant PrP^{Sc}

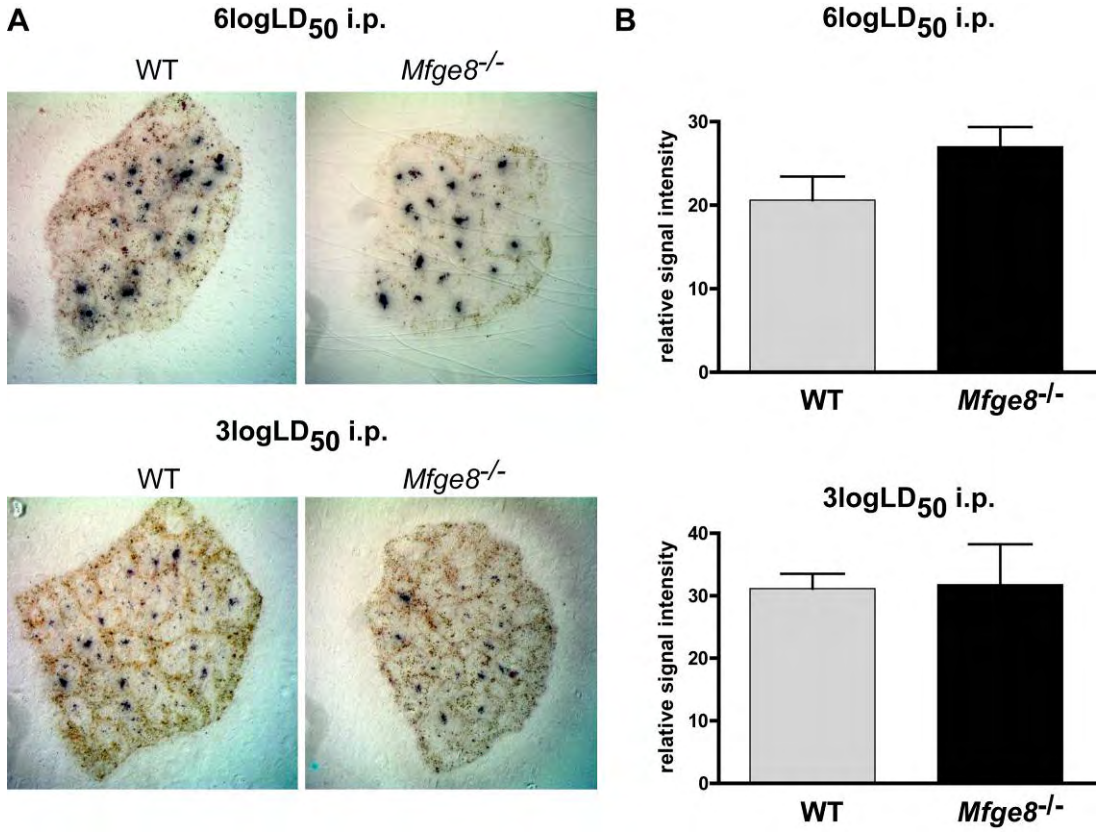

Figure 6.28 PrP^{Sc} accumulation in the spleen.
(A) Histoblots of spleens from high and low dose i.p. inoculated *Mfge8*$^{-/-}$ and WT mice showed accumulation of PK-resistant PrP^{Sc} on FDCs. No differences in the depostition of PrP^{Sc} could be observed between WT and *Mfge8*$^{-/-}$ mice. **(B)** PrP^{Sc} was quantified by densitometry on Western blots from PK-treated spleen homogenates from high and low dose inoculated WT and *Mfge8*$^{-/-}$ mice. Also there no significant differences were detected. N = 5 mice per group.

was visualized by histoblot. No obvious differences between *Mfge8*$^{-/-}$ mice and controls in accumulation of PrP^{Sc} by FDCs could be observed by this technique (Fig. 6.28A). Also quantification of PrP^{Sc} by densitometry on Western blots of PK-treated spleen homogenates did not reveal any significant differences in the amount of PrP^{Sc} (Fig.6.28B). Hence, it seems unlikely that Mfge8 produced by FDCs influences either the degradation or the replication of prions.

The most striking difference in incubation time was found after i.c inoculation. Therefore, it is likely that *Mfge8* deficiency alters prion replication or degradation in the CNS. This question was addressed by IHC for PrP^{Sc} aggregates using the anti-PrP antibody SAF84 and by Western blotting of brain tissue (Fig. 6.29). Immunohistochemistry using SAF84 and quantitation of PrP^{Sc} by Western blotting and densitometry revealed significantly increased levels of PrP^{Sc} in brains of *Mfge8*$^{-/-}$ mice, providing first evidence that Mfge8 might be involved in clearing prions from the brain (Fig. 6.29A and 6.29B). To ensure that this increase in PrP^{Sc} levels is not merely due to elevated levels of PrP^{C}, its levels were also quantified by Western blot. However, no significant difference between WT and *Mfge8*$^{-/-}$ mice was detectable (Fig. 6.29C), confirming a true increase in PrP^{Sc} levels. Consequently, *Mfge8*$^{-/-}$ accumulate more PrP^{Sc} within shorter time, since they succumb to disease more than 40 days earlier.

To see whether the increased PrP^{Sc} levels also manifest in more severe brain damage, the degree of spongiosis, astrogliosis and microgliosis was analyzed by H&E, GFAP and IBA1 stainings, respectively. However, there the severity of the spongiosis as well of the astrogliosis and the microgliosis was unaltered between WT and *Mfge8*$^{-/-}$ mice, but both groups showed extensive spongiosis and activation of astrocytes and microglia in the brain (Fig. 6.30). Apart from increased levels of PrP^{Sc} in the brains of *Mfge8*$^{-/-}$ mice no alterations in prion pathogenesis could be found.

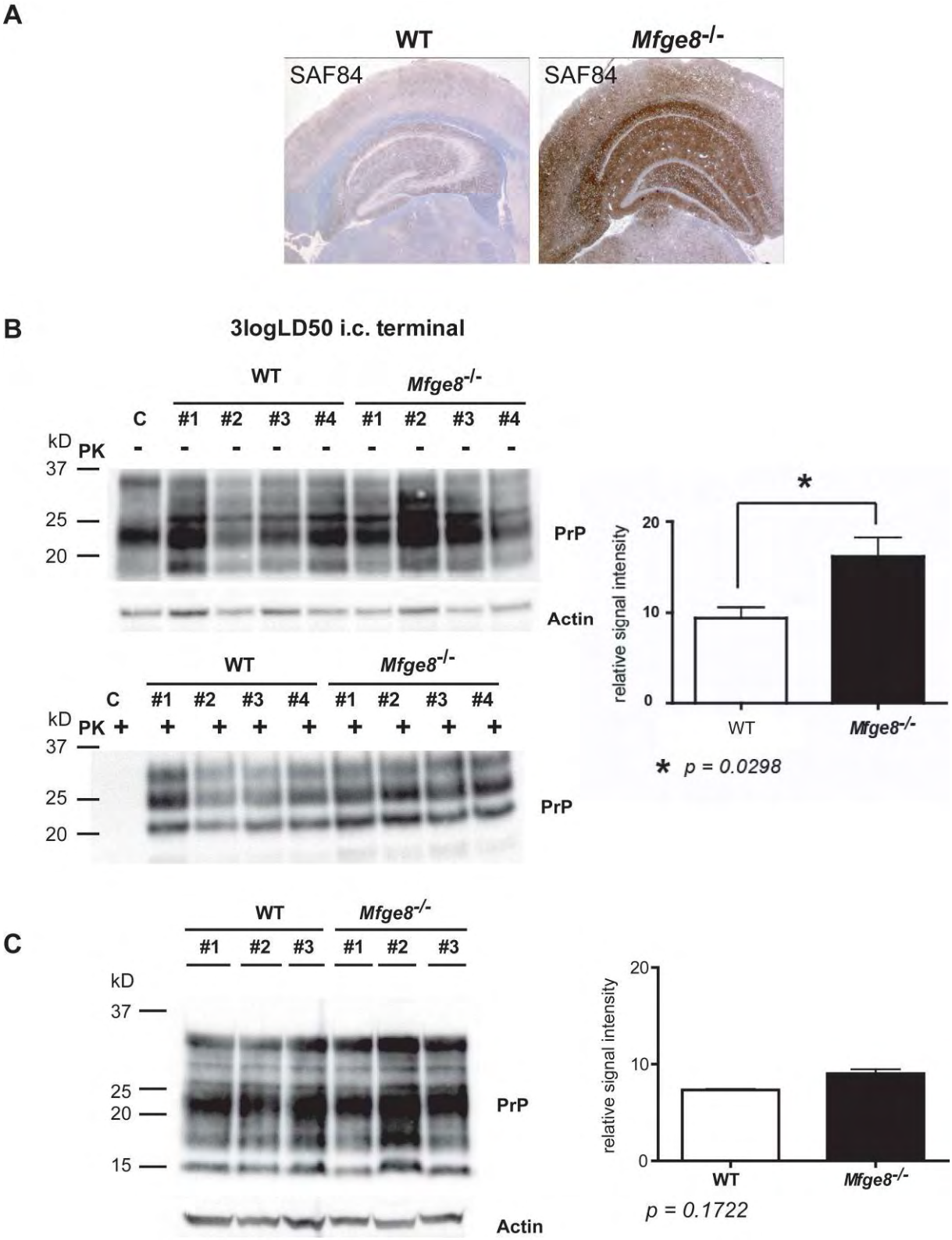

Figure 6.29 Increased PrP^{Sc} levels in the brain of *Mfge8*$^{-/-}$ mice.
(A) Stainings of brain section with the anti-PrP antibody SAF84 revealed increased deposition of PrP^{Sc} in the brains of *Mfge8*$^{-/-}$ mice. **(B)** Western blotting of brain homogenates from terminal i.c. inoculated WT and *Mfge8*$^{-/-}$ mice without (upper blot) and with PK (lower blot) shows increased levels of PrP^{Sc}. Quantitation by densitometry shows a siginificant increase of PrP^{Sc} of about 50%. **(C)** Western blotting of healthy WT and *Mfge8*$^{-/-}$ brain homogenates using anti-PrP antibodies with subsequent quantitation by densitometry showed that PrP^{C} levels were not different between WT and *Mfge8*$^{-/-}$ mice.
Graphs show average relative signal intensity, error bars represent the SD, n=4 (B) and n=3 (C). For statistical analysis Student´s T test was used.

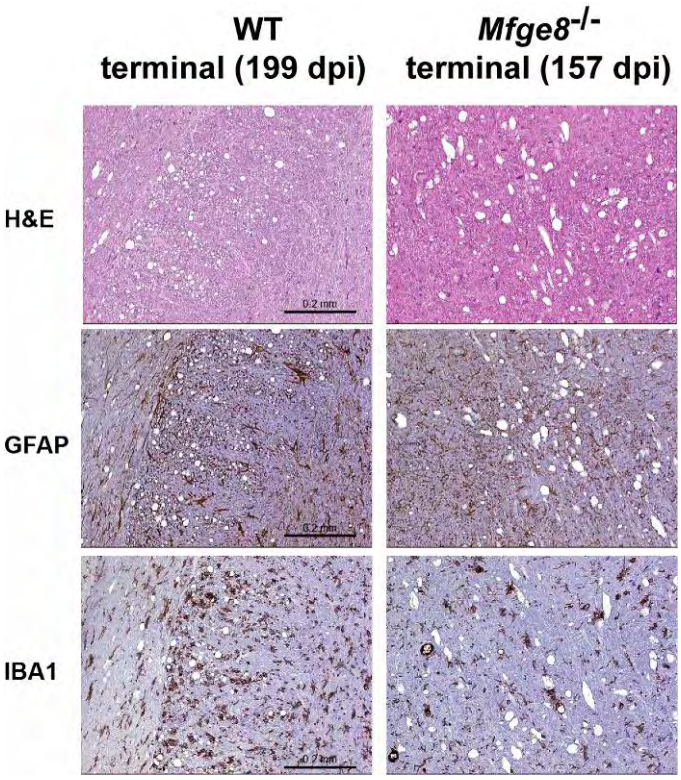

Figure 6.30 Histopathological analysis of terminal *Mfge8*$^{-/-}$ brains. Spongiform changes were analyzed on brain sections from terminal WT and *Mfge8*$^{-/-}$ mice by H&E staining. No difference between WT and *Mfge8*$^{-/-}$ brains was observed. Astrogliosis was analyzed by GFAP staining (middle panel) and microgliosis by IBA1 staining (lower panel). Also there was no obvious difference between WT and *Mfge8*$^{-/-}$ mice.

6.6.2 Analysis of Mfge8 expression in the brain

Since it was unknown whether *Mfge8* is expressed in the brain, different brain derived cells were analyzed by qPCR for *Mfge8* expression. Furthermore, the *Mfge8* expression pattern was determined by ISH on brain tissue (Fig. 6.31). Cultured astrocytes showed the highest *Mfge8* expression by quantitative qPCR. Only minimal *Mfge8* expression was detected by cultured neurons, oligodendrocytes or microglia (Fig. 6.31A). Either these cell types express *Mfge8* to very low levels, or the residual *Mfge8* expression originates from contaminating astroctyes.

ISH revealed a scattered *Mfge8* expression pattern in cortical brain areas. These cells might be astrocytes, since primary astrocyte-cultures showed abundant *Mfge8* expression by qPCR. But to determine the identity of these cells beyond any doubt further characterization needs to be performed. Also in the cerebellum *Mfge8*$^{+}$ cells were detected. These cells were located close to Purkinje neurons and most likely represent Bergman glia (Fig. 6.31B).

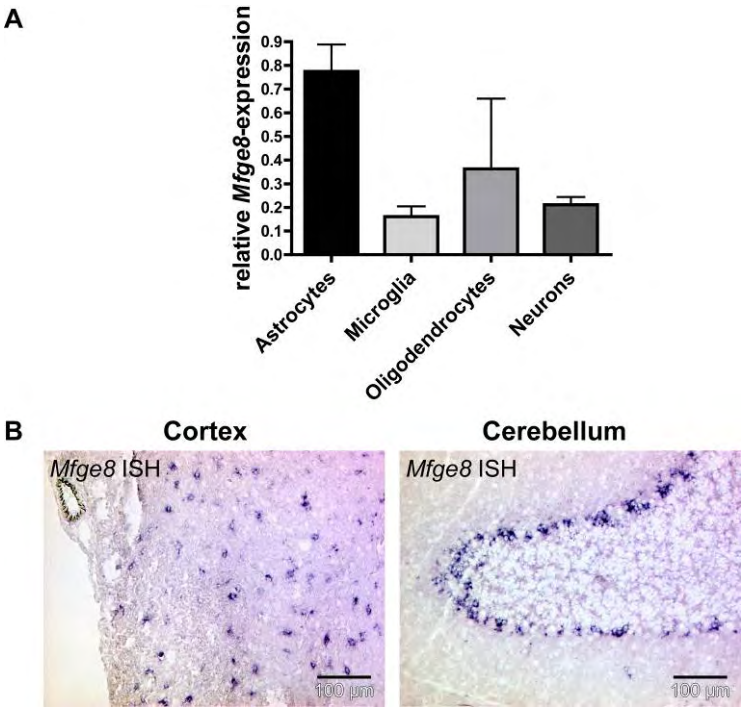

Figure 6.31 *Mfge8* expression analysis in the brain.
(A) Expression of *Mfge8* in cultured astrocytes, microglia, oligodendrocytes and neurons was quantified by qPCR. Only astrocytes showed abundant *Mfge8* expression. Error bar represent SD, n=3 indepent cultures per group. **(B)** ISH for *Mfge8* on brain cryosection. *Mfge8*$^{+}$ cells in the cortex might resemble astroglia. In the cerebellum *Mfge8* expression was found in Bergman glia. Scale bar 100 µm.

6.6.3 Influence of Mfge8 on prion pathogenesis is dependent on the genetic background

The *Mfge8*$^{-/-}$ mice used for the prion inoculation study where made in the R1 ES cell line, which was established from a (129X1/SvJ x 129S1)$_{F1}$ 3.5-day blastocyst (Nagy et al., 1993). The obtained founder was crossed once time with a C57BL/6 female. The resulting F1 generation was intercrossed with each other. Therefore, the mice used for this study were on a mixed B6x129 background. Unfortunately, many different sublines of the 129 background exist. Thus, it is almost impossible to find control mice that closely match the genetic background of the *Mfge8*$^{-/-}$ mice. Here, 129sv mice obtained from Charles River Laboratories were intercrossed with C57BL/6 mice. The F1 generation resulting from this intercrossing served as WT controls for the inoculation study, though the genetic backgrounds between controls and *Mfge8*$^{-/-}$ were only roughly matched. This fact raised some concerns that the accelerated prion pathogenesis in the *Mfge8*$^{-/-}$ might be an artefact caused by comparing them to mice of a different genetic background. To address these concerns, the inoculation study was repeated with *Mfge8*$^{-/-}$ mice which were backcrossed onto the C57BL/6 background for ten generations (B6-*Mfge8*$^{-/-}$) when these mice became available. For i.c. inoculation with a low dose of prions littermates that were either *Mfge8*$^{-/-}$, *Mfge8*$^{+/-}$ or *Mfge8*$^{+/+}$ were used. Surprisingly, there was no difference in incubation time between the three groups. The mean incubation time of all groups was around 180 days (Fig. 6.32A). To determine whether the B6-*Mfge8*$^{-/-}$

mice still exhibit increased levels of PrP^{Sc} in their brains at terminal stage, the PrP^{Sc} content was analyzed by Western blot. To this end, brain homogenates from terminal B6-*Mfge8*$^{+/+}$ and B6-*Mfge8*$^{-/-}$ mice were compared against each other. The PrP^{Sc} content showed strong variations between the individual mice, but over all there was no clear difference between the PrP^{Sc} levels of B6-*Mfge8*$^{+/+}$ and B6-*Mfge8*$^{-/-}$ mice. These results suggest that the phenotype observed in the mixed background *Mfge8*$^{-/-}$ mice is either an artefact caused by comparison of mice on a very different genetic background or is a real Mfge8-dependent effect, that only manifests on a certain genetic background. This question will be addressed in the future.

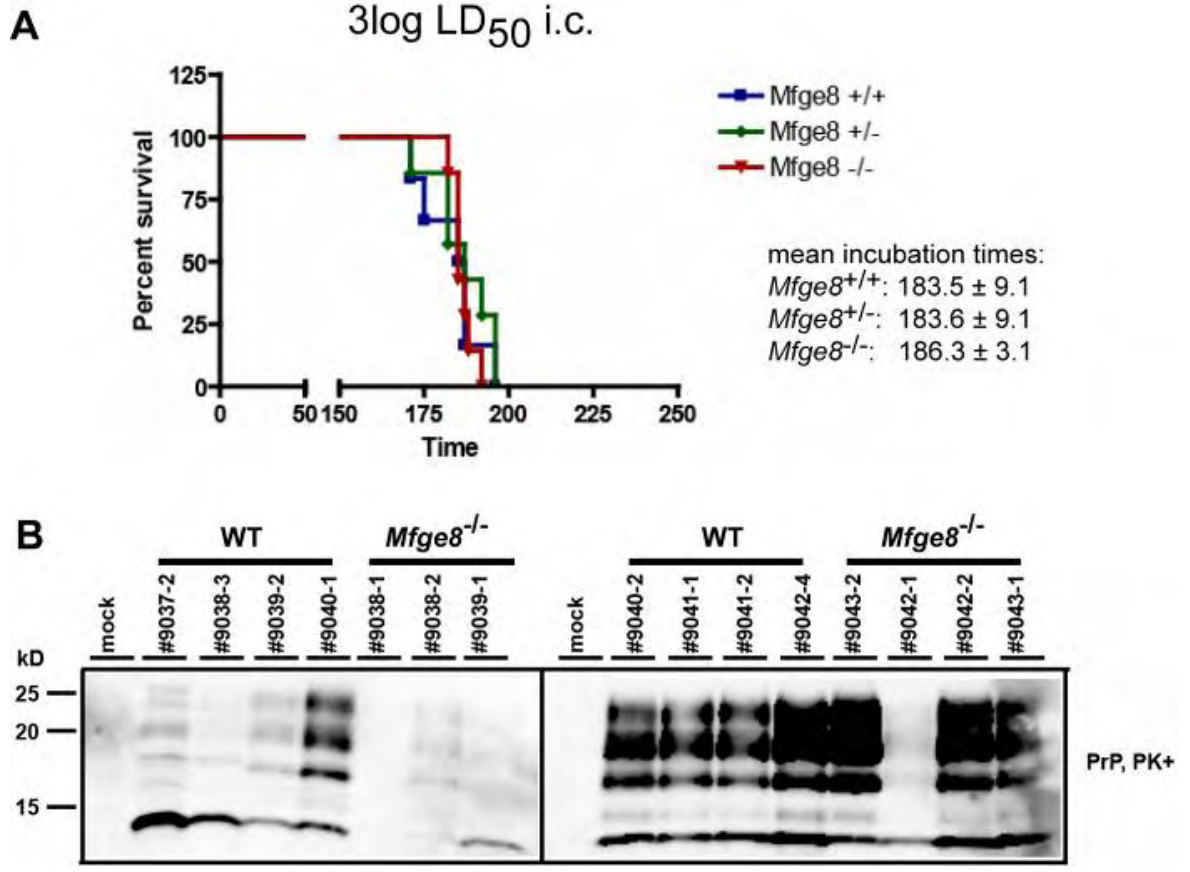

Figure 6.32 Inoculation of B6-*Mfge8*$^{-/-}$ mice.
(A) B6-*Mfge8*$^{+/+}$, B6-*Mfge8*$^{+/-}$ and B6-*Mfge8*$^{-/-}$ littermates were inoculated i.c. with 3logLD_{50} (n=7) of RML6 prions. The incubation time until terminal disease was monitored. The mean incubation times were 183.5 ± 9.1 in B6-*Mfge8*$^{+/+}$, 183.6 ± 9.1 in B6-*Mfge8*$^{+/-}$ and 186.3 ± 3.1 in B6-*Mfge8*$^{-/-}$ mice. **(B)** PrP-Western blotting of brain homogenates from terminal i.c. inoculated B6-*Mfge8*$^{+/+}$ (n=8) and B6-*Mfge8*$^{-/-}$ (n=7) mice after PK-digestion showed varying levels of PrP^{Sc} between individual mice, but no general increase in B6-*Mfge8*$^{-/-}$ mice.

7 Discussion

7.1 Identification of FDC-M1 as Mfge8 provides a new tool to study FDCs

The murine FDC-marker FDC-M1 is currently the most specific marker used to characterize FDCs. However, since the nature of the antigen was unknown, the scope of this marker was limited to histological studies of FDCs. This study identified FDC-M1 as Mfge8 by IF competition experiments (Fig. 6.3, 6.5 and 6.6), surface plasmon resonance (Fig. 6.7) and immunoprecipitation (Fig. 6.8).

The identification of the gene that encodes for FDC-M1 as *Mfge8* broadens the spectrum of techniques that can be used to analyze FDCs. Several new antibodies are now available, such as the anti-Mfge8 antibody clone 18A2-G10 which allows detection of FDC-M1/Mfge8 on formalin-fixed archived tissue (not shown) and in Western blot (Fig. 6.8), which was not possible with the anti-FDC-M1 antibody 4C11. Furthermore, the discovery that *Mfge8* is exclusively expressed by FDCs and few other stromal cells, that might represent FDC precursors, enables characterization of FDCs on RNA level. Quantitative studies are now possible using qPCR with *Mfge8*-specific primers. Also ISH with an *Mfge8* riboprobe will be a useful tool for histological studies of FDCs, especially since the Mfge8 ISH proved to be more sensitive than the FDC-M1 IHC. The Mfge8 ISH even detected *Mfge8*$^{+}$ cells in *Ltβr*$^{-/-}$ and *Rag1*$^{-/-}$ mice (Fig.6.23), where mature FDCs are absent. It will be very interesting to study whether these cells are indeed FDC precursors that are arrested in a premature stage due to impaired LTβR-signaling.

Since the *Mfge8* ISH was able to detect putative FDC precursors in a very early developmental stage this method might enable to follow FDC-maturation from early postnatal stages until first mature FDCs occur. If this leads to the discovery of an FDC-stem cell, the long-standing question of where FDCs come from and whether they are of stromal or hematopoietic origin might finally be answered.

The unexpected finding that *Mfge8* is already expressed in putative FDC precursors might hint to an additional function of Mfge8 in the spleen. Indeed, a role of Mfge8 in angiogenesis has been described and it might also be interesting to investigate whether Mfge8 produced by FDCs and their putative precursors are involved in the vascularization of the spleen and lymph nodes.

7.2 FDCs and not TBMϕs produce Mfge8 in the spleen

In 2004 Hanayama *et al*. published that Mfge8 is exclusively produced by TBMϕs in the spleen. Data from the study presented here and also other studies contradict this view. Huber *et al*. showed that *Mfge8* expression is increased in FDC-enriched versus FDC-depleted fractions. This was the first indication that also FDCs express *Mfge8*, but from this study it could not be excluded that TBMϕs are co-enriched together with the FDCs resulting in the observed increase in *Mfge8* expression. However, first *Mfge8* ISH results presented by Huber *et al*., suggested that TBMϕs cannot be the only source in the spleen (Huber et al., 2005).

In the current study the source of *Mfge8* expression was analyzed in detail. The fact that IF using anti-Mfge8 antibodies clearly stained FDC-networks and that the FDC-marker FDC-M1 was identified as Mfge8 gave strong support that FDCs indeed produce Mfge8. But to finally determine the source of Mfge8, *Mfge8* expression had to be analyzed on protein and RNA level by ISH in reciprocal BM-chimeras of WT and *Mfge8*$^{-/-}$ mice. Since FDCs are radiation resistant and TBMϕs radiation sensitive BM-chimeras where an adequate tool to answer this question. The surprising result was that Mfge8 protein could only be detected in TBMϕs when the stromal compartment was of WT origin, even with TBMϕs clearly being of *Mfge8*$^{-/-}$ origin (Fig. 6.12). These results illustrated first evidence that FDCs rather than TBMϕs are the actual source of Mfge8. This hypothesis was further corroborated by ISH analysis of the BM-chimeras. ISH and RT-PCR showed that all *Mfge8* RNA was of stromal and not of hematopoietic origin. Also ISH combined with IF for CD68 on WT mice showed that CD68^{+} TBMϕs did not contain any detectable *Mfge8* RNA. Therefore, the idea how Mfge8 functions in the GC had to be revised. Not the macrophages license themselves to remove apoptotic B cells, but FDCs by providing Mfge8, which opsonizes apoptotic cells and then targets them for uptake by TBMϕs. Hence, these results identified a novel function of FDCs: not only do they regulate the survival of GC B cells during a GC reaction, they also control their rapid removal after their death. This model would explain why TBMϕs can be detected as Mfge8^{+} cells by IHC upon ingestion of Mfge8-decorated apoptotic B cells. This model requires that two distinct cell types, FDCs and TBMϕs, collaborate in this removal process. This is plausible, because apoptosis is a rather frequent event in the GC, whereas TBMϕs are a rather rare cell type, which might limit the removal process. But if the removal is

not rapid enough, then autoimmunity impends. To ensure efficient removal, TBMϕs have to be guided specifically in a target-oriented manner to the apoptotic cell. This is best achieved by a local Mfge8-gradient produced by FDC that directs TBMϕs to the apoptotic cells. Since FDCs and B cells are in intimate contact, dying B cells can already be decorated with Mfge8 while still in contact with FDCs. This two-tiered mechanism may help ensuring that two rather few cell types – FDCs and TBMϕs - efficiently recognize and degrade large numbers of apoptotic cells (Fig. 7.1B).

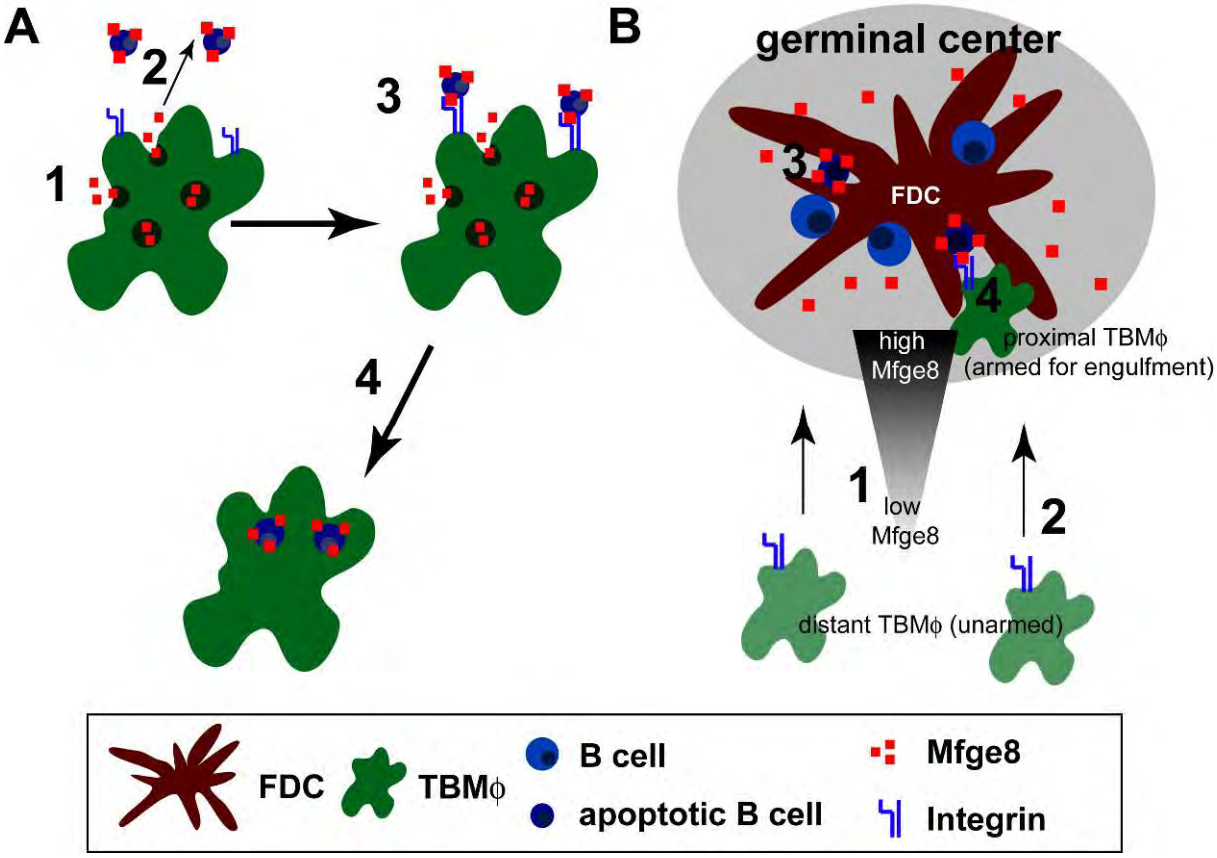

Figure 7.1 Models of Mfge8-dependent removal of apoptotic cells from the GC.
(A) Previous model of Mfge8-dependent engulfment of apoptotic cells. This model still holds true in acute inflammatory conditions, where macrophages are induced to express *Mfge8* themselves. Macrophages secrete Mfge8 (2) which subsequently targets apoptotic B cells (2). This allows macrophages to bind Mfge8-opsonized apoptotic cells via integrins (3). The interaction of Mfge8 with intregins induces the engulfment of the apoptotic cell (4). Adapted from Zullig and Hengartner, 2004.
(B) Revised model of Mfge8-dependent engulfment of apoptotic cells. In the spleen, Mfge8 is not produced by macrophages, but by FDCs. They establish a local Mfge8-gradient with the highest Mfge8-concentration in the GC (1). Along this gradient unarmed, distant TBMϕs are recruited directly to the location where apoptosis occurs (2). There, apoptotic cells become directly decorated with FDC-derived Mfge8 while still in contact with FDCs (3). Only proximal TBMϕs become armed for engulfment of apoptotic B cells in an Mfge8-dependent manner (4). This target-oriented two-tiered process allows two rare cell types to efficiently and rapidly remove apoptotic cells from the GC.

7.3 Complementary mechanism might control the removal of apoptotic cells from the GC

The rapid removal of apoptotic cells from the GC is of great importance, since upon impairment of this process, unremoved cells become necrotic, which results in release of DNA and other nuclear components. This is believed to be a cause of SLE, an autoimmune disease where systemic autoantibodies target nuclear components resulting in extensive tissue damage. *Mfge8*$^{-/-}$ mice were reported to develop SLE, though it appeared to be a rather mild form. They have a normal life span, increased levels of autoantibodies and glomerulonephritis that can only be observed at old age or after thorough immunization.

So far, no connection of FDCs and SLE has been described. However the above findings suggest that not only impaired TBMϕs function, but also impaired FDC function can cause SLE. Thus, the BM-chimeric mice were analyzed to determine whether stromal *Mfge8*-deficiency alone suffices to impair removal of apoptotic cells from the GC and to cause SLE. To this end, the amount of apoptotic cells associated with TBMϕs was quantified and revealed a mild increase in the case of complete (non-reconstituted *Mfge8*$^{-/-}$ mice or *Mfge8*$^{-/-}$→*Mfge8*$^{-/-}$ mice) or stromal (WT→*Mfge8*$^{-/-}$ mice) *Mfge8*-deficiency (Fig. 6.19). These results are in agreement with previous studies, although they seem to be less pronounced in the current study (Hanayama et al., 2004b). This observation can be interpreted as an impairment of the internalization and degradation of apoptotic cells. However, the EM analysis showed that even in the complete absence of Mfge8 (*Mfge8*$^{-/-}$→*Mfge8*$^{-/-}$) internalized lymphocytes in different degradation stages could be found within TBMϕs.

One possible explanation for this discrepancy is that several complementary mechanisms exist to ensure rapid removal of apoptotic cells. Plausible other candidates controlling the removal of apoptotic cells in the GC are complement factors which are known to target cells for phagocytosis. FDCs are a source of C1q and *C1q*-deficient mice also develop SLE (Schwaeble et al., 1995, Botto, 1998, Walport et al., 1998), underlining the importance of this cell type in regulating the removal of apoptotic cells in more than one way.

Unfortunately, the BM-chimeric mice proved to be not useful to study the SLE-induced glomerulonephritis, since all BM-chimeric mice developed a glomerulopathy due to the lethal irradiation which masked the autoimmune glomerulonephritis of *Mfge8*$^{-/-}$ mice (Fig. 6.22). The analysis of autoantibody levels did not yield evidence

supporting the presence of SLE in any of the analyzed mice, since autoantibody levels seemed unaltered in all chimeras (Fig. 6.21). Even in non-reconstituted mice no increased levels of autoantibodies could be detected. As mentioned above, the SLE in *Mfge8*$^{-/-}$ is rather mild and this might explain the difficulties in reproducing the elevated levels of autoantibodies. If the incidence of SLE in *Mfge8*$^{-/-}$ mice is low, development of SLE might depend on continous and extended stimulation with pathogens. Thus, the housing conditions and hygiene status of the mice might play an important role and could account for the differences between this study and previous reports.

Nevertheless, the above described findings raise the possibility that impaired FDC function can actively contribute to the development of SLE. It might be interesting to see, whether mice deficient for both, *Mfge8* and *C1q* exhibit a more dramatic SLE phenotype than knockout mice deficient of only one of these genes.

7.4 Acute inflammation induces *Mfge8* expression in macrophages

Regulation of *Mfge8* expression and of the removal of apoptotic cells seems to differ in organs other than the spleen During an acute inflammation, not stromal cells, but macrohages themselves produce Mfge8 (Fig. 6.24 and 6.25) (Hanayama et al., 2002). FDCs are only restricted to lymphoid organs and *Mfge8* expression has only been found in a few other stromal cells. But during acute inflammations, such as thioglycollate peritonitis or pulmonitis, extensive cell death occurs, hence *Mfge8* expression must be inducible throughout the whole body wherever extensive cell death requires it. This is best achieved by mobile cells that are efficiently recruited to the site of the inflammation during an immune response. Macrophages constitute such a cell type. However, *Mfge8* expression in macrophages seems to be tightly regulated. Interestingly, IL-4, but not IFNγ or LPS induced *Mfge8* expression. While IFNγ and LPS, inducers of the classical and innate macrophage-activation pathways promote an inflammatory response, IL-4, inducer of the alternative macrophage activation pathway, is thought to elicit an anti-inflammatory response. The anti-inflammatory macrophage response is associated with phagocytosis and increased antigen-presentation (Stein et al., 1992, Goerdt and Orfanos, 1999). It would be interesting to study the consequences of *Mfge8*-deficiency on disease-severity or

pathogen-load in different inflammatory disease models with profound Mϕ involvement.

The observation that the anti-inflammatory cytokine IL-4 induces *Mfge8* expression in Mϕs raises the possibility that Mfge8 is directly involved in this anti-inflammatory reaction. If this was true, then Mfge8 produced by FDCs could participate in the control of cell activation in the GC. In *Mfge8*$^{-/-}$ mice GC cells could therefore be hyperactive and a downregulation of the GC reaction might be impaired. This could lead to stronger and extended GC reactions and might, apart from the phagocytosis defect, contribute to the SLE and the enlarged spleen sizes observed in *Mfge8*$^{-/-}$ mice.

7.5 The role of Mfge8 in prion pathogenesis

While FDCs are the most important cell type for prion replication in lymphoid organs, it remains unclear why FDCs are so efficient in replication and accumulation of prions. Since FDCs are high expressors of Mfge8, the latter might have the potential to bind prions in order to target them for degradation by macrophages. To this end, *Mfge8*$^{-/-}$ mice were challenged with high and low doses of prions through the intraperitoneal (i.p.) and the intracerebral (i.c.) route.

Mfge8$^{-/-}$ mice on a mixed (B6x129) background exhibited a mild disease-acceleration after i.p. and a drastic acceleration after i.c. inoculation of prions. This acceleration is unlikely to be caused by altered prion replication or accumulation on FDCs, because the acceleration was most pronounced after i.c. inoculation, where disease progression is independent of the immune system. Furthermore, PrP^{Sc} accumulation in the spleen seemed to be unaltered in *Mfge8*$^{-/-}$ mice as assessed by histoblot and Western blot. In the brain however, increased levels of PrP^{Sc} were observed by IHC and Western blot. These results imply an involvement of Mfge8 in prion pathogenesis. Due to the known function of Mfge8 in the regulation of phagocytosis, it is likely that *Mfge8*-deficiency impairs either degradation of prions directly or the removal of apoptotic prion-infected cells. Both scenarios could explain the increased PrP^{Sc} levels in the brain.

The observed disease acceleration, however, seemed to be dependent on the genetic background of the mice. *Mfge8*$^{-/-}$ mice, that were backcrossed onto the C57BL/6 background for ten generations showed no alteration in prion pathogenesis.

Crossing the mixed background *Mfge8*$^{-/-}$ mice with the (B6x129) WT mice would help to exclude that the observed acceleration was an artefact caused by comparing incubation times of groups that differed too much in the genetic background. The resulting heterozygous F1 generation of this crossing has to be intercrossed and the disease progression of the *Mfge8*$^{+/+}$, *Mfge8*$^{+/-}$ and *Mfge8*$^{-/-}$ littermates of the F2-generation has to be compared. In addition to this, the *Mfge8*$^{-/-}$ mice could be crossed to another unrelated genetic background, like e.g. Balb/C. It would speak in favour for a true involvement of Mfge8 in prion pathogensis, if an acceleration can be observed in several very different genetic backgrounds or if a dose-dependent effect in *Mfge8*$^{+/-}$ mice can be observed

A possible explanation for the dependence of the disease acceleration on the genetic background could be that complementary molecular pathways, differently regulated in mice of different backgrounds, exist. One potential candidate is DEL-1, which has been shown to be a functional homolog of Mfge8 (Hanayama et al., 2004a, Hanayama et al., 2006). Therefore, it might be revealing to analyze DEL-1 expression in the brain of mice of different genetic backgrounds.

8 Materials and Methods

8.1 Mice

Mfge8$^{-/-}$ mice were generated in the lab of Shigekazu Nagata and were on a (C57BL/6x129)F_1 mixed (Hanayama et al., 2004b) or C57BL/6 background. As controls C57BL/6 (Harlan Laboratories) or F_1 offsprings of crossings between C57BL/6 and 129Sv mice (Charles River) were used. C57BL/6-CD45.1 mice were from Harlan Laboratories. All experiments were in accordance with Swiss federal legislation and had been approved by the local authorities.

8.2 Antibodies, recombinant proteins and other reagents

rEGF and rMfge8 were both from R&D Systems. rPrP was produced and purified as described (Zahn et al., 1997). 4C11 was from NovImmune SA, Geneva, Switzerland or from BD Pharmingen. Anti-Mfge8 clone 18A2-G10 was from MBL, International Corporation, and anti-Mfge8 clone 2422 from Alexis Biochemicals. Anti-CD21/35, FITC-labeled CD45.2, PE-labeled and biotinylated CD45.1 were from BD Pharmingen, biotinylated anti-CD68 clone FA-11, MOMA1 and rat IgG2c isotype control were from Serotec. ER-TR9 antibody was from Bachem AG, Switzerland. Anti-GFAP antibody was from DAKO, anti-IBA1 from Wako Chemicals and anti-PrP SAF84 antibody from SPI bio. Cy5-conjugated anti-PrP antibody POM2 was developed in house (Polymenidou et al., 2005). Secondary reagents were F(ab')$_2$ goat anti-hamster IgG FITC-labeled from Serotec, Alexa Fluor 594 goat anti-rat IgG (H+L), Streptavidin Alexa Fluor 647 from Molecular Probes and goat anti-Armenian hamster IgG-HRP from Santa Cruz Biotechnology. For *in vitro* stimulation of peritoneal macrophages LPS from *Salmonella abortus equi* (BioClot), IFNγ from R&D Systems and IL-4 from Sigma were used.

8.3 IHC, IF, TUNEL assay and competition with recombinant proteins

IHC for hematoxylin/eosin, FDC-M1 (1:50), CD21/35 (1:100) and CD68 (1:100) for light microscopy was performed on acetone-fixed spleen cryoscetions (5-10 μm) Blocking was performed in PBS containing 1% goat serum and 0.5% BSA. For detection, alkaline phosphatase (AP) conjugated secondary affinity-purified

polyclonal anti-Ig antibodies were used. AP was visualized using naphthol AS-BI phosphate and New Fuchsin as substrate, which yields a red precipitate. Endogenous AP was blocked by levamisole. Sections were counterstained with hematoxilin.

IHC for GFAP (1:1000) and IBA1 (1:1000) was performed on paraffin sections and detected with diaminobenzidine (Sigma). For PrP staining, formalin-fixed brain tissue were treated with concentrated formic acid for 60 min to inactivate prion infectivity. Postfixation in formalin was performed for at least 1 d, and tissues were embedded in paraffin. After deparaffination, sections (1-2 μm) were incubated for 6 min in 98% formic acid and washed in distilled water for 30 min. Sections were heated to 100°C in a steamer in citrate buffer (pH 6.0) for 3 min, and allowed to cool down to room temperature. Sections were incubated in VENTANA buffer and stains were performed on a NEXEX IHC robot (VENTANA instruments) using an IVIEW DAB Detection Kit (VENTANA Instruments). After incubation with protease 1 (VENTANA) for 16 min, sections were incubated with anti-PrP SAF-84 (1:200) for 32 min. Sections were counterstained with hematoxylin.

For IF, cyryosections were acetone-fixed and blocked (PBS containing 0.5% BSA and 1% goat serum), primary antibodies were added (2 μg/ml of 18A2-G10 and 2422 and 1 μg/ml of FDC-M1 or biotinylated anti-CD68). For competition, 18A2-G10 or FDC-M1 were incubated with 10 or 25 μg/ml rMfge8, rEGF or rPrP (1 hr, RT) before applying onto the sections. After washing secondary antibodies were added and analyzed by fluorescence microscopy (BX61, Olympus). TUNEL stainings were performed with the ApopTaq Plus Fluorescein In Situ Apoptosis Detection Kit (Chemicon) according to the manufacturer's instructions. Prior to TUNEL staining sections were fixed with 1% paraformaldehyde (PFA), washed, blocked and stained with biotinylated anti-CD68 (1 μg/ml) and postfixed again with PFA.

8.4 Immunoprecipitation and Western blotting

Paramagnetic beads (tosylactivated M280 Dynabeads, Dynal) were conjugated with purified 4C11, 2422 or rat IgG2c isotype control antibody according to the manufacturer's manual. Protein concentrations of 10% homogenates from WT and *Mfge8*$^{-/-}$ spleens were determined by BCA (bicinchoninic acid) Protein Assays (Pierce), according to the manufacturer's instructions. Homogenates were incubated

with 4C11-, 2422-, or IgG2c-beads, washed and resuspended in PBS containing sample buffer (NUPAGE® LDS Sample Buffer, Invitrogen) and subjected to Western blotting. Blots were blocked with 1x blocking buffer (Sigma) containing 1% goat serum and incubated with anti-Mfge8 antibody 18A2-G10 (0.5 μg/ml). For detection goat anti-Armenian hamster IgG-HRP (0.08 μg/ml) was used. After adding substrate (SuperSignal West Dura, Pierce) blots were analyzed with a FUJI LAS 3000 imaging system.

For detection of PrP^{Sc} by Western blot 50 μg of brain or spleen tissue homogentates were treated with proteinase K (50 μg/ml for brain, 20 μg/ml for spleen, 30 min, 37°C). Electrophoresis was done on 12% Bis-Tris NUPAGE gels (Invitrogen). Membranes were blocked (5% Topblock, Sigma) incubated with monoclonal antibody POM1 (1:10000) and detected with goat anti-mouse IgG1-HRP (1:10000), and visualized by enhanced chemiluminescence (ECL, Amersham).

8.5 Surface plasmon resonance (SPR) experiments

Surface plasmons are surface electromagnetic waves that propagate parallel along a metal interface. These waves oscillate at the boundary of the metal and the surrounding medium and are very sensitive to any changes of this boundary, such as the adsorption of molecules to the metal surface. Therefore, by recording changes in the electromagnetic waves using light beams that excite surface plasmons in a resonant manner, this technique can be used to measure interactions between molecules.

All experiments were performed with Biacore 3000. Rat IgG2c isotype control and 4C11 or 18A2-G10 antibodies were covalently captured on flow cells 1 and 2 respectively of a CM5 chip (Biacore) after activation with NHS/EDC at a flow rate of 5 μl/min. 5 μl of a 50 μg/ml antibody solution in acetate buffer (pH 4.5), were used to immobilize approx. 10’000 response units (RU) of covalently bound antibody. After surface inactivation with ethanolamine, the system was primed and a new sensogram was started with HBS-EP (Biacore) as running buffer. Similarly, approx. 15’000 RUs of each rPrP and rMfge8 were immobilized on the control and sample flow cell, respectively.

50 μl were used for all injections at a constant flow rate at 5 μl/min. All recombinant proteins or antibodies were injected at a concentration of 50 μg/ml diluted in HBS-EP

buffer (Biacore). For control, all protein-injections were made on two flow cells, where the first flow cell was coated with control protein or antibody and the second with the protein/antibody of interest. Regeneration of chip surfaces was achieved by 100 mM HCl. All sensograms represent changes in RUs on the flow cell immobilized with sample antibody or protein, after subtraction of changes in RUs on control flow cells.

8.6 Generation of BM chimeras and immunizations

BM cells were isolated from tibiae and femurs of donor mice and injected i.v. into the tail vein of previously irradiated (950 rad) hosts. Each mouse received i.v. $1x10^7$ donor BM cells. Reconstitution efficiency was assed after 5 weeks by FACS-analysis of CD45.1 and CD45.2 expression of blood leukocytes. 6 weeks post engraftment mice were immunized i.p. with 100 μg OVA (Sigma) in alum (Imject Alum, Pierce). 2 weeks later mice were boosted with the same dose of OVA in alum.

8.7 RNA isolation and cDNA synthesis

Total RNA from splenocytes or peritoneal macrophages was isolated using Trizol (Invitrogen). 1 μg RNA was used for cDNA synthesis. Prior to cDNA contaminating genomic DNA was removed. cDNA synthesis was done with QuantiTect Reverse Transcription Kit (Qiagen) according to the manufacturer's instruction. cDNA synthesis was tested by performing PCR (40 cycles) with primers specific for *Gapdh*. All samples were validated free of contaminating genomic DNA. PCR was performed with 2x PCR Master Mix (Promega).

8.8 quantitative Real Time PCR (QPCR) analysis and primers

Quantitative real-time PCR was performed using SYBR Green PCR Master Mix (Qiagen AG, Switzerland) on a 7900HT Fast Real-Time PCR System (Applied Biosystems) using default cycling conditions. Expression levels were normalized using *Gapdh*.

Gapdh forward primer: 5'-CCACCCCAGCAAGGAGACT-3'
Gapdh reverse primer: 5'-GAAATTGTGAGGGAGATGCT-3'
Mfge8 forward primer: 5'-ATATGGGTTTCATGGGCTTG-3'
Mfge8 reverse primer: 5'-GAGGCTGTAAGCCACCTTGA-3

Cxcl13 forward primer: 5'-TCGTGCCAAATGGTTACAAA-3'
Cxcl13 reverse primer: 5'-ACA AGG ATG TGG GTT GGG TA-3'
Ptprc forward primer: 5'-AAA CGA TCG GTG ACT TTT GG -3'
Ptprc reverse primer: 5'-AGC TCT TCC CCT TTC CAT GT-3'

8.9 FDC clusters isolation

To isolate FDCs, lymph nodes of 5 previously immunized and irradiated mice were dissected and enzymatically digested as described previously (Sukumar et al., 2006). The suspended cells from the digested lymph nodes were collected by centrifugation and resuspended in PBS containing FCS. The cells were then incubated with biotinylated 4C11 and mouse FcR blocking antibody (StemCell Technologies). Positive selection of $Mfge8^+$ cells was performed using the EasySep Biotin selection kit (StemCell Technologies). In brief, cells were incubated with EasySep Biotin selection cocktail. Then cells were further incubated with EasySep magnetic nanoparticles. Cells were then placed into the EasySep magnet. The two fractions (FDC-enriched and flow-through) were collected and lysed in Trizol, followed by RNA isolation and cDNA synthesis.

8.10 Stimulation of peritoneal Mϕs

Three months before use 30 g of fluid thioglycollate medium (Difco) were rehydrated in 1 l ddH_20 and autoclaved. Mice were injected i.p. with 1 ml thioglycollate suspension and 48h later, they were sacrificed and the peritoneum was flushed with cold PBS to harvest the Mϕs. For *in vitro* stimulation peritoneal Mϕs were isolated by peritoneal lavage and cultured over night in serum-free DMEM containing Pen/Strep. Then cells were washed and the adherent Mϕs were stimulated with either 100 ng/ml LPS, 100 ng/ml LPS and 10 ng/ml IFNγ (which was added 2h before the addition of LPS) or 20 ng IL-4 for 24h. Then cells were harvested and lysed in Trizol (Sigma). RNA and cDNA-synthesis followed and *Mfge8* expression was quantified by RT-PCR.

8.11 *In situ* RNA Hybridization

The *Mfge8* riboprobe was obtained by transcription of pBluescript II KS+ (Stratagene) containing the ORF of *Mfge8* using a DIG RNA Labeling Kit, Roche. ISH was

performed on spleen cryosections. For the fluorescent ISH, sections were prestained with biotinylated anti-CD68 antibody. Sections were post-fixed in 4% PFA in PBS followed by acetylation with 0.5% acetic anhydride in 0.1 M triethanolamine. Hybridization was carried out in buffer containing 50% formamide, 5x Saline Sodium Citrate (SSC) solution, 100 μg/ml E. coli t-RNA (Roche) and 5x Denhardt's solution. For *in situ* RNA hybridization 200 ng/ml DIG-labeled RNA probe was added to the hybridization buffer and incubated at 72°C overnight. For detection either anti-DIG-AP or anti-DIG-fluorescein antibody with a fluorescent enhancer kit (Roche) was used.

8.12 Electron microscopy

FDC clusters or tissue fragments from lymph nodes and spleens from BM-chimeras were fixed (60 min at 4°C) in a glutaraldehyde solution (2%) in 0.1 M cacodylate buffer (pH 7.4), washed and post-fixed for 30 min in a mixture of 1% OsO_4 and 1.5% $K_4Fe(CN)_6$ in 0.1 M cacodylate buffer (pH 7.4), dehydrated and embedded in EPON 812 (Fluka, Belgium). The resin specimens were trimmed and 70–90 nm sections were cut. Ultrathin sections were collected on copper 6200 girds and contrasted with uranyl acetate and lead acetate before examination with a Jeol CX 100 II transmission electron microscope at 80 kV.

8.13 Quantitation of autoantibodies by ELISA

To quantify serum levels of dsDNA and ANA antibodies, serum was collected from BM-chimeras 41 weeks post reconstitution. Titre-determination was done with the Anti-Nuclear Antibodies ELISA KIT and the Mouse Anti-dsDNA (IgG) Antibodies ELISA KIT from Alpha Diagostic according to the manufacturer´s instructions. In brief, appropriate serum dilutions were incubated on precoated ELISA plates. After addition of an HRP-conjugated anti-mouse Ig antibody, substrate was added. Enzymatic reaction was stopped after 15 min and absorbance was measured at 450 nm in an ELISA reader. Absorbance-values of the standard were plotted on a semi-log graph. After background-subtraction titre-concentrations of each sample was determined using the standard curve.

8.14 Prion inoculations

Mice were infected i.p. with 100 μl of brain homogenate diluted in PBS with 5% BSA and containing 3-6 $logLD_{50}$ units of the Rocky Mountain laboratory (RML) scrapie strain (passage 6, hence called RML6). For i.c. inoculations, 30 μl of inoculum with 3-6$logLD_{50}$ units were administered. Scrapie was diagnosed according to clinical criteria (ataxia, kyphosis, priapism and hind leg paresis). Mice were sacrificed on the day of onset of terminal clinical signs of scrapie.

8.15 Histoblotting

Spleen cryosections were blotted onto nitrocellulose membrane wetted in lysis buffer (0.5% Nonidet P-40/0.5% sodium deoxycholate/100 mM NaCi/lO mM EDTA/10 mM Tris-HCl, pH 7.8). For detection of PrP^{Sc} the membranes were thoroughly air dried, rehydrated for 1h in TBS-T and then subjected to limited proteolysis in digestion buffer (proteinase K at 400 μg/ml, for 18 hr at 37°C in 0.1% Brij 35/100mM NaCl/10 mM Tris-HCl, pH 7.8). To stop the reaction the blots were rinsed three times in TBS-T and incubated for 30 min in TBS-T/3 mM phenylmethylsulfonyl fluoride. Finally, the blots were incubated in 3 M GdnSCN/10 mM Tris HCl, pH 7.8, for 10 min and rinsed three times in TBS-T before immunostaining. The blots were then blocked with 5% Topblock and incubated the primary antibody (POM1). For detection a AP-conjugated secondary antibody was used.

9 References

Aguzzi, A., 2003. Prions and the immune system: a journey through gut, spleen, and nerves. Adv Immunol. 81, 123-171.

Aguzzi, A., 2006. Prion diseases of humans and farm animals: epidemiology, genetics, and pathogenesis. J Neurochem. 97, 1726-1739.

Aguzzi, A. and Polymenidou, M., 2004. Mammalian prion biology: one century of evolving concepts. Cell. 116, 313-327.

Aguzzi, A. and Sigurdson, C. J., 2004. Antiprion immunotherapy: to suppress or to stimulate? Nat Rev Immunol. 4, 725-736.

Ansel, K. M., McHeyzer-Williams, L. J., Ngo, V. N., McHeyzer-Williams, M. G. and Cyster, J. G., 1999. In vivo-activated CD4 T cells upregulate CXC chemokine receptor 5 and reprogram their response to lymphoid chemokines. J Exp Med. 190, 1123-1134.

Ansel, K. M., Ngo, V. N., Hyman, P. L., Luther, S. A., Forster, R., Sedgwick, J. D., Browning, J. L., Lipp, M. and Cyster, J. G., 2000. A chemokine-driven positive feedback loop organizes lymphoid follicles. Nature. 406, 309-314.

Balasubramanian, K. and Schroit, A. J., 2003. Aminophospholipid asymmetry: A matter of life and death. Annu Rev Physiol. 65, 701-734.

Balomenos, D., Martin-Caballero, J., Garcia, M. I., Prieto, I., Flores, J. M., Serrano, M. and Martinez, A. C., 2000. The cell cycle inhibitor p21 controls T-cell proliferation and sex-linked lupus development. Nat Med. 6, 171-176.

Baumann, I., Kolowos, W., Voll, R. E., Manger, B., Gaipl, U., Neuhuber, W. L., Kirchner, T., Kalden, J. R. and Herrmann, M., 2002. Impaired uptake of apoptotic cells into tingible body macrophages in germinal centers of patients with systemic lupus erythematosus. Arthritis Rheum. 46, 191-201.

Benschop, R. J. and Cambier, J. C., 1999. B cell development: signal transduction by antigen receptors and their surrogates. Curr Opin Immunol. 11, 143-151.

Boes, M., Schmidt, T., Linkemann, K., Beaudette, B. C., Marshak-Rothstein, A. and Chen, J., 2000. Accelerated development of IgG autoantibodies and autoimmune disease in the absence of secreted IgM. Proc Natl Acad Sci U S A. 97, 1184-1189.

Bofill, M., Akbar, A. N. and Amlot, P. L., 2000. Follicular dendritic cells share a membrane-bound protein with fibroblasts. J Pathol. 191, 217-226.

Bolland, S., Yim, Y. S., Tus, K., Wakeland, E. K. and Ravetch, J. V., 2002. Genetic modifiers of systemic lupus erythematosus in FcgammaRIIB(-/-) mice. J Exp Med. 195, 1167-1174.

Bolton, D. C., McKinley, M. P. and Prusiner, S. B., 1982. Identification of a protein that purifies with the scrapie prion. Science. 218, 1309-1311.

Botto, M., 1998. C1q knock-out mice for the study of complement deficiency in autoimmune disease. Exp Clin Immunogenet. 15, 231-234.

Brown, D. R., Qin, K., Herms, J. W., Madlung, A., Manson, J., Strome, R., Fraser, P. E., Kruck, T., von Bohlen, A., Schulz-Schaeffer, W., Giese, A., Westaway, D. and Kretzschmar, H., 1997a. The cellular prion protein binds copper in vivo. Nature. 390, 684-687.

Brown, D. R., Schulz-Schaeffer, W. J., Schmidt, B. and Kretzschmar, H. A., 1997b. Prion protein-deficient cells show altered response to oxidative stress due to decreased SOD-1 activity. Exp Neurol. 146, 104-112.

Burton, G. F., Conrad, D. H., Szakal, A. K. and Tew, J. G., 1993. Follicular dendritic cells and B cell costimulation. J Immunol. 150, 31-38.

Burton, G. F., Kosco, M. H., Szakal, A. K. and Tew, J. G., 1991. Iccosomes and the secondary antibody response. Immunology. 73, 271-276.

Campagnoli, C., Roberts, I. A., Kumar, S., Bennett, P. R., Bellantuono, I. and Fisk, N. M., 2001. Identification of mesenchymal stem/progenitor cells in human first-trimester fetal blood, liver, and bone marrow. Blood. 98, 2396-2402.

Castenholz, A., 1990. Architecture of the lymph node with regard to its function. Curr Top Pathol. 84 (Pt 1), 1-32.

Chen, L. L., Adams, J. C. and Steinman, R. M., 1978. Anatomy of germinal centers in mouse spleen, with special reference to "follicular dendritic cells". J Cell Biol. 77, 148-164.

Come, J. H., Fraser, P. E. and Lansbury, P. T., Jr., 1993. A kinetic model for amyloid formation in the prion diseases: importance of seeding. Proc Natl Acad Sci U S A. 90, 5959-5963.

Cyster, J. G., 1999. Chemokines and the homing of dendritic cells to the T cell areas of lymphoid organs. J Exp Med. 189, 447-450.

De Togni, P., Goellner, J., Ruddle, N. H., Streeter, P. R., Fick, A., Mariathasan, S., Smith, S. C., Carlson, R., Shornick, L. P., Strauss-Schoenberger, J. and et al.,

1994. Abnormal development of peripheral lymphoid organs in mice deficient in lymphotoxin. Science. 264, 703-707.

Desai-Mehta, A., Mao, C., Rajagopalan, S., Robinson, T. and Datta, S. K., 1995. Structure and specificity of T cell receptors expressed by potentially pathogenic anti-DNA autoantibody-inducing T cells in human lupus. J Clin Invest. 95, 531-541.

Dijkstra, C. D., Kamperdijk, E. W. and Dopp, E. A., 1984. The ontogenetic development of the follicular dendritic cell. An ultrastructural study by means of intravenously injected horseradish peroxidase (HRP)-anti-HRP complexes as marker. Cell Tissue Res. 236, 203-206.

Dijkstra, C. D., van Tilburg, N. J. and Dopp, E. A., 1982. Ontogenetic aspects of immune-complex trapping in the spleen and popliteal lymph nodes of the rat. Cell Tissue Res. 223, 545-552.

Felten, D. L. and Felten, S. Y., 1988. Sympathetic noradrenergic innervation of immune organs. Brain Behav Immun. 2, 293-300.

Flemming, W., 1885. Studien ueber Regeneration der Gewebe. Arch Mikr Anat 50.

Forster, R., Emrich, T., Kremmer, E. and Lipp, M., 1994. Expression of the G-protein--coupled receptor BLR1 defines mature, recirculating B cells and a subset of T-helper memory cells. Blood. 84, 830-840.

Fossum, S., 1980. The architecture of rat lymph nodes. IV. Distribution of ferritin and colloidal carbon in the draining lymph nodes after foot-pad injection. Scand J Immunol. 12, 433-441.

Fu, Y. X. and Chaplin, D. D., 1999. Development and maturation of secondary lymphoid tissues. Annu Rev Immunol. 17, 399-433.

Gaipl, U. S., Beyer, T. D., Heyder, P., Kuenkele, S., Bottcher, A., Voll, R. E., Kalden, J. R. and Herrmann, M., 2004. Cooperation between C1q and DNase I in the clearance of necrotic cell-derived chromatin. Arthritis Rheum. 50, 640-649.

Gaipl, U. S., Kuenkele, S., Voll, R. E., Beyer, T. D., Kolowos, W., Heyder, P., Kalden, J. R. and Herrmann, M., 2001. Complement binding is an early feature of necrotic and a rather late event during apoptotic cell death. Cell Death Differ. 8, 327-334.

Gaipl, U. S., Voll, R. E., Sheriff, A., Franz, S., Kalden, J. R. and Herrmann, M., 2005. Impaired clearance of dying cells in systemic lupus erythematosus. Autoimmun Rev. 4, 189-194.

Gajdusek, D. C., 1988. Transmissible and non-transmissible amyloidoses: autocatalytic post-translational conversion of host precursor proteins to beta-pleated sheet configurations. J Neuroimmunol. 20, 95-110.

Gibson, A., Wu, J., Edberg, J. C. and Kimberly, R. P., 1999. Fcgamma receptor polymorphism: insights into pathogenesis. Human Press, Inc.

Glatzel, M., Heppner, F. L., Albers, K. M. and Aguzzi, A., 2001. Sympathetic innervation of lymphoreticular organs is rate limiting for prion neuroinvasion. Neuron. 31, 25-34.

Goerdt, S. and Orfanos, C. E., 1999. Other functions, other genes: alternative activation of antigen-presenting cells. Immunity. 10, 137-142.

Gray, D., 1988. Recruitment of virgin B cells into an immune response is restricted to activation outside lymphoid follicles. Immunology. 65, 73-79.

Gretz, J. E., Norbury, C. C., Anderson, A. O., Proudfoot, A. E. and Shaw, S., 2000. Lymph-borne chemokines and other low molecular weight molecules reach high endothelial venules via specialized conduits while a functional barrier limits access to the lymphocyte microenvironments in lymph node cortex. J Exp Med. 192, 1425-1440.

Groeneveld, P. H., Erich, T. and Kraal, G., 1986. The differential effects of bacterial lipopolysaccharide (LPS) on splenic non-lymphoid cells demonstrated by monoclonal antibodies. Immunology. 58, 285-290.

Groscurth, P., 1980. [Non-lymphatic cells in the lymph node cortex of the mouse. II. Postnatal development of the interdigitating cells and the dendritic reticular cells (author's transl)]. Pathol Res Pract. 169, 235-254.

Guzman-Rojas, L., Sims-Mourtada, J. C., Rangel, R. and Martinez-Valdez, H., 2002. Life and death within germinal centres: a double-edged sword. Immunology. 107, 167-175.

Hanayama, R., Miyasaka, K., Nakaya, M. and Nagata, S., 2006. MFG-E8-dependent clearance of apoptotic cells, and autoimmunity caused by its failure. Curr Dir Autoimmun. 9, 162-172.

Hanayama, R. and Nagata, S., 2005. Impaired involution of mammary glands in the absence of milk fat globule EGF factor 8. Proc Natl Acad Sci U S A. 102, 16886-16891.

Hanayama, R., Tanaka, M., Miwa, K. and Nagata, S., 2004a. Expression of developmental endothelial locus-1 in a subset of macrophages for engulfment of apoptotic cells. J Immunol. 172, 3876-3882.

Hanayama, R., Tanaka, M., Miwa, K., Shinohara, A., Iwamatsu, A. and Nagata, S., 2002. Identification of a factor that links apoptotic cells to phagocytes. Nature. 417, 182-187.

Hanayama, R., Tanaka, M., Miyasaka, K., Aozasa, K., Koike, M., Uchiyama, Y. and Nagata, S., 2004b. Autoimmune disease and impaired uptake of apoptotic cells in MFG-E8-deficient mice. Science. 304, 1147-1150.

Hathaway, L. J. and Kraehenbuhl, J. P., 2000. The role of M cells in mucosal immunity. Cell Mol Life Sci. 57, 323-332.

Heikenwalder, M., Zeller, N., Seeger, H., Prinz, M., Klohn, P. C., Schwarz, P., Ruddle, N. H., Weissmann, C. and Aguzzi, A., 2005. Chronic lymphocytic inflammation specifies the organ tropism of prions. Science. 307, 1107-1110.

Heppner, F. L., Christ, A. D., Klein, M. A., Prinz, M., Fried, M., Kraehenbuhl, J. P. and Aguzzi, A., 2001. Transepithelial prion transport by M cells. Nat Med. 7, 976-977.

Heusermann, U., Zurborn, K. H., Schroeder, L. and Stutte, H. J., 1980. The origin of the dendritic reticulum cell. An experimental enzyme-histochemical and electron microscopic study on the rabbit spleen. Cell Tissue Res. 209, 279-294.

Hope, J., Ritchie, L., Farquhar, C., Somerville, R. and Hunter, N., 1989. Bovine spongiform encephalopathy: a scrapie-like disease of British cattle. Prog Clin Biol Res. 317, 659-667.

Huber, C., Thielen, C., Seeger, H., Schwarz, P., Montrasio, F., Wilson, M. R., Heinen, E., Fu, Y. X., Miele, G. and Aguzzi, A., 2005. Lymphotoxin-beta receptor-dependent genes in lymph node and follicular dendritic cell transcriptomes. J Immunol. 174, 5526-5536.

Humphrey, J. H., Grennan, D. and Sundaram, V., 1984. The origin of follicular dendritic cells in the mouse and the mechanism of trapping of immune complexes on them. Eur J Immunol. 14, 859-864.

Hutter, G., Heppner, F. L. and Aguzzi, A., 2003. No superoxide dismutase activity of cellular prion protein in vivo. Biol Chem. 384, 1279-1285.

Imai, Y. and Yamakawa, M., 1996. Morphology, function and pathology of follicular dendritic cells. Pathology International. 46, 807-833.

Imai, Y., Yamakawa, M., Masuda, A., Sato, T. and Kasajima, T., 1986. Function of the follicular dendritic cell in the germinal center of lymphoid follicles. Histol Histopathol. 1, 341-353.

Imazeki, N., Senoo, A. and Fuse, Y., 1992. Is the follicular dendritic cell a primarily stationary cell? Immunology. 76, 508-510.

Janeway, C. J., Travers, P., Walport, M. and Capra, J., 2001. Immunobiology. Garland Publishing, London.

Jarrett, J. T. and Lansbury, P. T., Jr., 1993. Seeding "one-dimensional crystallization" of amyloid: a pathogenic mechanism in Alzheimer's disease and scrapie? Cell. 73, 1055-1058.

Jeffrey, M., McGovern, G., Goodsir, C. M., Brown, K. L. and Bruce, M. E., 2000. Sites of prion protein accumulation in scrapie-infected mouse spleen revealed by immuno-electron microscopy. J Pathol. 191, 323-332.

Kamperdijk, E. W., Raaymakers, E. M., de Leeuw, J. H. and Hoefsmit, E. C., 1978. Lymph node macrophages and reticulum cells in the immune response. I. The primary response to paratyphoid vaccine. Cell Tissue Res. 192, 1-23.

Kapasi, Z. F., Burton, G. F., Shultz, L. D., Tew, J. G. and Szakal, A. K., 1993. Induction of functional follicular dendritic cell development in severe combined immunodeficiency mice. Influence of B and T cells. J Immunol. 150, 2648-2658.

Kapasi, Z. F., Qin, D., Kerr, W. G., Kosco-Vilbois, M. H., Shultz, L. D., Tew, J. G. and Szakal, A. K., 1998. Follicular dendritic cell (FDC) precursors in primary lymphoid tissues. J Immunol. 160, 1078-1084.

Kimberlin, R. H. and Walker, C. A., 1979. Pathogenesis of mouse scrapie: dynamics of agent replication in spleen, spinal cord and brain after infection by different routes. J Comp Pathol. 89, 551-562.

Klein, M. A., Frigg, R., Flechsig, E., Raeber, A. J., Kalinke, U., Bluethmann, H., Bootz, F., Suter, M., Zinkernagel, R. M. and Aguzzi, A., 1997. A crucial role for B cells in neuroinvasive scrapie. Nature. 390, 687-690.

Klein, M. A., Kaeser, P. S., Schwarz, P., Weyd, H., Xenarios, I., Zinkernagel, R. M., Carroll, M. C., Verbeek, J. S., Botto, M., Walport, M. J., Molina, H., Kalinke, U.,

Acha-Orbea, H. and Aguzzi, A., 2001. Complement facilitates early prion pathogenesis. Nat Med. 7, 488-492.

Koni, P. A. and Flavell, R. A., 1998. A role for tumor necrosis factor receptor type 1 in gut-associated lymphoid tissue development: genetic evidence of synergism with lymphotoxin beta. J Exp Med. 187, 1977-1983.

Koopman, G., Parmentier, H. K., Schuurman, H. J., Newman, W., Meijer, C. J. and Pals, S. T., 1991. Adhesion of human B cells to follicular dendritic cells involves both the lymphocyte function-associated antigen 1/intercellular adhesion molecule 1 and very late antigen 4/vascular cell adhesion molecule 1 pathways. J Exp Med. 173, 1297-1304.

Kosco, M. H., Monfalcone, A. P., Szakal, A. K. and Tew, J. G., 1988a. Germinal center B cells present antigen obtained in vivo to T cells in vitro and stimulate mixed lymphocyte reactions. Adv Exp Med Biol. 237, 883-888.

Kosco, M. H., Pflugfelder, E. and Gray, D., 1992. Follicular dendritic cell-dependent adhesion and proliferation of B cells in vitro. J Immunol. 148, 2331-2339.

Kosco, M. H., Szakal, A. K. and Tew, J. G., 1988b. In vivo obtained antigen presented by germinal center B cells to T cells in vitro. J Immunol. 140, 354-360.

Kraal, G., Hardy, R. R., Gallatin, W. M., Weissman, I. L. and Butcher, E. C., 1986. Antigen-induced changes in B cell subsets in lymph nodes: analysis by dual fluorescence flow cytofluorometry. Eur J Immunol. 16, 829-834.

Kraal, G., Rep, M. and Janse, M., 1987. Macrophages in T and B cell compartments and other tissue macrophages recognized by monoclonal antibody MOMA-2. An immunohistochemical study. Scand J Immunol. 26, 653-661.

Lansbury, P. T., Jr. and Caughey, B., 1995. The chemistry of scrapie infection: implications of the 'ice 9' metaphor. Chem Biol. 2, 1-5.

Lasmezas, C. I., Deslys, J. P., Robain, O., Jaegly, A., Beringue, V., Peyrin, J. M., Fournier, J. G., Hauw, J. J., Rossier, J. and Dormont, D., 1997. Transmission of the BSE agent to mice in the absence of detectable abnormal prion protein. Science. 275, 402-405.

Ledbetter, J. A. and Herzenberg, L. A., 1979. Xenogeneic monoclonal antibodies to mouse lymphoid differentiation antigens. Immunol Rev. 47, 63-90.

Lee, I. Y. and Choe, J., 2003. Human follicular dendritic cells and fibroblasts share the 3C8 antigen. Biochem Biophys Res Commun. 304, 701-707.

Lindhout, E. and de Groot, C., 1995. Follicular dendritic cells and apoptosis: life and death in the germinal centre. Histochem J. 27, 167-183.

Liu, Y. J., Zhang, J., Lane, P. J., Chan, E. Y. and MacLennan, I. C., 1991. Sites of specific B cell activation in primary and secondary responses to T cell-dependent and T cell-independent antigens. Eur J Immunol. 21, 2951-2962.

Lorenz, M. and Radbruch, A., 1996. Developmental and molecular regulation of immunoglobulin class switch recombination. Curr Top Microbiol Immunol. 217, 151-169.

Mabbott, N. A., Bruce, M. E., Botto, M., Walport, M. J. and Pepys, M. B., 2001. Temporary depletion of complement component C3 or genetic deficiency of C1q significantly delays onset of scrapie. Nat Med. 7, 485-487.

Mabbott, N. A., Farquhar, C. F., Brown, K. L. and Bruce, M. E., 1998. Involvement of the immune system in TSE pathogenesis. Immunol Today. 19, 201-203.

MacLennan, I. C., 1994. Germinal centers. Annu Rev Immunol. 12, 117-139.

McBride, P. A., Eikelenboom, P., Kraal, G., Fraser, H. and Bruce, M. E., 1992. PrP protein is associated with follicular dendritic cells of spleens and lymph nodes in uninfected and scrapie-infected mice. J Pathol. 168, 413-418.

Miyasaka, K., Hanayama, R., Tanaka, M. and Nagata, S., 2004. Expression of milk fat globule epidermal growth factor 8 in immature dendritic cells for engulfment of apoptotic cells. Eur J Immunol. 34, 1414-1422.

Moens, U., Seternes, O. M., Hey, A. W., Silsand, Y., Traavik, T., Johansen, B. and Rekvig, O. P., 1995. In vivo expression of a single viral DNA-binding protein generates systemic lupus erythematosus-related autoimmunity to double-stranded DNA and histones. Proc Natl Acad Sci U S A. 92, 12393-12397.

Mohan, C., Adams, S., Stanik, V. and Datta, S. K., 1993. Nucleosome: a major immunogen for pathogenic autoantibody-inducing T cells of lupus. J Exp Med. 177, 1367-1381.

Muramatsu, M., Kinoshita, K., Fagarasan, S., Yamada, S., Shinkai, Y. and Honjo, T., 2000. Class switch recombination and hypermutation require activation-induced cytidine deaminase (AID), a potential RNA editing enzyme. Cell. 102, 553-563.

Nagata, S. and Suda, T., 1995. Fas and Fas ligand: lpr and gld mutations. Immunol Today. 16, 39-43.

Nagy, A., Rossant, J., Nagy, R., Abramow-Newerly, W. and Roder, J. C., 1993. Derivation of completely cell culture-derived mice from early-passage embryonic stem cells. Proc Natl Acad Sci U S A. 90, 8424-8428.

Nakatani, H., Aoki, N., Nakagawa, Y., Jin-No, S., Aoyama, K., Oshima, K., Ohira, S., Sato, C., Nadano, D. and Matsuda, T., 2006. Weaning-induced expression of a milk-fat globule protein, MFG-E8, in mouse mammary glands, as demonstrated by the analyses of its mRNA, protein and phosphatidylserine-binding activity. Biochem J. 395, 21-30.

Napirei, M., Karsunky, H., Zevnik, B., Stephan, H., Mannherz, H. G. and Moroy, T., 2000. Features of systemic lupus erythematosus in Dnase1-deficient mice. Nat Genet. 25, 177-181.

Neutra, M. R. and Kraehenbuhl, J. P., 1992. Transepithelial transport and mucosal defence I: the role of M cells. Trends Cell Biol. 2, 134-138.

Ngo, V. N., Korner, H., Gunn, M. D., Schmidt, K. N., Riminton, D. S., Cooper, M. D., Browning, J. L., Sedgwick, J. D. and Cyster, J. G., 1999. Lymphotoxin alpha/beta and tumor necrosis factor are required for stromal cell expression of homing chemokines in B and T cell areas of the spleen. J Exp Med. 189, 403-412.

Ogata, T., Yamakawa, M., Imai, Y. and Takahashi, T., 1996. Follicular dendritic cells adhere to fibronectin and laminin fibers via their respective receptors. Blood. 88, 2995-3003.

Pasparakis, M., Kousteni, S., Peschon, J. and Kollias, G., 2000. Tumor necrosis factor and the p55TNF receptor are required for optimal development of the marginal sinus and for migration of follicular dendritic cell precursors into splenic follicles. Cell Immunol. 201, 33-41.

Patton, S. and Keenan, T. W., 1975. The milk fat globule membrane. Biochim Biophys Acta. 415, 273-309.

Phan, T. G., Grigorova, I., Okada, T. and Cyster, J. G., 2007. Subcapsular encounter and complement-dependent transport of immune complexes by lymph node B cells. Nat Immunol. 8, 992-1000.

Polymenidou, M., Stoeck, K., Glatzel, M., Vey, M., Bellon, A. and Aguzzi, A., 2005. Coexistence of multiple PrPSc types in individuals with Creutzfeldt-Jakob disease. Lancet Neurol. 4, 805-814.

Prinz, M., Heikenwalder, M., Junt, T., Schwarz, P., Glatzel, M., Heppner, F. L., Fu, Y. X., Lipp, M. and Aguzzi, A., 2003a. Positioning of follicular dendritic cells within the spleen controls prion neuroinvasion. Nature. 425, 957-962.

Prinz, M., Huber, G., Macpherson, A. J., Heppner, F. L., Glatzel, M., Eugster, H. P., Wagner, N. and Aguzzi, A., 2003b. Oral prion infection requires normal numbers of Peyer's patches but not of enteric lymphocytes. Am J Pathol. 162, 1103-1111.

Prusiner, S. B., 1982. Novel proteinaceous infectious particles cause scrapie. Science. 216, 136-144.

Prusiner, S. B., 1991. Molecular biology of prion diseases. Science. 252, 1515-1522.

Prusiner, S. B., Bolton, D. C., Groth, D. F., Bowman, K. A., Cochran, S. P. and McKinley, M. P., 1982. Further purification and characterization of scrapie prions. Biochemistry. 21, 6942-6950.

Prusiner, S. B. and DeArmond, S. J., 1990. Prion diseases of the central nervous system. Monogr Pathol, 86-122.

Prusiner, S. B., McKinley, M. P., Bowman, K. A., Bolton, D. C., Bendheim, P. E., Groth, D. F. and Glenner, G. G., 1983. Scrapie prions aggregate to form amyloid-like birefringent rods. Cell. 35, 349-358.

Rabinowitz, S. S. and Gordon, S., 1991. Macrosialin, a macrophage-restricted membrane sialoprotein differentially glycosylated in response to inflammatory stimuli. J Exp Med. 174, 827-836.

Ree, H. J., Khan, A. A., Elsakr, M., Liau, S. and Teplitz, C., 1993. Intercellular adhesion molecule-1 (ICAM-1) staining of reactive and neoplastic follicles. ICAM-1 expression of neoplastic follicle differs from that of reactive germinal center and is independent of follicular dendritic cells. Cancer. 71, 2817-2822.

Rekvig, O., 1997. Polyoma induced autoimmunity to DNA; experimental systems and clinical observations in human SLE. Lupus. 6, 325-326.

Rennert, P. D., Browning, J. L. and Hochman, P. S., 1997. Selective disruption of lymphotoxin ligands reveals a novel set of mucosal lymph nodes and unique effects on lymph node cellular organization. Int Immunol. 9, 1627-1639.

Rennert, P. D., Browning, J. L., Mebius, R., Mackay, F. and Hochman, P. S., 1996. Surface lymphotoxin alpha/beta complex is required for the development of peripheral lymphoid organs. J Exp Med. 184, 1999-2006.

Roufosse, C. A., Direkze, N. C., Otto, W. R. and Wright, N. A., 2004. Circulating mesenchymal stem cells. Int J Biochem Cell Biol. 36, 585-597.

Sailer, A., Bueler, H., Fischer, M., Aguzzi, A. and Weissmann, C., 1994. No propagation of prions in mice devoid of PrP. Cell. 77, 967-968.

Schwaeble, W., Schafer, M. K., Petry, F., Fink, T., Knebel, D., Weihe, E. and Loos, M., 1995. Follicular dendritic cells, interdigitating cells, and cells of the monocyte-macrophage lineage are the C1q-producing sources in the spleen. Identification of specific cell types by in situ hybridization and immunohistochemical analysis. J Immunol. 155, 4971-4978.

Sigurdson, C. J. and Aguzzi, A., 2007. Chronic wasting disease. Biochim Biophys Acta. 1772, 610-618.

Smith, J. P., Burton, G. F., Tew, J. G. and Szakal, A. K., 1998. Tingible body macrophages in regulation of germinal center reactions. Dev Immunol. 6, 285-294.

Smith, J. P., Kosco, M. H., Tew, J. G. and Szakal, A. K., 1988. Thy-1 positive tingible body macrophages (TBM) in mouse lymph nodes. Anat Rec. 222, 380-390.

Smith, J. P., Lister, A. M., Tew, J. G. and Szakal, A. K., 1991. Kinetics of the tingible body macrophage response in mouse germinal center development and its depression with age. Anat Rec. 229, 511-520.

Stein, M., Keshav, S., Harris, N. and Gordon, S., 1992. Interleukin 4 potently enhances murine macrophage mannose receptor activity: a marker of alternative immunologic macrophage activation. J Exp Med. 176, 287-292.

Strasser, A., 1995. Life and death during lymphocyte development and function: evidence for two distinct killing mechanisms. Curr Opin Immunol. 7, 228-234.

Sukumar, S., Szakal, A. K. and Tew, J. G., 2006. Isolation of functionally active murine follicular dendritic cells. J Immunol Methods. 313, 81-95.

Swartzendruber, D. C. and Congdon, C. C., 1963. Electron Microscope Observations on Tingible Body Macrophages in Mouse Spleen. J Cell Biol. 19, 641-646.

Szabo, M. C., Butcher, E. C. and McEvoy, L. M., 1997. Specialization of mucosal follicular dendritic cells revealed by mucosal addressin-cell adhesion molecule-1 display. J Immunol. 158, 5584-5588.

Szakal, A. K., Gieringer, R. L., Kosco, M. H. and Tew, J. G., 1985. Isolated follicular dendritic cells: cytochemical antigen localization, Nomarski, SEM, and TEM morphology. J Immunol. 134, 1349-1359.

Szakal, A. K., Holmes, K. L. and Tew, J. G., 1983. Transport of immune complexes from the subcapsular sinus to lymph node follicles on the surface of nonphagocytic cells, including cells with dendritic morphology. J Immunol. 131, 1714-1727.

Szakal, A. K., Kosco, M. H. and Tew, J. G., 1988. A novel in vivo follicular dendritic cell-dependent iccosome-mediated mechanism for delivery of antigen to antigen-processing cells. J Immunol. 140, 341-353.

Szakal, A. K., Kosco, M. H. and Tew, J. G., 1989. Microanatomy of lymphoid tissue during humoral immune responses: structure function relationships. Annu Rev Immunol. 7, 91-109.

Tanaka, H., Saito, S., Sasaki, H., Arai, H., Oki, T. and Shioya, N., 1994. Morphological aspects of LFA-1/ICAM-1 and VLA4/VCAM-1 adhesion pathways in human lymph nodes. Pathol Int. 44, 268-279.

Tenner-Racz, K., Racz, P., Schmidt, H., Dietrich, M., Kern, P., Louie, A., Gartner, S. and Popovic, M., 1988. Immunohistochemical, electron microscopic and in situ hybridization evidence for the involvement of lymphatics in the spread of HIV-1. Aids. 2, 299-309.

Tew, J. G., Thorbecke, G. J. and Steinman, R. M., 1982. Dendritic cells in the immune response: characteristics and recommended nomenclature (A report from the Reticuloendothelial Society Committee on Nomenclature). J Reticuloendothel Soc. 31, 371-380.

Timens, W., 1991. The human spleen and the immune system: not just another lymphoid organ. Res Immunol. 142, 316-320.

Tsunoda, R., Nakayama, M., Heinen, E., Miyake, K., Suzuki, K., Sugai, N. and Kojima, M., 1992. Emperipolesis of lymphoid cells by human follicular dendritic cells in vitro. Virchows Arch B Cell Pathol Incl Mol Pathol. 62, 69-78.

van Eijk, M., Medema, J. P. and de Groot, C., 2001. Cutting edge: cellular Fas-associated death domain-like IL-1-converting enzyme-inhibitory protein protects germinal center B cells from apoptosis during germinal center reactions. J Immunol. 166, 6473-6476.

van Keulen, L. J., Schreuder, B. E., Meloen, R. H., Mooij-Harkes, G., Vromans, M. E. and Langeveld, J. P., 1996. Immunohistochemical detection of prion protein in lymphoid tissues of sheep with natural scrapie. J Clin Microbiol. 34, 1228-1231.

Voll, R. E., Roth, E. A., Girkontaite, I., Fehr, H., Herrmann, M., Lorenz, H. M. and Kalden, J. R., 1997. Histone-specific Th0 and Th1 clones derived from systemic lupus erythematosus patients induce double-stranded DNA antibody production. Arthritis Rheum. 40, 2162-2171.

Walport, M. J., Davies, K. A. and Botto, M., 1998. C1q and systemic lupus erythematosus. Immunobiology. 199, 265-285.

Ware, C. F., VanArsdale, T. L., Crowe, P. D. and Browning, J. L., 1995. The ligands and receptors of the lymphotoxin system. Curr Top Microbiol Immunol. 198, 175-218.

Weinstein, P. D. and Cebra, J. J., 1991. The preference for switching to IgA expression by Peyer's patch germinal center B cells is likely due to the intrinsic influence of their microenvironment. J Immunol. 147, 4126-4135.

Weinstein, P. D., Schweitzer, P. A., Cebra-Thomas, J. A. and Cebra, J. J., 1991. Molecular genetic features reflecting the preference for isotype switching to IgA expression by Peyer's patch germinal center B cells. Int Immunol. 3, 1253-1263.

Weissmann, C., 2004. The state of the prion. Nat Rev Microbiol. 2, 861-871.

Wells, G. A., Dawson, M., Hawkins, S. A., Green, R. B., Dexter, I., Francis, M. E., Simmons, M. M., Austin, A. R. and Horigan, M. W., 1994. Infectivity in the ileum of cattle challenged orally with bovine spongiform encephalopathy. Vet Rec. 135, 40-41.

Whitacre, C. C., Reingold, S. C. and O'Looney, P. A., 1999. A gender gap in autoimmunity. Science. 283, 1277-1278.

Witmer, M. D. and Steinman, R. M., 1984. The anatomy of peripheral lymphoid organs with emphasis on accessory cells: light-microscopic immunocytochemical studies of mouse spleen, lymph node, and Peyer's patch. Am J Anat. 170, 465-481.

Yoshida, K., Kaji, M., Takahashi, T., van den Berg, T. K. and Dijkstra, C. D., 1995. Host origin of follicular dendritic cells induced in the spleen of SCID mice after transfer of allogeneic lymphocytes. Immunology. 84, 117-126.

Zabel, M. D., Heikenwalder, M., Prinz, M., Arrighi, I., Schwarz, P., Kranich, J., von Teichman, A., Haas, K. M., Zeller, N., Tedder, T. F., Weis, J. H. and Aguzzi, A., 2007. Stromal complement receptor CD21/35 facilitates lymphoid prion colonization and pathogenesis. J Immunol. 179, 6144-6152.

Zahn, R., von Schroetter, C. and Wuthrich, K., 1997. Human prion proteins expressed in Escherichia coli and purified by high-affinity column refolding. FEBS Lett. 417, 400-404.

Zullig, S. and Hengartner, M. O., 2004. Cell biology. Tickling macrophages, a serious business. Science. 304, 1123-1124.

Zwart, B., Ciurana, C., Rensink, I., Manoe, R., Hack, C. E. and Aarden, L. A., 2004. Complement activation by apoptotic cells occurs predominantly via IgM and is limited to late apoptotic (secondary necrotic) cells. Autoimmunity. 37, 95-102.

10 Curriculum Vitae

Name: Jan Kranich

Date of birth: 09.05.1978

Place of birth: Ulm, Germany

Nationality: German

Education

1984 - 1988	Ludwig-Uhland Schule Langenau, Germany
1988 - 1997	Robert-Bosch-Gymnasiums Langenau, Germany
1997	Abitur at the Robert-Bosch-Gymnasium Langenau
1997 to 1998	Military service at Luftwaffensanitätsstaffel, Mengen, Germany
1998 to 2002	Biology-studies at the University of Freiburg, Germany
2001	"Vordiplom" at the University of Freiburg
09/2001	practical training in the lab of Dr. Gabor Igloi at the University of Freiburg
03/2002	practical training in the lab of Prof. Bodo Rak at the University of Freiburg
04-05/2002	practical training in the lab of Dr. Viktor Steimle at the Max-Planck-Institute for Immunobiology, Freiburg, Germany
2002	"Diplomprüfung" at the University of Freiburg Major subject: Immunology Minor subjects: Genetics, Bioinformatics, Informatics
01-12/2003	Diploma thesis at the Max-Planck-Institut for Immunbiology Freiburg, Germany in the lab of Dr. Jörg Kirberg Title: "Altered B cell function in BKLF transgenic mice".
01-02/2004	Scientific Assistant at the Max-Planck-Institut for Immunology in the group of Dr. Jörg Kirberg.
2004 - present	PhD thesis at the Institute of Neuropathology, University Hospital Zurich, Switzerland; Director: Prof. Dr. Adriano Aguzzi Title: "Novel Functional Aspects of Follicular Dendritic Cells".

11 Presentations and Publications

Presentations

Poster presentation at the 34th DGFI-Meeting, 2003 in Berlin, Germany (Title: "**BKLF overexpression results in altered B cell development**").

Poster presentation at the Prion2005 Meeting, Düsseldorf, Germany (Title: "**Using shRNA-mediated knockdown of PrP in vitro to reveal the function of the prion protein**").

Poster presentation at the Prion2007 Meeting, Edinburgh, UK (Title: "**CD21/35 - A Peripheral Prion Receptor?**").

Oral presentation at the EU Prions Conference 2005, Crete, Greece (Title: "**Peripheral and central modifiers of prion disease**").

Oral presentation at the Prion2006 Meeting, Torino, Italy (Title: "**The Role of Mfge8 in Prion Pathogenesis**").

Oral presentation at the Alpine Meeting "Molecular basis of disease", Valens, Switzerland, 2007 (Title: "**Follicular dendritic cells provide Mfge8 to tingible-body macrophages and enable engulfment of apoptotic B cells** ").

Oral presentation at IMMUNORIO 2007: 13th International Congress of Immunology, Rio de Janeiro, Brasil, 2007 (Title: "**Follicular dendritic cells provide Mfge8 to tingible-body macrophages and enable engulfment of apoptotic B cells**").

Publications

Follicular dendritic cells control engulfment of apoptotic bodies by secreting Mfge8. Jan Kranich, Nike Julia Krautler, Ernst Heinen, Magdalini Polymenidou, Claire Bridel, Anita Schildknecht, Christoph Huber, Marie H. Kosco-Vilbois, Rolf Zinkernagel, Gino Miele, and Adriano Aguzzi; (manuscript in preparation).

Coincident scrapie infection and nephritis lead to urinary prion excretion. Seeger H, Heikenwalder M, Zeller N, **Kranich J**, Schwarz P, Gaspert A, Seifert B, Miele G, Aguzzi A.; Science, 2005 Oct 14;310(5746):324-6.

Stromal complement receptor CD21/35 facilitates lymphoid prion colonization and pathogenesis. Zabel MD, Heikenwalder M, Prinz M, Arrighi I, Schwarz P, **Kranich J**, von Teichman A, Haas KM, Zeller N, Tedder TF, Weis JH, Aguzzi A.; J Immunol. 2007 Nov 1;179(9):6144-52.

Transcriptional Stability of Cultured Cells upon Prion Infection. Julius C, Hutter G, Wagner U, Seeger H, Kana V, **Kranich J**, Klöhn P, Weissmann C, Miele G, Aguzzi A.; J Mol Biol. 2007 Nov 12; [Epub ahead of print]

12 Acknowledgments

I am very grateful to Prof. Adriano Aguzzi for giving me the opportunity to work on this interesting project, for his critical supervision and for his great support during my PhD thesis.

I would like to thank Prof. Annette Oxenius and Prof. Manfred Kopf for their support and help as members of my PhD committee.

I also would like to thank Dr. Gino Miele, for his superb supervision and very helpful discussions during the first two years of my PhD thesis.

Then I would like to thank Nike Kräutler who contributed a lot to the success of this work for the excellent collaboration.

I am also very thankful to Petra Schwarz for the mouse work, all the uncountable cryosections and stainings she made and also for all the cookies, chocolate and wine.

Furthermore I would like to thank:
Prof. Ernst Heinen for the electron microscopy, Magdalini Polymenidou for the Biacore study, Claire Bridel and Anita Schildknecht who also contributed to the success of this project and Dr. Marie Kosco-Vilbois for the stimulating discussions, Dr. Shigekazu Nagata for the *Mfge8*$^{-/-}$ mice and Dr. Ariana Gaspert for the help with the kidney analysis.
Mirzet Delic and the whole BZL-team for the great support in the animal facility.
Rita Moos, Audrey Marcel and Li-Chun Infanger for the excellent technical support.
Christian Julius, Anna Maria Callela, Mathias Heikenwälder, Jeppe Falsig, José Barros, Gregor Hutter, Dorothea Rutishauser, Kalina Draganova, Christina Sigurdson, Peter Nilsson, Frank Baumann, Mark Zabel, Harald Seeger and Sei-ichi Yusa for all the interesting discussions, help and support.